ION CYCLOTRON RESONANCE STUDIES OF VIBRATIONALLY EXCITED IONS. I. LOW INTENSITY MULTIPHOTON DISSOCIATION OF GAS PHASE IONS USING CW CO_2 LASER RADIATION. II. INFRARED RADIATIVE STABILIZATION OF ENERGIZED SPECIES IN THE GAS PHASE.

Thesis by

Richard Lawrence Woodin

In Partial Fulfillment of the Requirements

For the Degree of

Doctor of Philosophy

California Institute of Technology

Pasadena, California

1979

(Submitted January 3, 1979)

ACKNOWLEDGMENTS

First and foremost I would like to sincerely thank my advisor, Professor J. L. Beauchamp, for his tutelage and guidance during my stay at Caltech, in both the pursuit and presentation of science. I also wish to thank Professor W. A. Goddard III for his interest and assistance in several projects.

During the course of the past year I have been privileged to work with David Bomse on the laser photodissociation experiments. His contributions, especially his wry humor on those late nights when the experiment died, have been invaluable. It has been a great pleasure to work with Frances Houle and Ben Freiser on several projects. Reed Corderman has been a good friend throughout my graduate career, and I thank him for many instructive conversations over the years. To the rest of the Beauchamp research group, past and present, I would like to express my thanks for their assistance and many good times both in and out of the lab.

I am indebted to Bill Schuelke and Anton Stark for their expert technical assistance in modifying and maintaining the ICR apparatus. Joyce Lundstedt deserves special thanks for her efforts in the final assembly of this thesis.

To my parents I owe a tremendous debt for their unflagging encouragement in all of my endeavors. Largely through their efforts have I been able to come this far. I wish that my father might be here to share in my achievement. To my wife, Signe, I owe a double

debt of gratitude for not only having to put up with me during the writing of this thesis, but also with the rigors of her job in these final days. I thank her for her love and understanding over the past several years.

Finally, I express my appreciation to the California Institute of Technology for financial support during my graduate studies.

ABSTRACT

This thesis is divided into two general topics; vibrational excitation of gas phase molecules using cw CO_2 laser radiation (Chapters II and III) and stabilization of chemically activated species by infrared radiative emission (Chapters IV-VI). Chapter I is a brief introduction to the topics discussed in Chapters II-VI.

Multiphoton dissociation of molecules is observed using low intensity (1-100 W cm^{-2}) cw CO_2 laser radiation. Ion cyclotron resonance techniques allow gas phase ions to be stored and irradiated for times approaching several seconds prior to mass analysis. Chapter II describes multiphoton dissociation of ions derived from diethyl ether $[(C_2H_5)_2O]$ while Chapter III describes multiphoton dissociation of $C_3F_6^+$ from perfluoropropylene (C_3F_6). Energy fluence thresholds and cross-sections for multiphoton dissociation measured using low intensity radiation qualitatively agree with similar measurements using megawatt pulsed infrared lasers. For all ions which photodissociate only the lowest activation energy process is observed. Effects of bimolecular interactions, varying laser intensity, and laser wavelength on photodissociation probabilities are explored. At high pressures collisions are observed to deactivate vibrationally excited ions. At low pressures, however, $C_3F_6^+$ photodissociation is enhanced by collisions. The consequences of collisional enhancement of multiphoton absorption are discussed.

ICR techniques are uniquely suited for studying ion-molecule reactions under nearly collisionless conditions. Chapters IV and V

discuss direct association reactions of Li^+ with $(C_2H_5)_2CO$, $CH_3COC_2H_5$, $(CH_3)_2CO$, $(CD_3)_2CO$, CH_3CHO, and H_2CO at pressures low enough ($< 10^{-6}$ Torr) to preclude collisional stabilization of the chemically activated adduct. The stabilization mechanism is assumed to be via infrared emission, and calculated attachment rates are in good agreement with experiment.

In experiments similar to those described above, rates of direct electron attachment to C_6F_6 (perfluorobenzene), C_7F_8 (perfluorotoluene), c-C_4F_8 (perfluorocyclobutane), and C_7F_{14} (perfluoromethylcyclohexane) are measured at low pressure by ICR techniques. Rate constants measured by ICR are found to be one to two orders of magnitudes smaller than high pressure swarm measurements. The results are discussed in terms of radiative stabilization at low pressure versus collisional stabilization at high pressure. Combination of data from time-of-flight, electron beam-swarm, and ICR experiments allows estimates of infrared radiative lifetimes to be made. These fall in the range 0.4-3.0 msec, which are typical of infrared radiative processes. Data are also presented for dissociative electron attachment of CCl_4.

TABLE OF CONTENTS

CHAPTER I

INTRODUCTION

The variety of chemical and physical phenomena amenable to study is largely dictated by available techniques for detecting concentrations of atoms and molecules, or detecting changes in some physical property associated with atomic and molecular processes. Thus, historically, chemical insight first dealt with easily obtainable bulk material properties, for example, color, vapor pressure, melting point and boiling point. As experimental technology has evolved, increasingly discerning measurement capability has become available such that current techniques now allow observation of physical and chemical phenomena associated with isolated molecules.[1] Examples of particularly elegant studies involve infrared multiphoton dissociation of isolated molecules in molecular beams using infrared lasers.[2] A disadvantage of beam techniques for isolating molecules is the inherently short interaction time involved. Storage of particles in a spatially well defined volume for long periods of time (several seconds) under collisionless conditions should allow a host of hitherto unexplored processes to be observed. No such storage is available as yet for neutral species. However, the electric charge associated with ions provides a means of spatially confining particles.

The ability to manipulate charged particles via electric and magnetic fields has been known for many years,[3] and gave rise to the field of mass spectrometry. A particularly versatile mass

spectrometric technique is ion cyclotron resonance spectroscopy (ICR).[4] ICR utilizes crossed electric and magnetic fields to spatially trap ions for up to several seconds, during which time stored ions may react with neutral molecules. Mass detection depends upon the relation between cyclotron frequency and charge to mass ratio.[4] In the past ICR has been used primarily to study the reactions of ions with neutral molecules. Such studies include determining acid-base thermochemical properties,[5] reaction mechanisms,[4] and metal-ligand binding energies.[6] At sufficiently low pressures ($< 10^{-7}$ Torr) ions may be trapped for times approaching several seconds under essentially collisionless conditions. By avoiding collisional effects, processes with lifetimes approaching 1 sec can be observed. This thesis deals primarily with the interactions of gas phase ions with infrared radiation. By using the ion trapping capability of ICR spectroscopy, the absorption of many quanta of cw infrared laser radiations by ions has been studied (Chapters II and III), as well as the complementary process of stabilization of chemically activated species by infrared emission (Chapters IV-VI). The time scale of these processes (1-1000 msec) is such that under more usual conditions encountered in the laboratory they are not observable. ICR thus provides a unique method for observing these phenomena. Table I lists previous publications by the author which are relevant to this thesis.

While molecular beam experiments have clearly demonstrated that pulsed megawatt infrared lasers can energize isolated molecules

Table I. Published Work Related to This Thesis

1. Sequential Deuterium Exchange Reactions of Protonated Benzenes with D_2O in the Gas Phase by Ion Cyclotron Resonance Spectroscopy

   B. S. Freiser, R. L. Woodin, and J. L. Beauchamp
   J. Am. Chem. Soc., 97, 6893 (1975)

2. The Nature of the Bonding of Li^+ to H_2O and NH_3; Ab Initio Studies

   R. L. Woodin, F. A. Houle, and W. A. Goddard III
   Chem. Phys., 14, 461 (1976)

3. Binding of Li^+ to Lewis Bases in the Gas Phase. Reversals in Methyl Substituent Effects for Different Reference Acids

   R. L. Woodin and J. L. Beauchamp
   J. Am. Chem. Soc., 100, 501 (1978)

4. Multiphoton Dissociation of Molecules with Low Power Continuous Wave Infrared Laser Radiation

   R. L. Woodin, D. S. Bomse, and J. L. Beauchamp
   J. Am. Chem. Soc., 100, 3248 (1978)

5. Multiphoton Dissociation of Molecules with Low Power CW Infrared Lasers

   D. S. Bomse, R. L. Woodin, and J. L. Beauchamp
   In "Advances in Laser Chemistry," A. H. Zewail, ed., Springer Series in Chemical Physics, Springer, Berlin, Heidelberg, New York, 1978

6. Multiphoton Dissociation of Gas Phase Ions Using Low Intensity CW Laser Radiation

   R. L. Woodin, D. S. Bomse, and J. L. Beauchamp
   In "Chemical and Biochemical Applications of Lasers," C. Bradley Moore, ed., Vol. IV, Academic Press, New York, 1978

to above the dissociation threshold,[2] the experiments are difficult and in many respects not quantitative due to spatial and temporal inhomogeneities inherent in focused pulsed laser radiation. Chapters II and III detail studies of low intensity infrared multiphoton dissociation of ions using spatially and temporally uniform cw laser radiation. Chapter II deals with multiphoton dissociation of ions derived from diethyl ether, while Chapter III discusses multiphoton dissociation of $C_3F_6^+$. A number of comparisons and contrasts are drawn between the present work using a cw laser, and experiments using megawatt pulsed lasers.

A complementary process to the infrared excitation described above is stabilization of molecules by infrared emission. This is particularly applicable to chemical reactions in the collisionless realm of interstellar space.[7] A number of interstellar molecules (ions) are thought to be formed by bimolecular association, process 1.[8, 9, 10] In the absence of collisions the chemically activated adduct

$$A^+ + B \rightarrow [AB^+]^{\ddagger} \qquad \Delta H = -D_0(B\text{-}A^+) \tag{1}$$

$[AB^+]^{\ddagger}$ retains the reaction exothermicity, $D_0(B\text{-}Li^+)$, as internal excitation. The adduct may subsequently decompose or be stabilized by another mechanism, usually postulated as infrared emission. While radiative association reactions have been proposed to explain certain interstellar molecular abundances,[11] no direct experimental evidence has previously been obtained to verify radiative association. Using trapped ion techniques association reactions of Li^+ to a number

of aliphatic carbonyl compounds have been observed, and are discussed in Chapters IV and V. Pressures are low enough (10^{-7}-10^{-6} Torr) to render collisional stabilization unlikely, and the experimental results are interpreted in terms of an infrared radiative mechanism.

Chapter VI deals with a similar chemical activation process, direct electron attachment at low pressure. It has been known for some time that molecules such as SF_6 or C_6F_6 attach low energy electrons in both high pressure (1-10 Torr) and low pressure ($< 10^{-6}$ Torr) experiments.[12-14] Discrepancies in both attachment rates and negative ion lifetimes between high and low pressure data has led to confusion as to the nature of the process. Utilizing data from time-of-flight measurements, high pressure swarm experiments and low pressure ICR results, electron attachment is discussed in Chapter VI in terms of infrared emission stabilizing initially excited molecular negative ions. Comparison of data from these various experiments allows estimates of radiative rates to be made.

References

1. See for example, R. D. Levine and R. B. Bernstein, "Molecular Reaction Dynamics," Oxford University Press, New York, 1974.
2. M. J. Coggiola, P. A. Schulz, Y. T. Lee, and Y. R. Shen, Phys. Rev. Lett., 38, 17 (1977); Aa. S. Sudbo, P. A. Schulz, E. R. Grant, Y. R. Shen, and Y. T. Lee, J. Chem. Phys., 68, 1306 (1978).
3. J. D. Jackson, "Classical Electrodynamics," John Wiley and Sons, Inc., New York, 1975.
4. T. A. Lehman and M. M. Bursey, "Ion Cyclotron Resonance Spectrometry," Wiley-Interscience, New York, 1976; J. L. Beauchamp, Ann. Rev. Phys. Chem., 22, 527 (1971).
5. J. F. Wolf, R. H. Staley, I. Koppel, M. Taagepera, R. T. McIver, Jr., J. L. Beauchamp, and R. W. Taft, J. Am. Chem. Soc., 99, 5417 (1977), and references contained therein.
6. R. R. Corderman and J. L. Beauchamp, J. Am. Chem. Soc., 98, 3998 (1976).
7. E. Herbst and W. Klemperer, Phys. Tod., June, 32 (1976).
8. E. Herbst, Astrophys. J., 205, 94 (1976).
9. D. Smith and N. G. Adams, Astrophys. J., 220, L87 (1978).
10. J. H. Black and A. Dalgarno, Astrophys. Lett., 15, 79 (1973).
11. D. Smith and N. G. Adams, Astrophys. J., 217, 741 (1977).
12. L. G. Christophorou, Adv. Electron. and Electron Phys., 46, 55 (1978)

13. L. G. Christophorou, "Atomic and Molecular Radiation Physics," Wiley-Interscience, New York, 1971.

14. M. S. Foster and J. L. Beauchamp, Chem. Phys. Lett., 31, 482 (1975).

CHAPTER II

Molecular Activation with Low Intensity CW Infrared Laser Radiation. Multiphoton Dissociation of Ions Derived from Diethyl Ether.

D. S. Bomse,[1] R. L. Woodin,[2] and J. L. Beauchamp

Contribution No. 5932 from the Arthur Amos Noyes Laboratory of Chemical Physics, California Institute of Technology, Pasadena, California 91125

ABSTRACT

Low intensity cw CO_2 laser radiation (10. 6 μm) induced multiphoton dissociation of gas phase ions derived from diethyl ether is reported. Techniques of ion cyclotron resonance spectroscopy are used to store ions, allowing irradiation for up to 2 seconds with intensities of 1-100 W cm^{-2}. Measured energy fluence thresholds and dissociation rates are comparable to data derived from pulsed laser experiments. For all ions which photodissociate only the decomposition process of lowest activation energy is observed. Effects of bimolecular interactions, varying laser intensity, and laser wavelength on photodissociation probabilities are explored. The present work is compared and contrasted with pulsed infrared laser experiments, and mechanistic implications are discussed.

Introduction

A reasonable description of infrared multiphoton excitation using megawatt pulsed lasers is now beginning to emerge. It is generally agreed that initial excitation is by coherent absorption of 3-5 infrared photons in one vibrational mode.[3] Typically, at this level of excitation the rates of intramolecular V-V transfer are sufficient to allow rapid energy transfer to other vibrational modes.[4] Subsequent excitation then proceeds through a sequential incoherent absorption process.[3,5] Standard statistical theories[6] accurately model the unimolecular reactions which occur when the internal excitation of a molecule exceeds threshold.[5,7] Key results from megawatt pulsed laser experiments are: (1) Multiphoton dissociation is observed under collisionless conditions.[8] (2) Decomposition via the lowest energy pathway is always observed, but is not necessarily the exclusive reaction channel.[9] (3) The spectrum obtained by monitoring the probability of dissociation as a function of laser wavelength is shifted to lower energies and broadened relative to the corresponding infrared absorption spectrum.[3,10,11] Where isotopic substitution introduces shifts in the absorption spectrum, multiphoton dissociation is isotopically selective.[3,11,12] (4) Collisionless dissociation probabilities are uniquely determined by the total laser pulse energy, independent of peak power.[13] (5) There appears to be an energy fluence (energy cm^{-2}) threshold below which dissociation does not occur.[8,14] (6) Collisions during the laser pulse decrease the fraction of molecules dissociated yet increase the total number of photons absorbed.[3,15,16]

(7) Multiphoton excitation rates are sufficiently rapid that molecules may absorb as many as 10 photons in excess of the thermodynamic threshold prior to reaction.[8, 17]

Typical energy fluence thresholds for multiphoton dissociation processes are measured to be 1-2 J cm^{-2}.[8, 14] Since the level of multiphoton excitation depends on energy fluence rather than intensity one infers multiphoton dissociation can be effected using ~ 1 W cm^{-2} provided the target molecules are irradiated under collisionless conditions for at least 1 second. This rather stringent criterion can be satisfied by molecules in an interstellar medium or, more conveniently, in the laboratory using the techniques of ion cyclotron resonance spectroscopy. An obvious requirement for the success of such an experiment is that net absorption rates must exceed spontaneous emission rates. Our recent observation of multiphoton dissociation of gas phase ions using cw laser intensities of less than 100 W cm^{-2} adds an exciting new dimension to the field of multiphoton activation.[18] Thus photodissociation experiments need not be limited to excitation by megawatt pulsed lasers. In the present study we detail our investigations of low intensity multiphoton dissociation of ions derived from diethyl ether. Effects of bimolecular interactions, varying laser intensity, and laser wavelength on photodissociation probabilities are explored. Infrared photodissociation spectra of gas phase ions promises to be a source of previously unobtainable ion structural conformation.

Experimental

The theory, techniques and instrumentation of trapped ion ICR spectroscopy have been previously described in detail.[19] The spectrometer used in this study was built at Caltech and incorporates a 15 inch electromagnet capable of 23.4 kG. A flat ICR cell is utilized, illustrated in Figure 1, in which the upper source plate is replaced with a 92% transmittance mesh to allow irradiation of trapped ions.

All ICR experiments were carried out in the range 10^{-7}-10^{-5} Torr, corresponding to neutral particle densities of 3×10^{9} - 3×10^{11} molecules cm^{-3}. Pressure is measured with a Schulz-Phelps type ionization gauge calibrated against an MKS Instruments Baratron Model 90H1-E capacitance manometer. It is expected that absolute pressure determinations are within ± 20% using this method, with pressure ratios being somewhat more accurate. Sample mixtures are prepared directly in the instrument using three sample inlets and the Schulz-Phelps gauge.

Diethyl ether, sulphur hexafluoride, isobutane, and cyclohexane were obtained from commercial sources. Perdeuterated diethyl ether was provided by Professor J. D. Roberts and $(C_2H_5)(C_2D_5)O$ was prepared by D. Holtz. All reagents were used without further purification except for the removal of noncondensible gases by several freeze-pump-thaw cycles. Mass spectrometry revealed no detectable impurities. Diethyl ether -d_{10} and $(C_2H_5)(C_2D_5)_2O$ were measured to be $>$ 99 and 98.6 atom percent pure, respectively.

FIGURE 1

Cutaway view of cyclotron resonance cell. The electron beam is collinear with the magnetic field. Laser beam positioning is indicated for low intensity laser photodissociation studies.

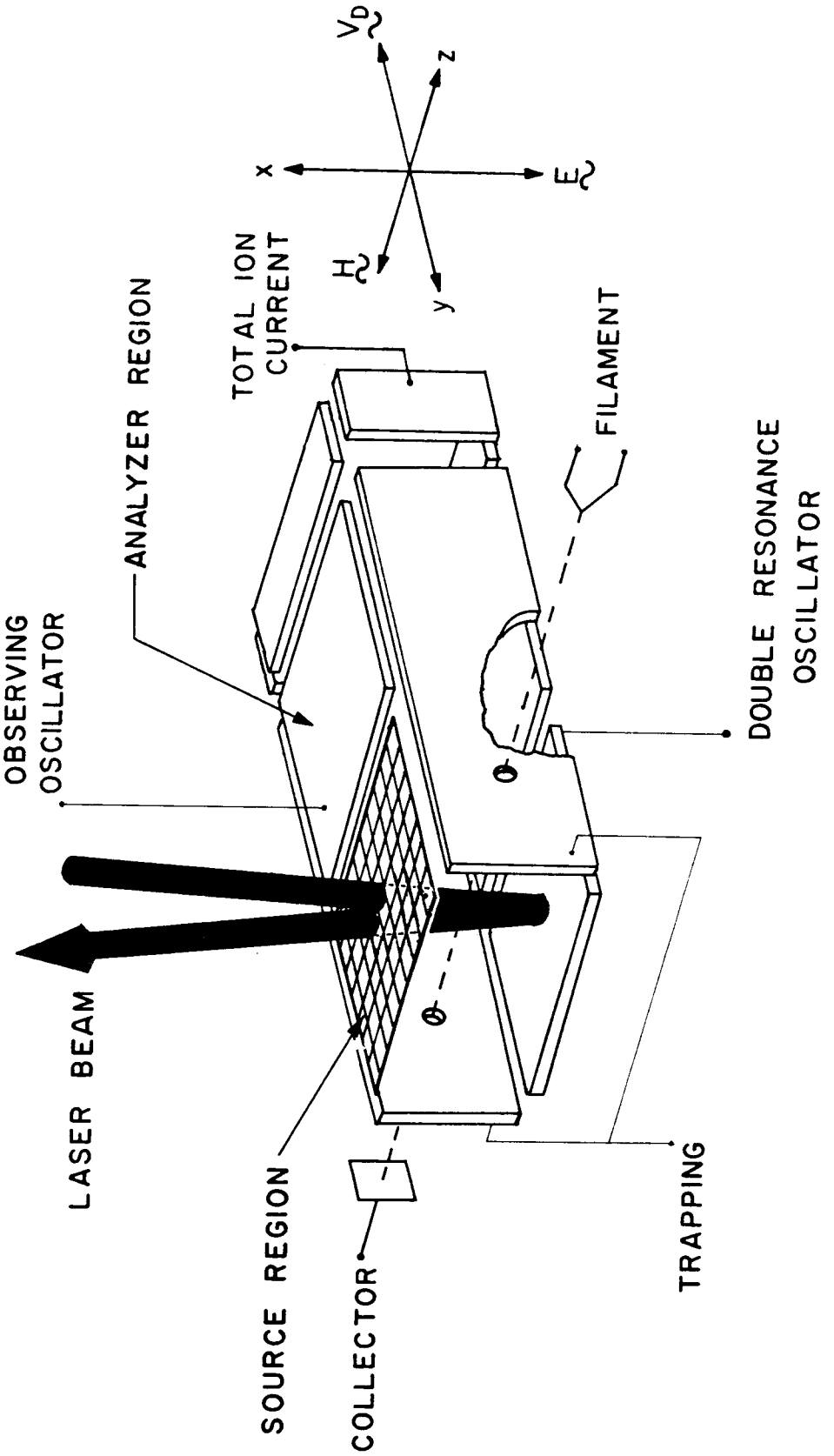
V_D
z
x
E
H
y
TOTAL ION CURRENT
ANALYZER REGION
FILAMENT
OBSERVING OSCILLATOR
DOUBLE RESONANCE OSCILLATOR
LASER BEAM
SOURCE REGION
COLLECTOR
TRAPPING

Gas phase infrared spectra were obtained using a Perkin-Elmer 257 grating spectrometer. Samples were contained in a 10 cm path length cell equipped with NaCl windows. Wavelength calibration was with polystyrene film.

A schematic view of the experimental apparatus is shown in Figure 2. The laser is an Apollo Model 550A grating tuned cw CO_2 laser. The laser beam profile is nearly Gaussian (FWHM = 6 mm) as determined by measuring the power transmitted through a 1 mm diameter pinhole translated across the beam. Infrared beam intensities quoted in this paper are calculated by dividing the total power in the beam by the area of the 6 mm diameter beam. Beam shape is monitored with an Optical Engineering Model 22A thermal imaging plate. Infrared laser wavelengths are measured with an Optical Engineering Model 16A spectrum analyzer. Bandwidths are estimated to be 50 MHz. A fraction (25%) of the beam is reflected by a calibrated ZnSe beam splitter (supplied by II-VI Inc.) to a Laser Precision Corp. Model RkP-345 pyroelectric radiometer allowing continuous power measurement. Power fluctuations are typically less than $\pm$ 5% during an experiment. Maximum stability is achieved by running the laser continuously and controlling irradiation of ions with a Uniblitz Model 225LOA14x5 mechanical shutter. The shutter opening time is measured to be 5 msec.

A turning mirror (Figure 2) directs the beam transverse to the magnetic field into the source region of the ICR cell. The infrared beam enters the vacuum system through an antireflection coated ZnSe window (25.4 mm dia. $\times$ 3.5 mm thick) supplied by II-VI, Inc. A

FIGURE 2

Schematic view of the experimental apparatus.

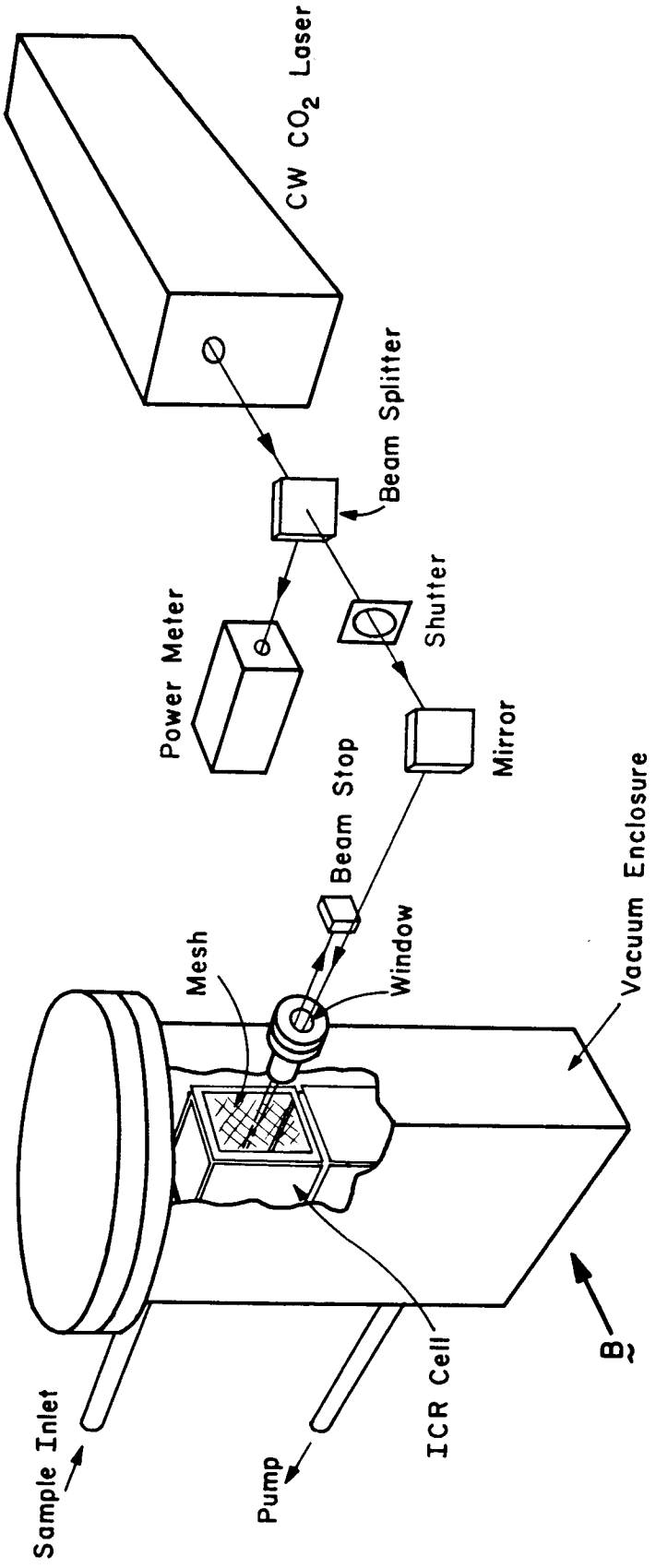
CW CO_2 Laser
Beam Splitter
Power Meter
Shutter
Mirror
Beam Stop
Window
Mesh
Vacuum Enclosure
Sample Inlet
Pump
ICR Cell
B

mirror finish on the lower source plate (Figure 1) reflects the beam through the source region and out of the apparatus to a graphite beam stop. Laser intensity in the cell can be varied from 1-100 W cm^{-2}. Irradiation of stored ions is uniform as indicated by the fact that small translations of the laser beam do not alter photodissociation rates.

Observed ion decompositions obey first order kinetics and it is possible to dissociate 100% of the ions. The timing sequence for a typical experiment is illustrated in Figure 3. A 10 msec electron beam pulse generates ions (typically 10^5 ions cm^{-3}) which can be stored for several seconds during which time reactions may occur. The ions are then mass analyzed to determine concentrations of the various species present. [20] Ions of a particular charge to mass ratio can be selectively ejected by ICR double resonance[19] allowing positive identification of reaction pathways. Electronic control of the optical shutter allows the infrared beam to irradiate ions during any portion of the trapping sequence. Ions can be irradiated on alternate trapping cycles and corresponding ion intensities (laser on and laser off) are monitored by a two channel boxcar integrator. These signals are then processed in a straightforward fashion to yield photodissociation rate constants, even in the presence of ion loss due to diffusion and reaction. [21]

Results and Discussion

A. Ion-Molecule Chemistry of Diethyl Ether. Electron impact ionization of diethyl ether at electron energies greater than 15 eV

FIGURE 3

Timing sequence for trapped ion ICR photodissociation experiments. Ions may be irradiated during any portion of the trapping period.

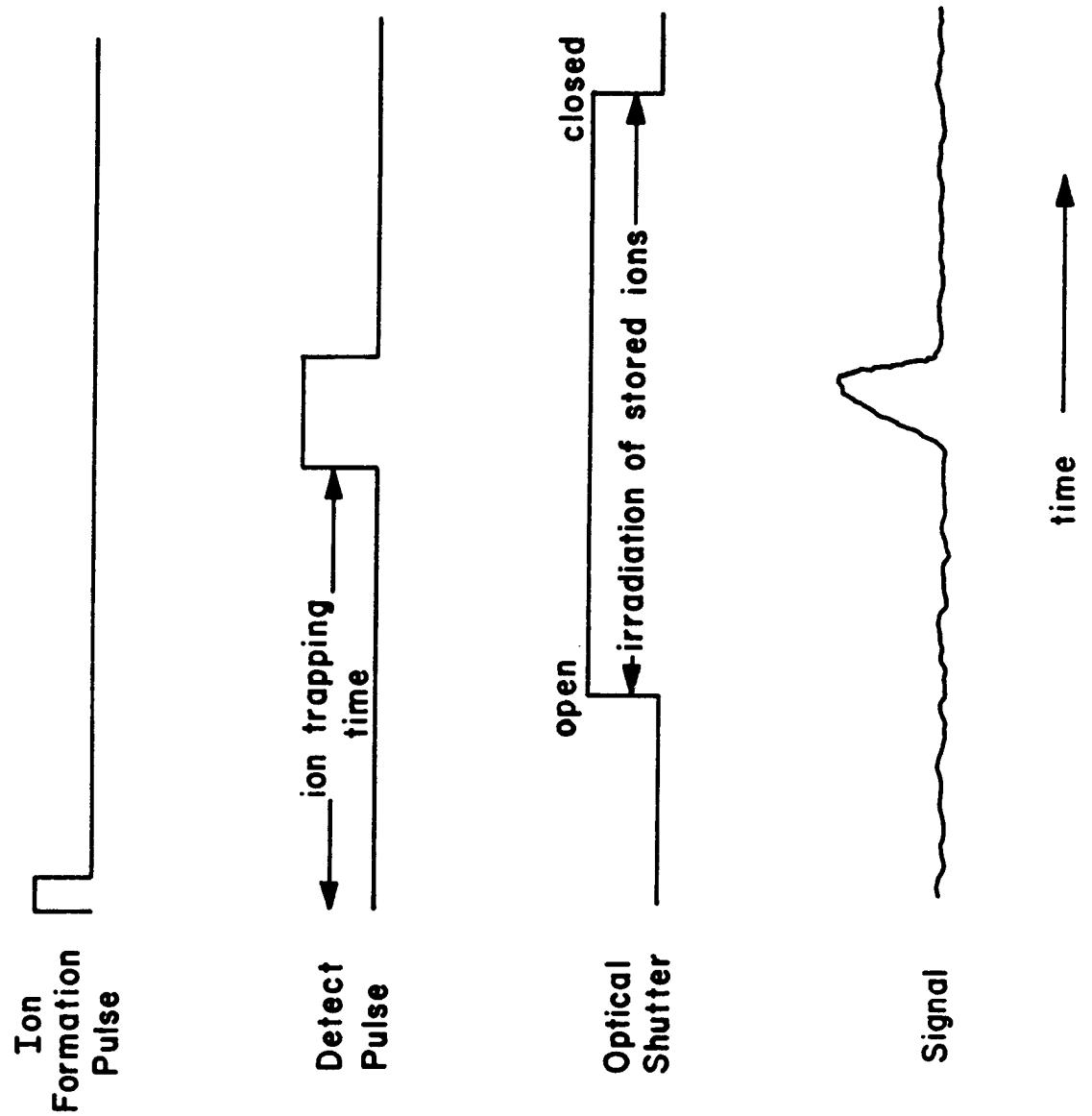
Ion Formation Pulse
Detect Pulse
ion trapping time
Optical Shutter
open
irradiation of stored ions
closed
Signal
time

results in a large variety of fragmentation products. The breakdown diagram shown in Figure 4 illustrates the variation with electron energy of the major ion abundances. Data in Figure 4 are obtained at low pressure and short trapping times to avoid bimolecular reactions. Relative contributions of CHO^+ and $C_2H_5^+$ to the m/e 29 signal are ascertained by comparison with the $(C_2D_5)_2O$ breakdown diagram. Similar comparisons indicate that ions observed at m/e 43 and m/e 45 are due exclusively to $C_2H_3O^+$ and $C_2H_5O^+$, respectively.

Ion-molecule reactions which occur in diethyl ether involve proton transfer, hydride abstraction and bimolecular clustering.[22] Proton transfer from fragment ions and parent cation to diethyl ether results in formation of $(C_2H_5)_2OH^+$, process 1, where RH^+ includes

$$RH^+ + (C_2H_5)_2O \rightarrow (C_2H_5)_2OH^+ + R \qquad (1)$$

$C_2H_3^+$, $C_2H_5^+$, CHO^+, CH_2OH^+, $C_2H_3O^+$, $C_2H_5O^+$, $C_2H_7O^+$, and $C_4H_{10}O^+$. In some cases proton transfer is sufficiently exothermic to induce fragmentation of protonated ether yielding protonated ethanol, process 2, where RH^+ includes $C_2H_3^+$, $C_2H_5^+$, and CHO^+. These

$$RH^+ + (C_2H_5)_2O \rightarrow [(C_2H_5)_2OH^+]^* + R \qquad (2a)$$

$$[(C_2H_5)_2OH^+]^* \rightarrow C_2H_5OH_2^+ + C_2H_4 \qquad (2b)$$

reactions are confirmed by ICR double resonance.

At pressures greater than 5×10^{-7} Torr and for trapping times greater than 0.5 sec $(C_2H_5)_2OH^+$ is observed to react with diethyl ether

FIGURE 4

Variation of ion abundance with ionization energy for diethyl ether. Diethyl ether pressure is 6×10^{-7} Torr.

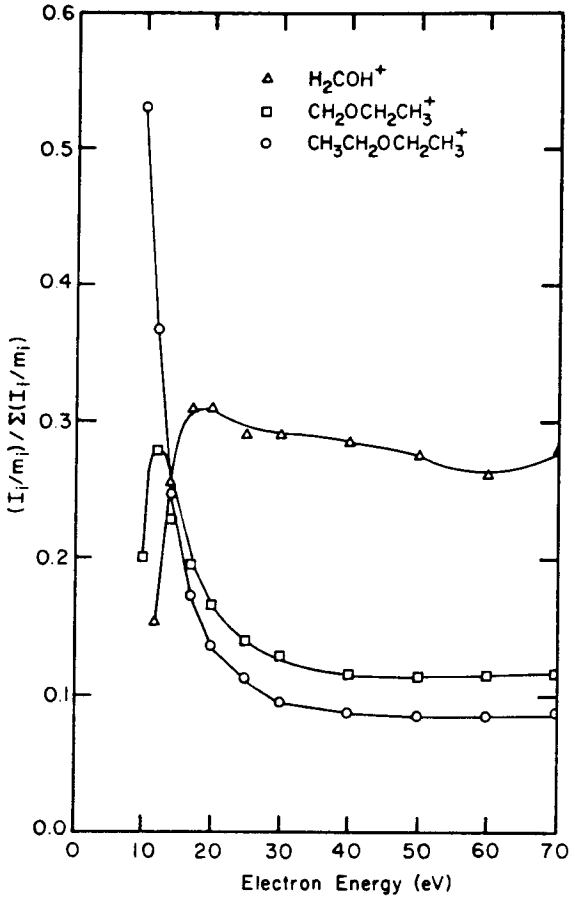
0.6
0.5
0.4
0.3
0.2
0.1
0.0
0
10
20
30
40
50
60
70
Electron Energy (eV)
$(I_i/m_i)/\Sigma(I_i/m_i)$
H_2COH^+
$CH_2OCH_2CH_3^+$
$CH_3CH_2OCH_2CH_3^+$

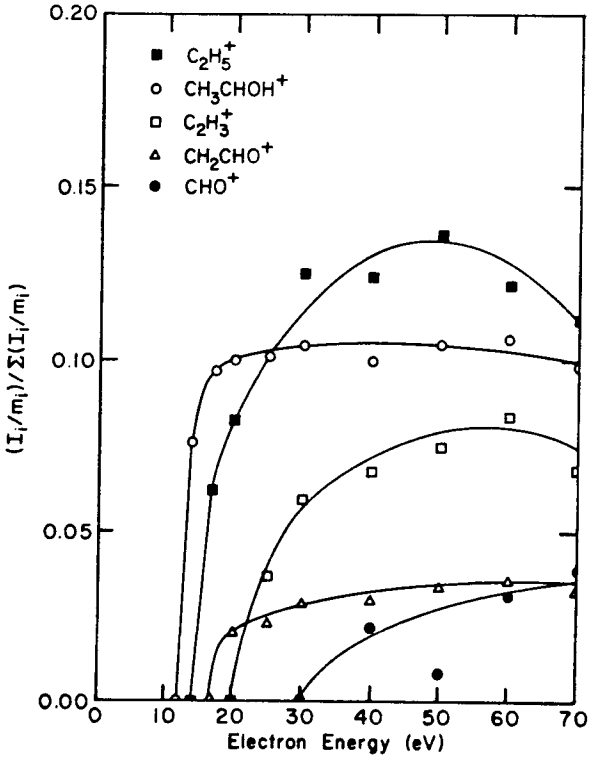
0.20
0.15
0.10
0.05
0.00
0
10
20
30
40
50
60
70
Electron Energy (eV)
$(I_i/m_i)/\Sigma(I_i/m_i)$
$C_2H_5^+$
CH_3CHOH^+
$C_2H_3^+$
CH_2CHO^+
CHO^+

to produce the proton bound dimer of diethyl ether, process 3.

$$(C_2H_5)_2OH^+ + (C_2H_5)_2O \rightarrow [(C_2H_5)_2O]_2H^+ \quad (3)$$

The rate of proton bound dimer formation measured at these pressures indicated process 3 is bimolecular with a rate constant of 1.7×10^{-11} cm^3 $molecule^{-1}$ sec^{-1}. The rate constant for formation of $[(C_2H_5)_2O]_2H^+$ is obtained from data such as shown in Figure 5. This figure displays the temporal variation of major ion abundances at a diethyl ether pressure of 4.9×10^{-7} Torr and ionizing energy of 14 eV. Also shown are the data for the hydride abstraction reaction, process 4. The measured rate for this reaction is 3.3×10^{-10} cm^3

$$CH_2OC_2H_5^+ + (C_2H_5)_2O \rightarrow CH_3CHOC_2H_5^+ + CH_3OC_2H_5 \quad (4)$$

$molecule^{-1}$ sec^{-1}. Not shown in Figure 5 is another hydride abstraction, process 5, which gives rise to only a minor fraction ($< 10\%$)

$$C_3H_5^+ + (C_2H_5)_2O \rightarrow CH_3CHOC_2H_5^+ + C_3H_6 \quad (5)$$

of the $CH_3CHOC_2H_5^+$ abundance.

As reported previously,[18] both $(C_2H_5)_2OH^+$ and $[(C_2H_5)_2O]_2H^+$ undergo multiphoton dissociation on a time scale such that collisions may deactivate vibrationally excited species. For $(C_2H_5)_2OH^+$ the most obvious deactivation process is symmetric proton transfer.[23] The use of isotopically labeled ether allows detection of symmetric proton transfer, reaction 6.

$$(C_2H_5)_2OH^+ + (C_2D_5)_2O \longrightarrow (C_2H_5)_{20} + (C_2D_5)_2OH^+ \quad (6)$$

FIGURE 5

Variation of ion abundance with trapping time for the major ions derived from diethyl ether. Ions are produced by a 10 msec 14 eV electron beam pulse.

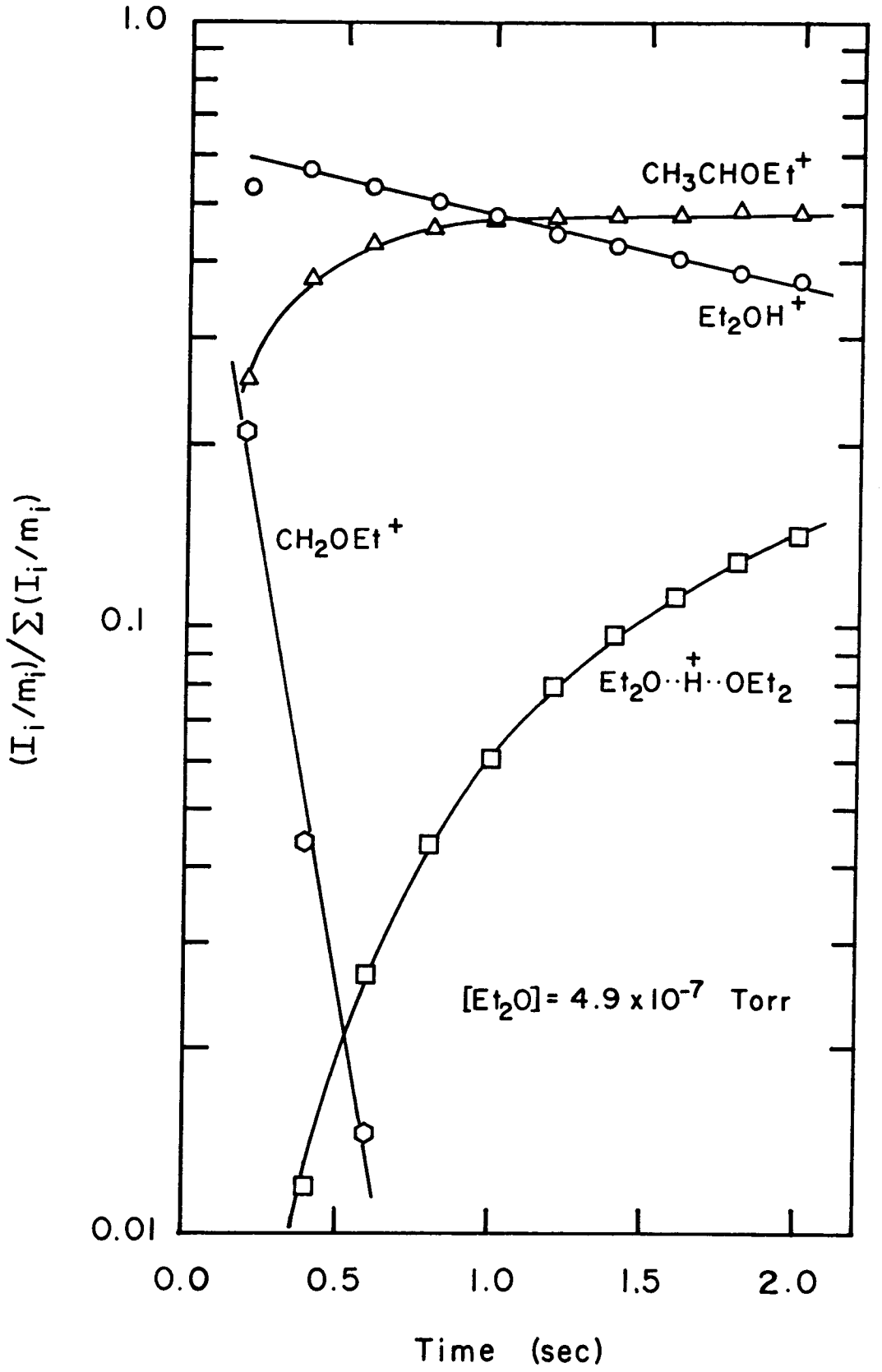
1.0
0.1
0.01
$(I_i/m_i)/\Sigma(I_i/m_i)$
CH_3CHOEt^+
Et_2OH^+
CH_2OEt^+
$Et_2O\cdot\overset{+}{H}\cdot OEt_2$
$[Et_2O] = 4.9 \times 10^{-7}$ Torr
0.0
0.5
1.0
1.5
2.0
Time (sec)

Double resonance ejection of $(C_2D_5)_2OH^+$ prevents the reverse of reaction 6 and leads to exponential decay of $(C_2H_5)_2OH^+$ with decay rate equal to the proton transfer rate. This is determined to be 3.9×10^{-10} cm^3 $molecule^{-1}$ sec^{-1}. Similarly, symmetric ether exchange is a possible route for deactivation of laser excited $[(C_2H_5)_2O]_2H^+$. Again, the rate can be measured using a mixture of diethyl ether and diethyl ether-d_{10}. For reaction 7, the rate constant

$$[(C_2H_5)_2O]_2H^+ + (C_2D_5)_2O \rightarrow (C_2H_5)_2OH^+O(C_2D_5)_2 + (C_2H_5)_2O \qquad (7)$$

is 5.3×10^{-12} cm^3 $molecule^{-1}$ sec^{-1} which corresponds to approximately 1 exchange for every 200 ion-molecule collisions.[24]

B. Infrared Laser Photochemistry of $[(C_2H_5)_2O]_2H^+$. Although infrared absorption bands for ions derived from diethyl ether are unknown, multiphoton dissociation of species such as $[(C_2H_5)_2O]_2H^+$ was anticipated based on strong absorption bands of $(C_2H_5)_2O$ in the 900-1100 cm^{-1} region.[25] Under infrared laser irradiation the proton bound dimer of diethyl ether is observed to decompose according to eq 8.[18] This dissociation reaction is estimated to be 31 ± 2 kcal/mol

$$[(C_2H_5)_2O]_2H^+ \rightarrow (C_2H_5)_2OH^+ + (C_2H_5)_2O \qquad (8)$$

endothermic, corresponding to absorption of at least 12 photons at the laser wavelengths used.[26] Rupture of the hydrogen bond is not expected to have an activation energy in excess of the reaction endothermicity. At laser intensities sufficient to decompose $[(C_2H_5)_2O]_2H^+$, no dissociation of $(C_2H_5)_2OH^+$ is observed and the increase in abundance of $(C_2H_5)_2OH^+$ exactly matches the decrease in abundance

of $[(C_2H_5)_2O]_2H^+$, verifying eq 8 as the only decomposition pathway.

A typical experiment monitoring $[(C_2H_5)_2O]_2H^+$ is shown in Figure 6. Ions are produced by a 10 msec electron beam pulse and stored for up to 2 sec. At 1 sec of trapping time the remaining $(C_2H_5)_2OH^+$ is ejected by ICR double resonance in a time short compared with the time between collisions, thus preventing further formation of the dimer, process 3. This is evidenced (Figure 6, upper trace) by the constant abundance of $[(C_2H_5)_2O]_2H^+$ after 1 sec. The laser, tuned to 944 cm^{-1}, is gated on at 1 sec of trapping time coincident with ejection of $(C_2H_5)_2OH^+$ and effects an exponential decay of the dimer (Figure 6, lower trace).

For data such as presented in Figure 6, the dissociation kinetics are characterized by an induction period followed by an exponential (first order) decay of the irradiated species. These two features are evident in Figure 7 which shows the logarithm of fractional ion abundance as a function of trapping time with laser irradiation commencing at 1.0, 1.3, 1.6, and 1.9 seconds, respectively. In all cases double resonance ejection of $(C_2H_5)_2OH^+$ commences at 1.0 sec.

The induction period is defined as the time between the shutter opening (vertical arrows in Figure 7) and first observable dissociation. The variation of induction period with laser irradiance is illustrated in Figure 8 for $[(C_2H_5)_2O]_2H^+$ at constant ether pressure. When corrected for a shutter opening time of 5 msec, the data in Figure 8 fit eq 9 closely (solid line in Figure 8), where I_{las} is the laser

FIGURE 6

Ion abundance versus trapping time for a typical multiphoton dissociation experiment. Ions are found by a 10 msec 70 eV electron beam pulse. The upper trace is the proton bound dimer signal with the laser off. Ejection of $(C_2H_5)_2OH^+$ beginning at 1 sec trapping time halts further dimer formation. CW irradiation by the infrared laser at 14 W cm^{-2} coincident with ejection of $(C_2H_5)_2OH^+$ (lower trace) results in photodissociation of the dimer.

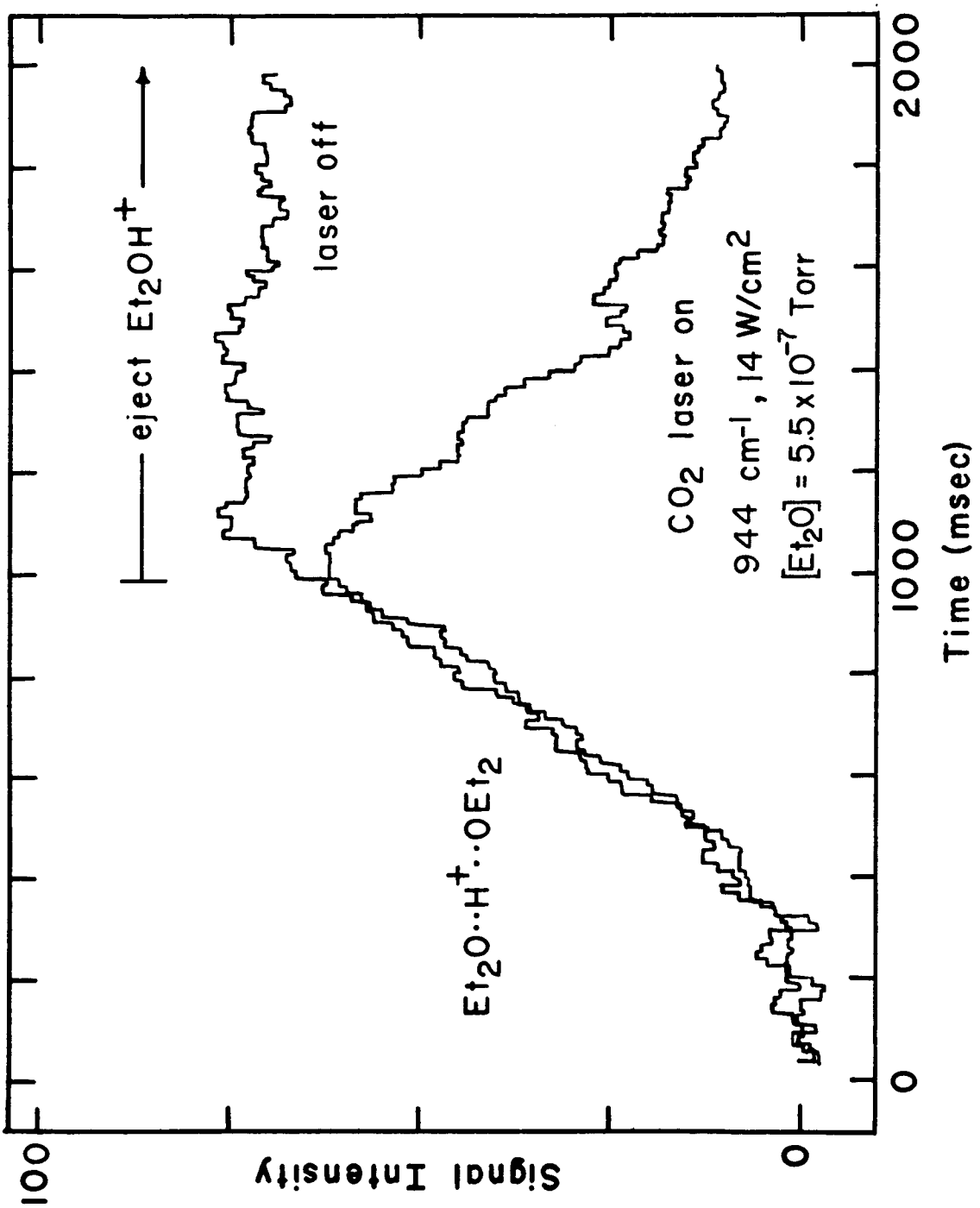
100
0
Signal Intensity
0
1000
2000
Time (msec)
eject Et_2OH^+
laser off
CO_2 laser on
944 cm^{-1}, 14 W/cm^2
$[Et_2O] = 5.5 \times 10^{-7}$ Torr
$Et_2O \cdot H^+ \cdot OEt_2$

FIGURE 7

Semilog plot of fractional ion abundance versus trapping time for multiphoton dissociation of $[(C_2H_5)_2O]_2H^+$. Data labeled A, B, C, and D are for increasing delays of 0, 300, 600, and 900 msec prior to irradiation. Double resonance ejection of $(C_2H_5)_2OH^+$ begins at 1 sec of trapping time. Ions are formed by a 10 msec 14 eV electron beam pulse.

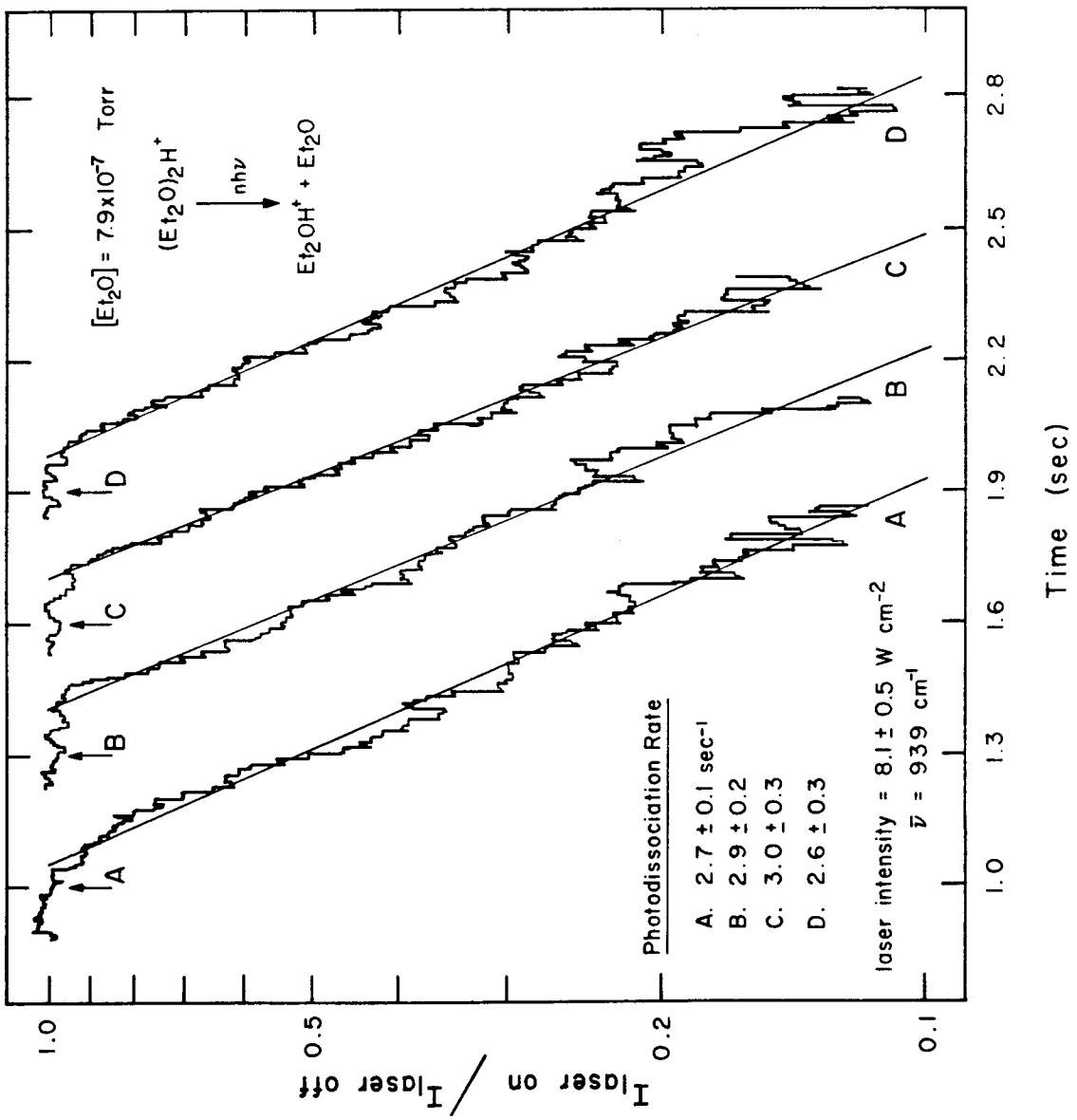
[Et2O] = 7.9x10-7 Torr
(Et2O)2H+
nhν
Et2OH+ + Et2O
A
B
C
D
Photodissociation Rate
A. 2.7 ± 0.1 sec-1
B. 2.9 ± 0.2
C. 3.0 ± 0.3
D. 2.6 ± 0.3
laser intensity = 8.1 ± 0.5 W cm-2
ν̄ = 939 cm-1
I laser on / I laser off
1.0
0.5
0.2
0.1
1.0
1.3
1.6
1.9
2.2
2.5
2.8
Time (sec)

FIGURE 8

Induction period (defined in text) for multiphoton dissociation of $[(C_2H_5)_2O]_2H^+$ as a function of laser intensity. Ions are formed by a 10 msec 14 eV electron beam pulse. The timing sequence is the same as for Figure 6. The solid line is a plot of eq 9, corrected for the 5 msec shutter opening time.

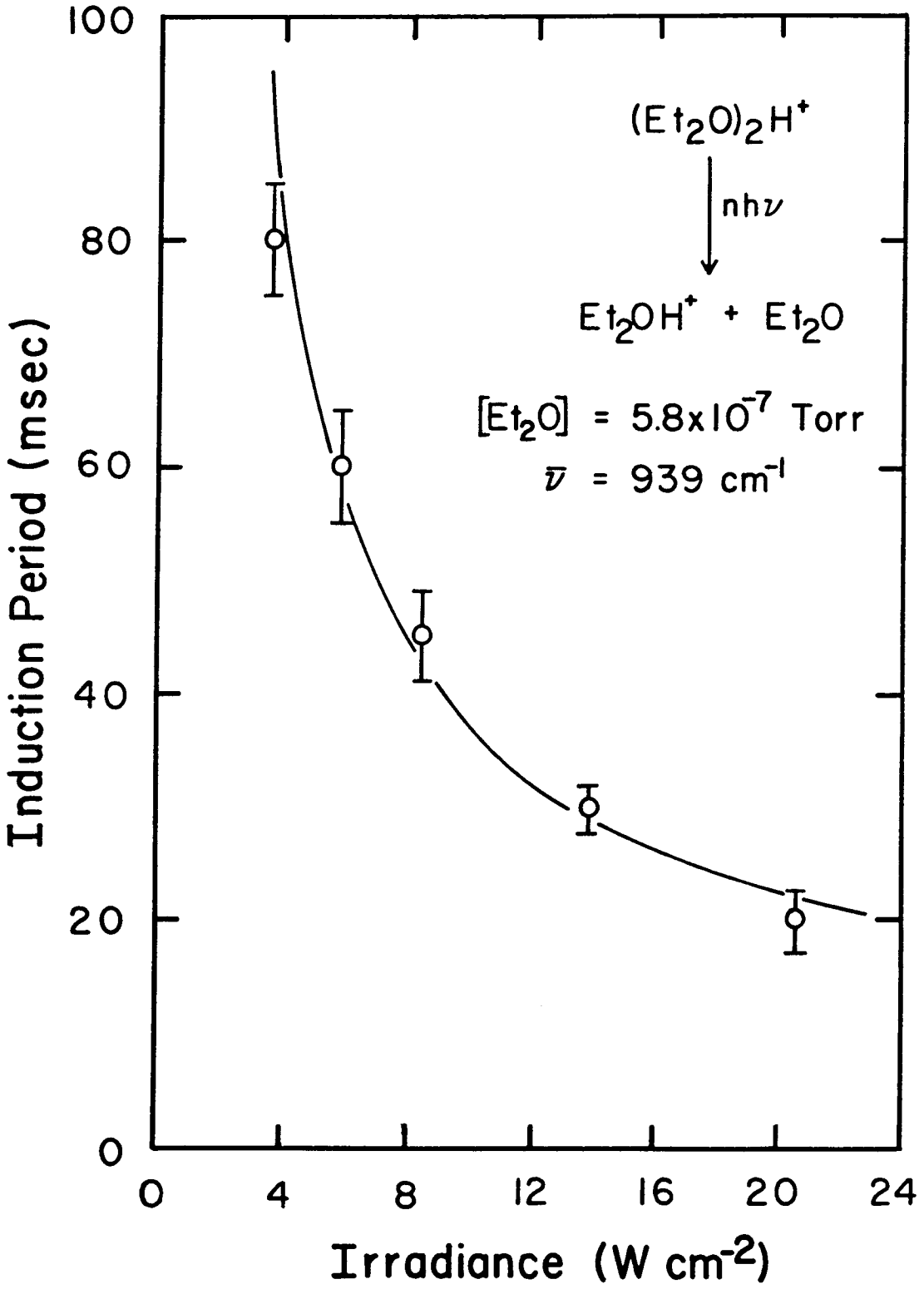
100
80
60
40
20
0
0
4
8
12
16
20
24
Induction Period (msec)
Irradiance (W cm^{-2})
$(Et_2O)_2H^+$
$nh\nu$
$Et_2OH^+ + Et_2O$
$[Et_2O] = 5.8 \times 10^{-7}$ Torr
$\bar{\nu} = 939$ cm^{-1}

$$(\text{Induction period}) \times I_{las} = 0.3 \text{ J cm}^{-2} \quad (9)$$

irradiance in W cm^{-2}. Eq 9 indicates an energy fluence threshold of 0.3 J cm^{-2} for the observed multiphoton dissociation.

Collisional effects both prior to and during irradiation have been studied in the decomposition of $[(C_2H_5)_2O]_2H^+$. Data in Figure 9 show photodissociation rate constants decrease with increasing pressure at constant laser intensity, which is the expected effect of collisional deactivation processes. In addition to diethyl ether, results obtained by adding the buffer gases SF_6 and i-C_4H_{10} to a small amount (3.7×10^{-7} Torr) of $(C_2H_5)_2O$ are included in Figure 9. To allow direct comparison of deactivation efficiencies of the three gases, dissociation rates are plotted as a function of ion-molecule collision frequency.[27] In diethyl ether alone collision rates 10 times the dissociation rate reduce the latter by roughly a factor of two. For a comparable reduction in dissociation rate, collisions with isobutane and SF_6 are, respectively, $1\frac{1}{2}$ and $2\frac{1}{2}$ times as effective as diethyl ether. Thus vibrationally excited ions are quenched by encounters with buffer gas molecules, probably through intermolecular V–V transfer. In the special case where diethyl ether is used as the collision partner, symmetric ether exchange with the proton bound dimer (eq 7) is too slow to account for the observed deactivation efficiency. As mentioned previously, only one collision out of 200 results in ether exchange. It is possible to obtain information regarding the collision free photodissociation of $[(C_2H_5)_2O]_2H^+$ by extrapolating the data to a low pressure limit. Here the low pressure limit is defined by requiring the time between collisions to be

FIGURE 9

$[(C_2H_5)_2O]_2H^+$ multiphoton dissociation rate as a function of added buffer gases $(C_2H_5)_2O$, SF_6, and $\underline{i}$-C_4H_{10}. Dissociation rate is plotted as a function of total collision rate[27] [$(C_2H_5)_2O$ plus buffer gas] to allow direct comparison of collision efficiencies. SF_6 and $\underline{i}$-C_4H_{10} are added to 3.7×10^{-7} Torr of diethyl ether. Ionization energy is 14 eV.

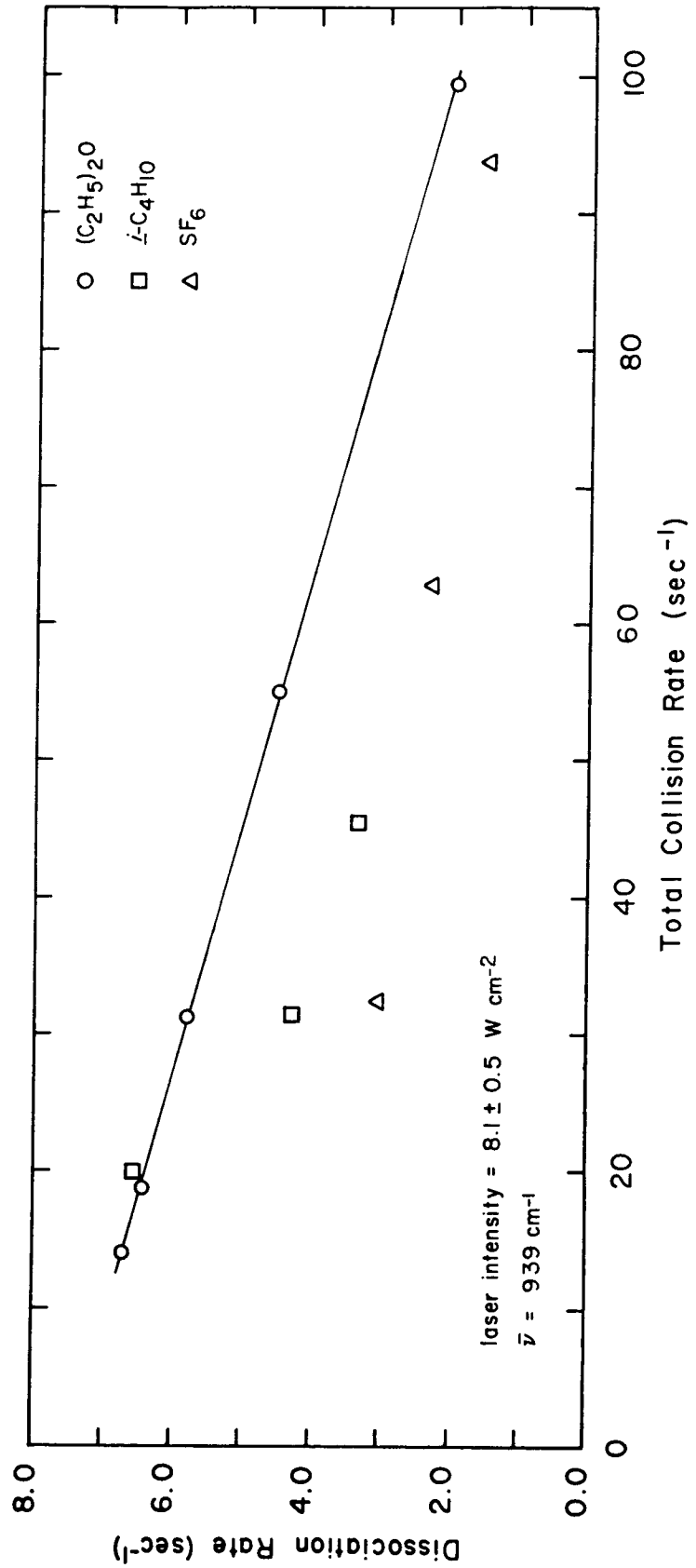
Dissociation Rate (sec^{-1})
Total Collision Rate (sec^{-1})
$(C_2H_5)_2O$
i-C_4H_{10}
SF_6
laser intensity = 8.1 ± 0.5 W cm^{-2}
$\bar{\nu}$ = 939 cm^{-1}
0.0
2.0
4.0
6.0
8.0
0
20
40
60
80
100

long compared with the time for excitation and dissociation of an irradiated ion. The latter is the induction period at the particular laser intensity used. Data, such as shown in Figure 9, were obtained at four different laser powers (1 to 4 W cm^{-2}). A low pressure dissociation rate was obtained for each laser power. Figure 10 shows the logarithm of the low pressure rates as a function of the logarithm of irradiance. Within experimental error the points lie on a straight line of unit slope, implying $[(C_2H_5)_2O]_2H^+$ photodissociation rate is first order in photon flux. At the low pressure limit, eq 10

$$k = \sigma_D \Phi \tag{10}$$

relates the dissociation rate k to a phenomenologically defined cross section, σ_D, and photon flux Φ. The measured cross section is $\sigma_D = 2.0 \pm 0.5 \times 10^{-20}$ cm^2.

Since formation of $[(C_2H_5)_2O]_2H^+$ is bimolecular (eq 3) and exothermic the proton bound dimer may contain up to 31 kcal/mol of internal energy prior to laser photolysis. To probe the effects of vibrational excitation preceding photolyses, an experiment similar to the one depicted in Figure 6 was carried out, modified such that the irradiation was delayed following onset of $(C_2H_5)_2OH^+$ ejection for up to 900 msec. Some of the results from this experiment are presented in Figure 7. Within experimental error, the four multi-photon dissociation rates are identical as are the observed induction periods. For all buffer gas [$(C_2H_5)_2O$, SF_6, and $\underline{i}$-C_4H_{10}] pressures up to 4×10^{-6} Torr no change in $[(C_2H_5)_2O]_2H^+$ induction period or photodissociation rate is observed with increasing laser delay. The

FIGURE 10

Log-log plot indicating the dependence of $[(C_2H_5)_2O]_2H^+$ low pressure photodissociation rate on the first power of laser intensity.

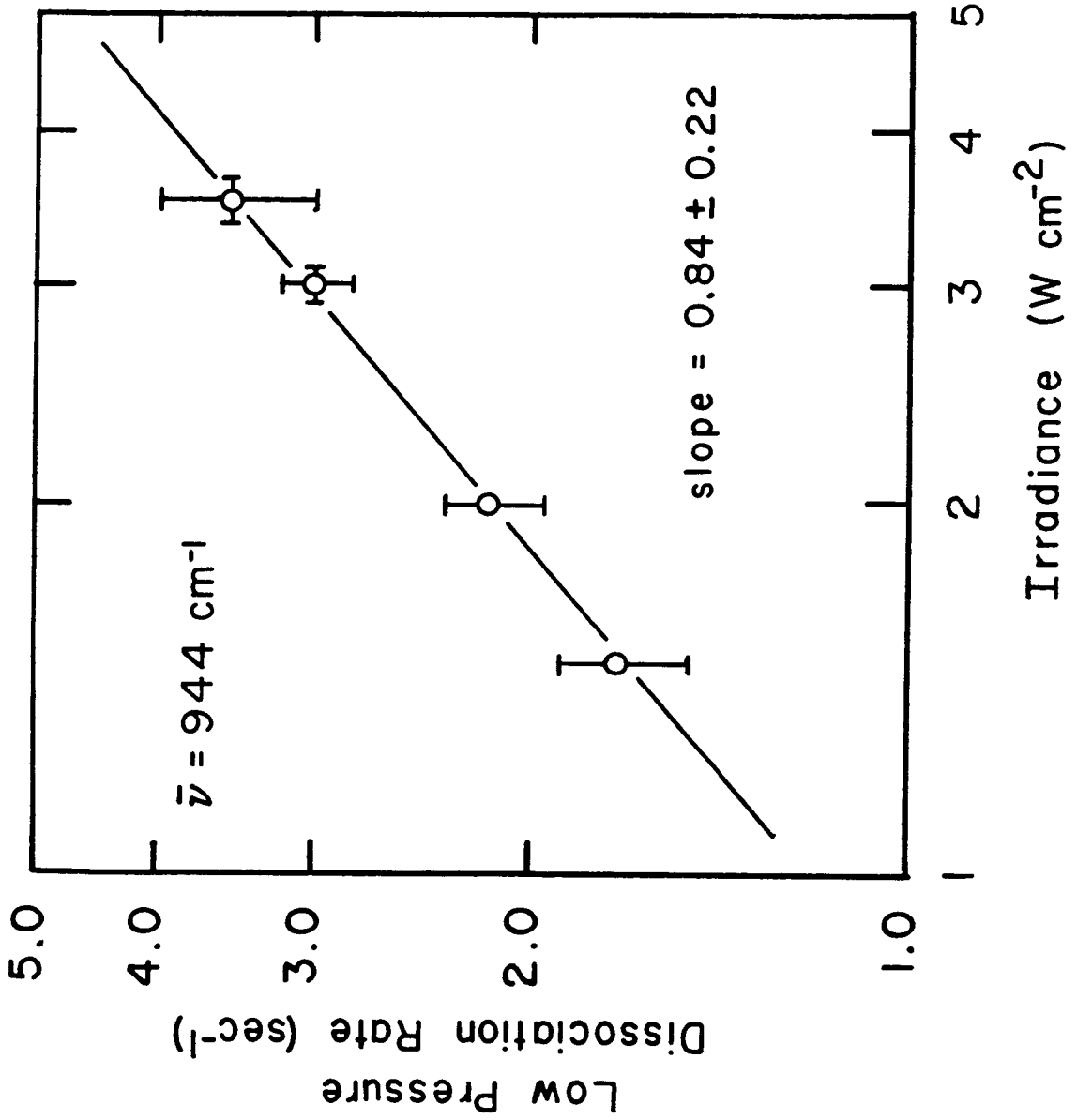
Low Pressure
Dissociation Rate (sec⁻¹)
5.0
4.0
3.0
2.0
1.0
1
2
3
4
5
Irradiance (W cm⁻²)
ν̄ = 944 cm⁻¹
slope = 0.84 ± 0.22

anticipated effect of vibrational excitation in ions prior to irradiation is an enhanced dissociation rate once irradiation commences. Collisions prior to excitation have no effect on $[(C_2H_5)_2O]_2H^+$ dissociation rates, (Figure 7), in contrast to the effect of collisions during irradiation (Figure 9) which inhibit excitation. The invariance of dissociation rate with delay of excitation indicates that $[(C_2H_5)_2O]_2H^+$ ions are vibrationally relaxed after only several collisions.

The ability to photodissociate the entire $[(C_2H_5)_2O]_2H^+$ population (Figure 6) at even the lowest pressures (corresponding to ~ 10 collisions sec^{-1}) implies that all ions absorb energy over the entire band.[28] This homogeneous behavior may be the result of multiple overlapping vibrational transitions (section 4) or broadening due to rapid intramolecular V–V transfer.[4]

C. Infrared Laser Photochemistry of $(C_2H_5)_2OH^+$, $(C_2D_5)_2OD^+$ and $(C_2H_5)(C_2D_5)OH^+$. At low pressures where proton bound dimer formation is not significant multiphoton dissociation of the protonated ether can be studied. The laser induced process and postulated four center intermediate[29] are shown in eq 11.[30] Both direct observation

$$(C_2H_5)_2OH^+ + nh\nu \rightarrow \left[C_2H_5\text{–}\overset{H}{\overset{\vdots}{O^+}}\cdots\overset{\vdots}{\underset{\vdots}{H}}\cdots\overset{:}{\underset{:}{CH_2}} \right]^* \longrightarrow C_2H_5OH_2^+ + C_2H_4 \qquad \Delta H = 27 \text{ kcal/mol} \qquad (11)$$

of $C_2H_5OH_2^+$ formation and ICR double resonance confirm (11) as the reaction pathway. By analogy with similar β-hydrogen transfer processes the activation energy for reaction 11 is expected to be

no more than ~2 kcal/mol in excess of the reaction endothermicity.[31] While a less endothermic decomposition route exists,[32] process 12,

$$(C_2H_5)_2OH^+ + nh\nu \rightarrow CH_3CHOH^+ + C_2H_6 \quad \Delta H = 15 \text{ kcal/mol} \qquad (12)$$

infrared laser photolyses of $(C_2H_5)_2OH^+$ yields exclusively $C_2H_5OH_2^+$. This is consistent with decomposition of vibrationally excited $(C_2H_5)_2OH^+$ formed via exothermic proton transfer (reaction 2) which produces only $C_2H_5OH_2^+$.[22] Thus the activation energy for α-hydrogen transfer to carbon (process 12) must be larger than for β-hydrogen transfer to oxygen (process 11).

Consistent with the results of infrared laser photolyses of $[(C_2H_5)_2O]_2H^+$, photodissociation of $(C_2H_5)_2OH^+$ exhibits an induction period between the start of laser irradiation and the onset of decomposition. Analysis similar to that for $[(C_2H_5)_2]_2H^+$ (eq 9) indicates that the energy fluence threshold for decomposition of $(C_2H_5)_2OH^+$ is approximately 2 J cm^{-2}. The cross section for photodissociation is estimated to be $\sigma_D \cong 1 \times 10^{-21}$ cm^2.

Ions derived from electron impact ionization of $(C_2H_5)_2O$ undergo the identical reactions as do the corresponding unlabeled species. However, with the partially deuterated ether, $C_2H_5OC_2D_5$, an interesting isotope effect is observed in the decomposition of the protonated molecular ion. Chemical ionization of $C_2D_5OC_2H_5$ at low (12 eV) electron energies using cyclohexane as protonating agent allows for selective formation of $(C_2H_5)(C_2D_5)OH^+$ with only trace amounts of $(C_2H_5)(C_2D_5)OD^+$. By analogy with eq 11 there are two

possible product ions from the decomposition of $(C_2H_5)(C_2D_5)OH^+$, eq 13. Yet during laser irradiation, $C_2D_5OH_2^+$ is the only product

$$(C_2H_5)(C_2D_5)OH^+ + nh\nu \begin{cases} \longrightarrow C_2D_5OH_2^+ + C_2H_4 & (13a) \\ \longrightarrow C_2H_5OHD^+ + C_2D_4 & (13b) \end{cases}$$

detected, process 13a. Thus β-hydrogen transfer in the four center intermediate is more facile than β-deuterium transfer. Consideration of ion detection limits in this experiment provides a lower limit for the combined primary and secondary isotope effects (defined as the ratio of rates of product ion formation) as ≥ 6. In comparison, when $(C_2H_5)(C_2D_5)OH^+$ is formed by highly exothermic proton transfer such that the protonated ether internal energy greatly exceeds the decomposition threshold, the observed isotope effect is ~ 2.[33] These results suggest that multiphoton dissociation occurs at an energy only slightly in excess of thermodynamic threshold. Large primary isotope effects have also been reported for metastable ion decompositions at threshold energies.[34] Thus the excitation rate must be slow compared to the unimolecular decomposition rate.

The relatively slow time scale for low intensity infrared laser excitation implies that standard statistical treatments of unimolecular reactions[6] can be utilized to describe the decomposition of multiphoton excited ions. RRKM calculations on $(C_2H_5)(C_2D_5)OH^+$ decomposition indicate dissociation rates become extremely large ($> 10^3$ sec^{-1}) within several kcal/mol above decomposition threshold, in agreement with the conclusions drawn from experimental results.

Figure 11 shows the calculated isotope effect in decomposition of $(C_2H_5)(C_2D_5)OH^+$ as a function of internal energy in excess of threshold. The experimentally measured value of ≥ 6 from infrared photodissociation is consistent with decomposition close to threshold. At higher energies, the isotope effect is ~ 2, in agreement with the chemical activation experiments. For these calculations, vibrational frequencies are assumed similar to the neutral molecule with appropriate frequencies added involving proton vibration. A tight transition state is assumed, in accordance with standard treatments for four-centered transition states[6, 34, 35] (eq 11).

As each of the proton transfer reactions which produce $(C_2H_5)_2OH^+$ (eq 1) is exothermic, the protonated ether may be vibrationally excited in the absence of deactivating collisions. The distribution of internal energies is quite complex because each of the eight proton transfer reactions imparts a different amount of energy to $(C_2H_5)_2OH^+$. Changing the ionization energy alters the relative abundances of fragment ions (Figure 4) which lead to formation of $(C_2H_5)_2OH^+$ and so varies the internal energy content of the protonated ether. The results of using ionization energies of 14 and 70 eV are shown in Figure 12. Laser irradiation is continuous in this experiment. The increase in photodissociation rate with 70 eV electrons compared to 14 eV electrons, readily apparent in Figure 12, is most likely due to proton transfer reactions of greater exothermicity at 70 eV. Although symmetric proton transfer, reaction 6, represents an efficient deexcitation process, the low pressures used to study

FIGURE 11

Calculated isotope effect in decomposition of $(C_2H_5)(C_2D_5)OH^+$ as a function of internal energy in excess of decomposition threshold.

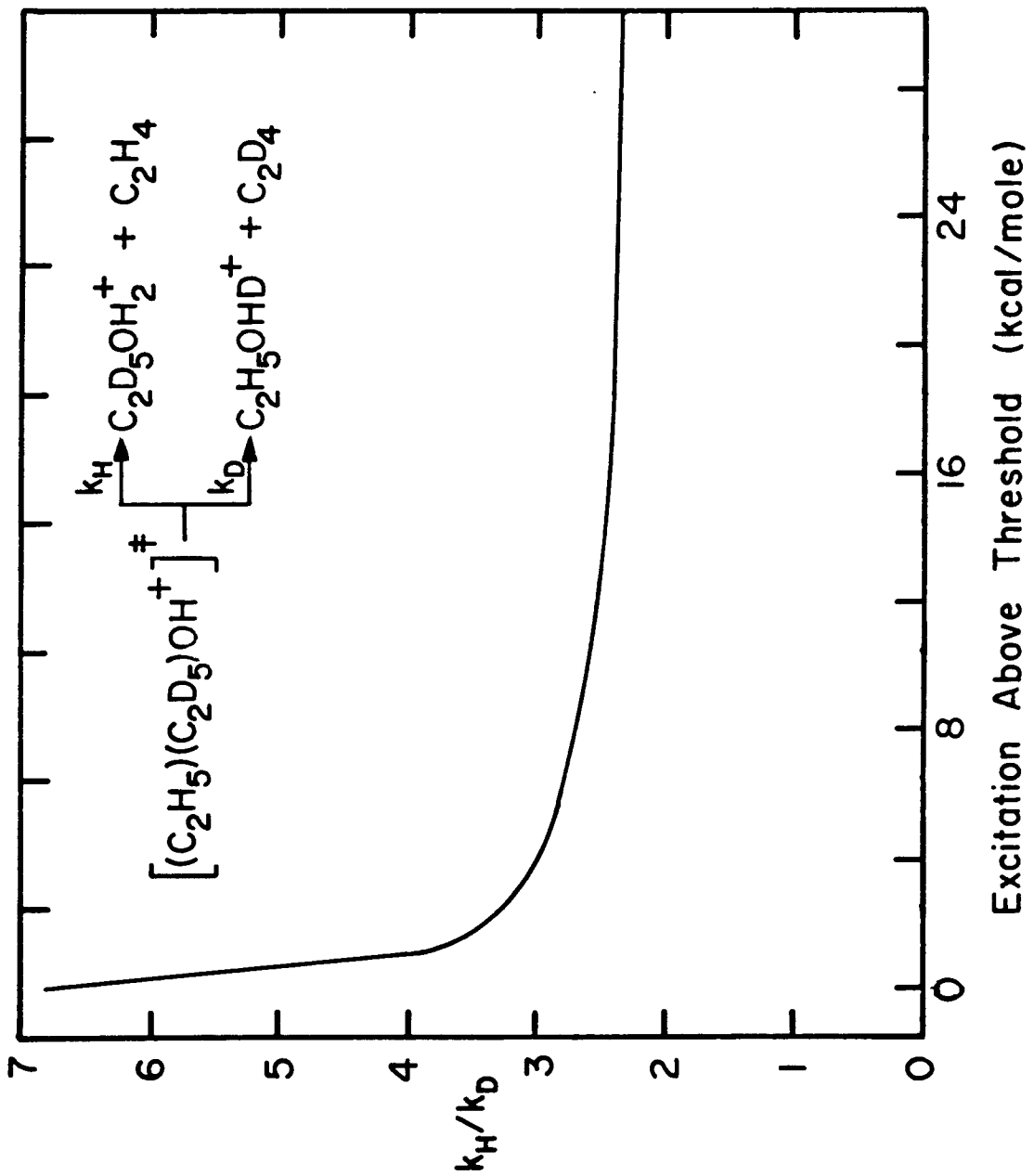
k_H/k_D
Excitation Above Threshold (kcal/mole)
0
1
2
3
4
5
6
7
0
8
16
24
$[(C_2H_5)(C_2D_5)OH^+]^\ddagger$
k_H
k_D
$C_2D_5OH_2^+ + C_2H_4$
$C_2H_5OHD^+ + C_2D_4$

FIGURE 12

Fractional ion abundance versus trapping time for multiphoton dissociation of $(C_2H_5)_2OH^+$. Data are shown for laser off conditions, and laser on conditions where the ionization energy is 14 eV and 70 eV. The laser off curve is the same for both 14 and 70 eV ionization energies. Laser irradiation is continuous beginning at t = 0 sec.

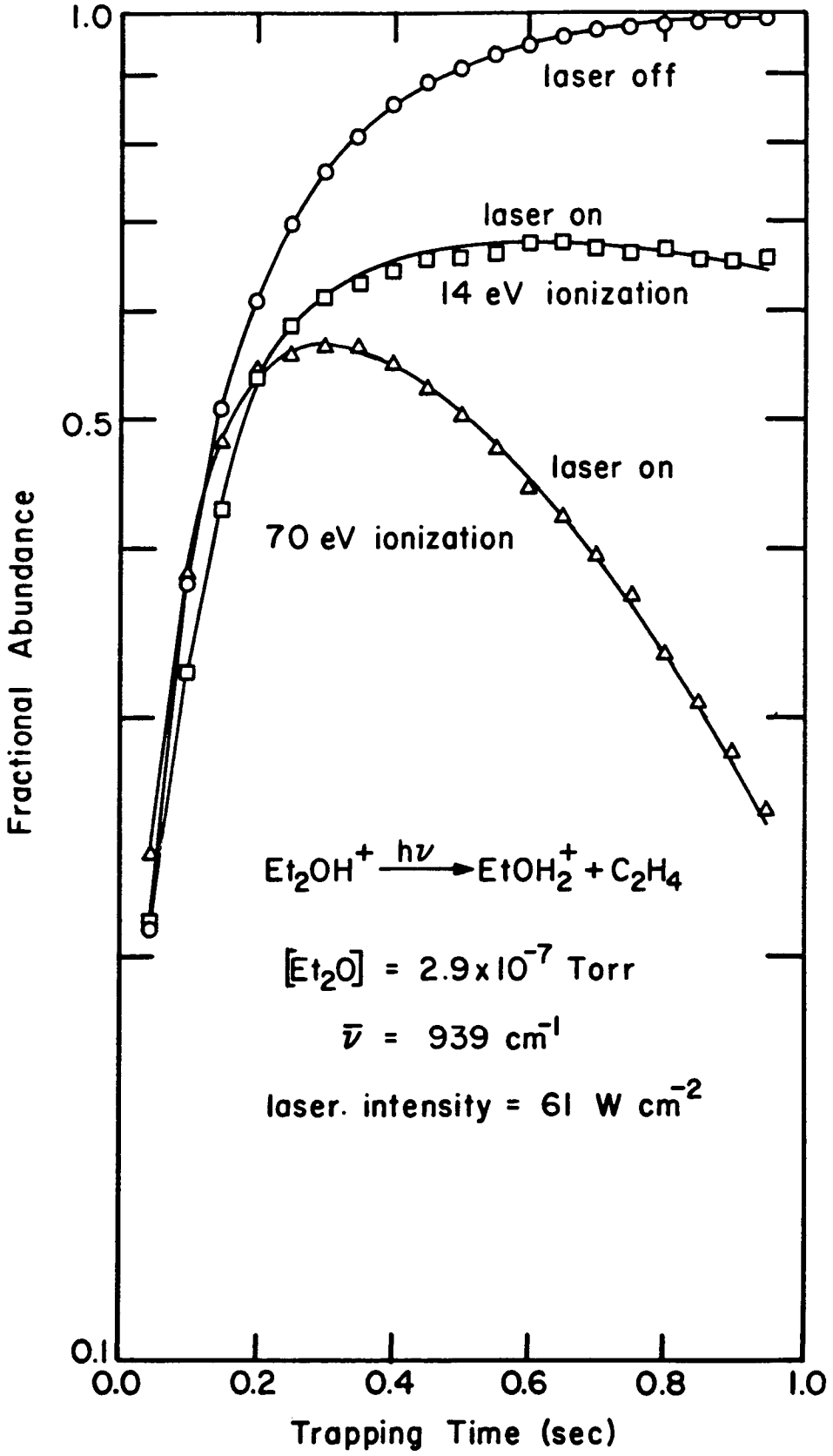
1.0
0.5
0.1
Fractional Abundance
laser off
laser on
14 eV ionization
laser on
70 eV ionization
$Et_2OH^+ \xrightarrow{h\nu} EtOH_2^+ + C_2H_4$
$[Et_2O] = 2.9 \times 10^{-7}$ Torr
$\bar{\nu} = 939\ cm^{-1}$
laser. intensity = 61 W cm^{-2}
0.0
0.2
0.4
0.6
0.8
1.0
Trapping Time (sec)

$(C_2H_5)_2OH^+$ limit the total ion-molecule collision rate to less than 15 sec^{-1}.[27] Low diethyl ether pressure is necessary to minimize proton bound dimer formation. Thus vibrationally excited ions are sufficiently long-lived to be observed in the multiphoton dissociation process, Figure 12. Quantitative determination of the effects of prior vibrational excitation on $(C_2H_5)_2OH^+$ decomposition were not pursued due to complications caused by the presence of a multitude of proton transfer reactions forming $(C_2H_5)_2OH^+$, and the necessity of accounting for $(C_2H_5)_2OH^+$ formation during irradiation (Figure 12).

D. Infrared Laser Photochemistry of $CH_3CHOC_2H_5^+$, $C_2H_5OH_2^+$ and CH_3CHOH^+. Photodissociation of $CH_3CHOC_2H_5^+$ is observed at laser intensities similar to those required for dissociation of $(C_2H_5)_2OH^+$.[18] ICR double resonance confirms process 14 as the only decomposition pathway,[30] which is also the decomposition of lowest endothermicity.

$$CH_3CHOC_2H_5^+ + nh\nu \rightarrow CH_3CHOH^+ + C_2H_4 \qquad \Delta H = 34 \text{ kcal/mol} \qquad (14)$$

σ_D estimated for this process is $\sim 4 \times 10^{-22}$ cm^2. Since reaction 14 involves β-hydrogen transfer in a four-center intermediate similar to process 11, the activation energy is again assumed to be less than $\sim$ 2 kcal/mol in excess of the reaction endothermicity.

Higher laser intensities than those required for photodissociation of $(C_2H_5)_2OH^+$ or $CH_3CHOC_2H_5^+$ result in decomposition of $C_2H_5OH_2^+$. Of the low enthalpy dissociation pathways available,[30] reaction 15, the observed process with laser irradiation and confirmed

$$C_2H_5OH_2^+ + nh\nu \begin{cases} \longrightarrow H_3O^+ + C_2H_4 & \Delta H = 27 \text{ kcal/mol} \quad (15a) \\ \longrightarrow CH_3CHOH^+ + H_2 & \Delta H = 21 \text{ kcal/mol} \quad (15b) \end{cases}$$

by double resonance, is reaction 15a. This result is consistent with results from decomposition of chemically activated $C_2H_5OH_2^+$.[36] While reaction 15b has a lower ΔH, chemical ionization studies of protonated methanol decomposition indicate a barrier of approximately 1 eV in excess of the reaction endothermicity for hydrogen elimination, and no activation energy above the endothermicity for loss of H_3O^+.[36] The observed laser induced photodissociation process is thus the decomposition of lowest activation energy.[37] σ_D for infrared multiphoton dissociation of $C_2H_5OH_2^+$ is $\sim 1 \times 10^{-22}$ cm^2. No dissociation of CH_3CHOH^+ is observed with infrared laser radiation in the 900-1100 cm^{-1} region.

E. Photodissociation Spectra. For all systems studied the photodissociation products are invariant to change in laser wavelength. The wavelength dependences for multiphoton dissociation of $(C_2H_5)_2OH^+$ and $[(C_2H_5)_2O]_2H^+$ are shown in Figure 13a and data for $(C_2D_5)_2OD^+$ are shown in Figure 13b. Also shown are the gas phase absorption spectra of the corresponding neutrals over the range of CO_2 laser wavelengths (note the change of scale in the axes for percent transmission). P_D is defined as the fractional dissociation yield for a particular irradiation time and laser intensity. For both $(C_2H_5)_2OH^+$ and $(C_2D_5)_2OD^+$ experimental conditions are nearly identical; therefore, differences in P_D values for the monomer species are a direct measure of differences in cross sections for multiphoton dissociation

FIGURE 13

(a) Photodissociation spectra of $(C_2H_5)_2OH^+$ and $[(C_2H_5)_2O]_2H^+$ over the CO_2 laser spectral range. For $(C_2H_5)_2OH^+$, P_D is the fraction of ions dissociated after 1. 9 seconds of irradiation at 48 W cm^{-2}; $(C_2H_5)_2O$ pressure is 8.8×10^{-8} Torr. P_D for $[(C_2H_5)_2O]_2H^+$ is defined as the fraction of ions dissociated after 2. 0 seconds of irradiation at 10 W cm^{-2}; $(C_2H_5)_2O$ pressure is 4.7×10^{-7} Torr. Ionization energy for both experiments is 14 eV. Dotted line is the infrared absorption spectrum of diethyl ether at 20 Torr.

(b) Photodissociation spectrum of $(C_2D_5)_2OD^+$ over the CO_2 laser spectral range. Experimental conditions are the same as for photodissociation of $(C_2H_5)_2OH^+$ in (a). Dotted line is the infrared absorption spectrum of $(C_2D_5)_2O$ at 16 Torr.

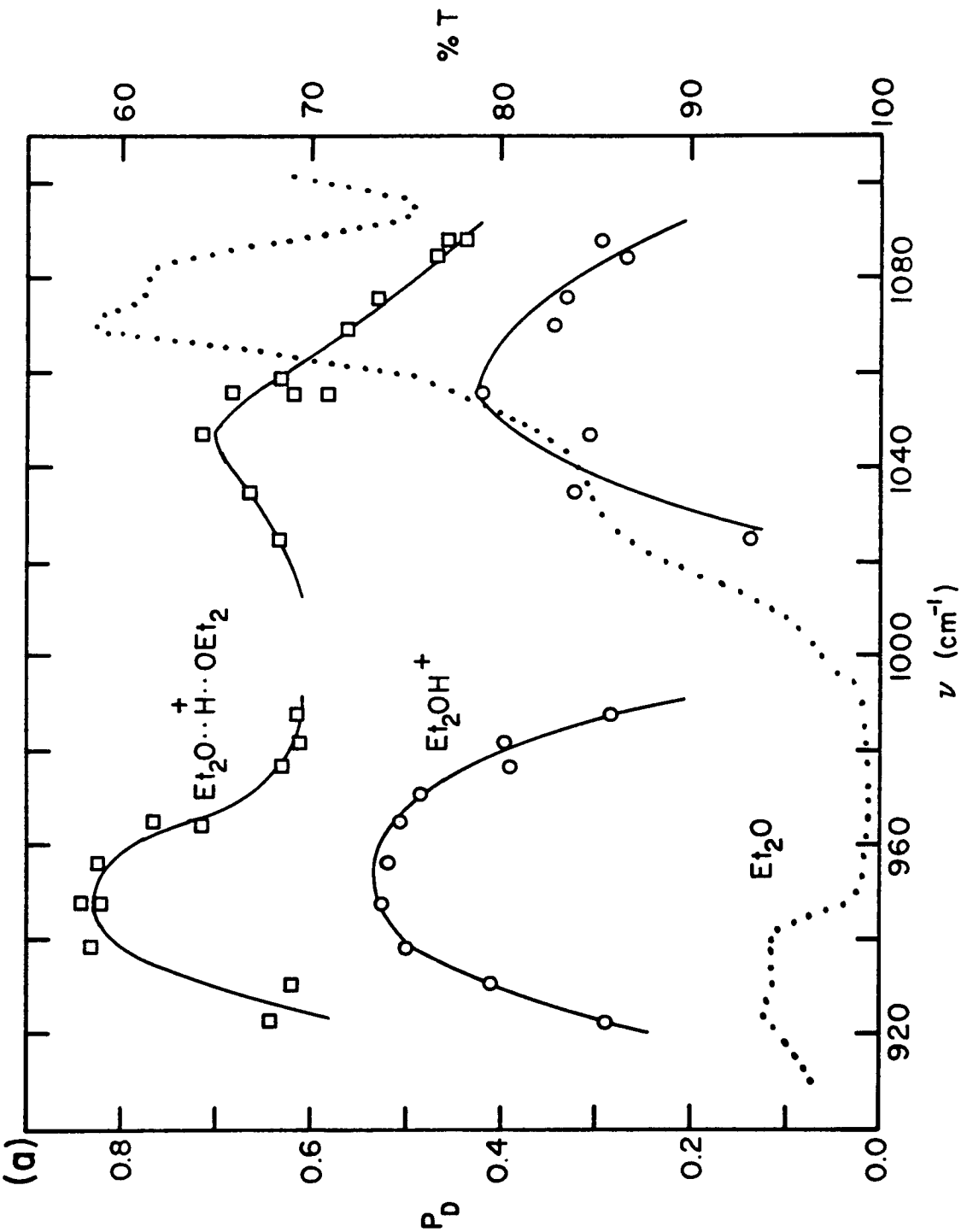
(a)
$Et_2O\cdots H^+\cdots OEt_2$
Et_2OH^+
Et_2O
P_D
% T
ν (cm^{-1})
0.0
0.2
0.4
0.6
0.8
60
70
80
90
100
920
960
1000
1040
1080

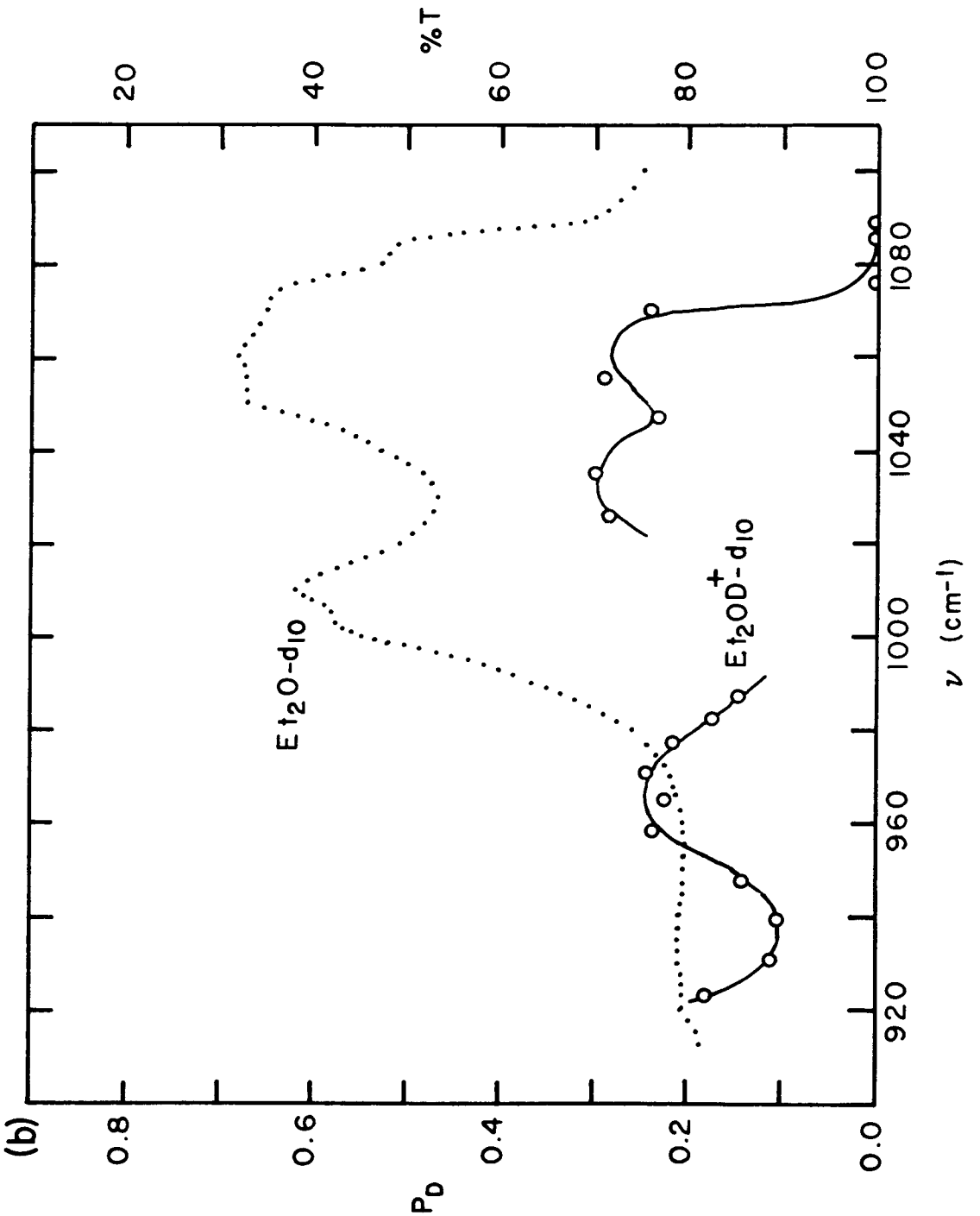
(b)
P_D
%T
ν (cm^{-1})
Et_2O-d_{10}
Et_2OD^+-d_{10}

at each wavelength. No such direct comparison regarding dissociation cross sections can be made between the protonated ether and the proton bound dimer owing to differences in laser intensity and ether pressure for the two experiments.

Analysis of the infrared photodissociation spectra (Figures 13 a, b) rests on the assumption that multiphoton dissociation spectra somewhat mimic small signal absorption spectra, as is observed in infrared laser photolyses of neutrals.[3, 10, 11] Observed bands in the infrared spectrum of diethyl ether from 900-1100 cm^{-1} are assigned to combinations of C–C stretches, C–O stretches, and methylene wags.[25] Protonation of the ether should not significantly affect the C–C stretch and methylene wag frequencies. It is seen in Figure 13a that the $(C_2H_5)_2OH^+$ photodissociation spectrum exhibits local maxima at roughly the same wavelengths as the diethyl ether absorption spectrum. Vibrational frequencies of protonated ether and the proton bound dimer are expected to be similar with the exception of low frequency skeletal torsions, and vibrations associated with proton motion. Neither of these special cases is expected to involve vibration in the 900-1100 cm^{-1} region excited in photodissociation experiments. Thus the photodissociation spectra of $(C_2H_5)_2OH^+$ and $[(C_2H_5)_2O]_2H^+$ show nearly identical maxima.

Theoretical Implications

While it is tempting to apply current theories for megawatt pulsed laser multiphoton dissociation[3, 5, 7, 38a-i] to low intensity infrared photolyses of gas phase ions, there are

inherent differences between the two types of experiments which necessitate modification of the existing developed theories. In particular, the time scale of the ICR experiments requires consideration of spontaneous emission (typically 1-100 sec^{-1}[39]) as a viable deactivation mechanism. Equally important, the low laser intensities obviate power broadening[40] as a mechanism for overcoming anharmonicities in hot band absorptions.

Several authors point out that at high levels of internal excitation vibrational state densities become large, guaranteeing the availability of at least one vibrational state within the laser bandwidth.[3] This defines the quasi-continuum of vibrational states. Theories of excitation through the quasi-continuum treat the process as a sequence of incoherent single photon absorptions.[5, 7, 8, 14, 38c] Model calculations[5] of sequential absorption through the quasi-continuum using cross sections obtained from photoacoustic spectra[7] agree well with pulsed laser multiphoton dissociation yields.

If absorption through the quasi-continuum is facile due to the availability of resonant transitions, then the ability to photodissociate a molecule with low intensity radiation depends on the ease of populating the quasi-continuum. Molecules in which the quasi-continuum is attained by absorption of a single photon are expected to photodissociate most readily, while molecules requiring absorption of two or more photons should, in the absence of power broadening, be much more difficult to photodissociate. Molecules possessing many degrees of freedom will have a significant amount of internal energy at ambient temperature.[28] The combination of

many vibrational modes and appreciable thermal energy content serves to locate such molecules very nearly in the quasi-continuum prior to laser excitation. Although not all vibrational frequencies of $[(C_2H_5)_2O]_2H^+$ and $(C_2H_5)_2OH^+$ are known, approximating the frequencies with those reported for diethyl ether[25] permits an estimate of the density of vibrational states in the ions. Using the well-known Whitten-Rabinovitch approximation,[6] the densities of states in $[(C_2H_5)_2O]_2H^+$ at energies corresponding to absorption of one and two infrared photons (1000 cm^{-1}) are 120 states/cm^{-1} and 9×10^4 states/cm^{-1}, respectively. The cw CO_2 laser bandwidth of ~ 0.001 cm^{-1} implies that for the proton bound dimer, the quasi-continuum is accessible following resonant absorption of a single infrared photon. In comparison, the estimated densities of states in $(C_2H_5)_2OH^+$ corresponding to absorption of one and two infrared photons are 2 states/cm^{-1} and 94 states/cm^{-1}. For the protonated ether, the quasi-continuum is not reached until the absorption of four infrared photons (density of states $\cong 2.32 \times 10^4$ states/cm^{-1}) occurs. These arguments concerning the densities of states in the ions explain why multiphoton dissociation of $[(C_2H_5)_2O]_2H^+$ is facile while decomposition of the $(C_2H_5)_2OH^+$ requires considerably higher laser powers. In fact, at room temperature, the proton bound dimer contains 3-4 kcal/mol in excess of the zero point energy due to thermal population of vibrational states. This energy is comparable to excitation by a single infrared photon. The availability of many overlapping vibrational transitions allows all ions to absorb over a wide range of

frequencies. Dissociation of the entire population is thus possible even under collisionless conditions.

If in fact the proton bound dimer is very nearly in the quasi-continuum prior to excitation then the same analysis used for pulsed laser model calculations[5] should apply to low intensity photolyses with allowances made for deactivation due to spontaneous emission. Applying eq 9 to megawatt powers and short pulse duration predicts induction periods commensurate with the pulsed laser model calculations mentioned above. In a complementary fashion, scaling the model calculations[5] to low laser intensities yields results very similar to experimentally observed multiphoton dissociation reactions with cw radiation. Scheme I illustrates the sequential mechanism assumed for low intensity infrared multiphoton dissociation, where both

Scheme I

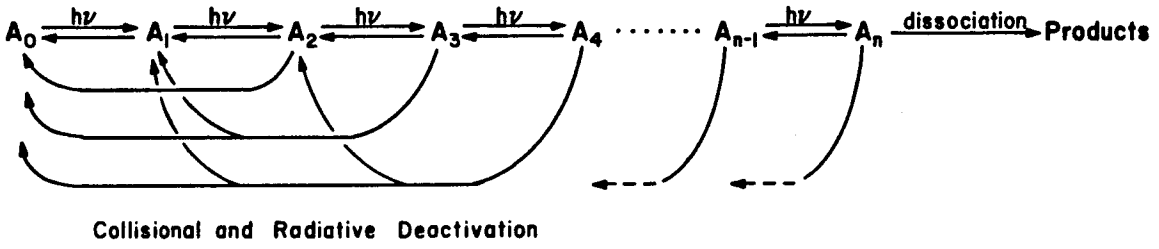

collisions and spontaneous emission are deactivation processes. Assuming absorption cross sections are similar to those derived for SF_6, preliminary model calculations following Scheme I and including only excitation processes are shown in Figure 14. The form for the absorption cross section used is given in eq 16,[7] where

FIGURE 14

Model calculations of slow multiphoton dissociation. The calculation follows Scheme I, assuming n = 12 and only excitation processes are involved. The form of the absorption cross section at each level of excitation is given by eq 16.

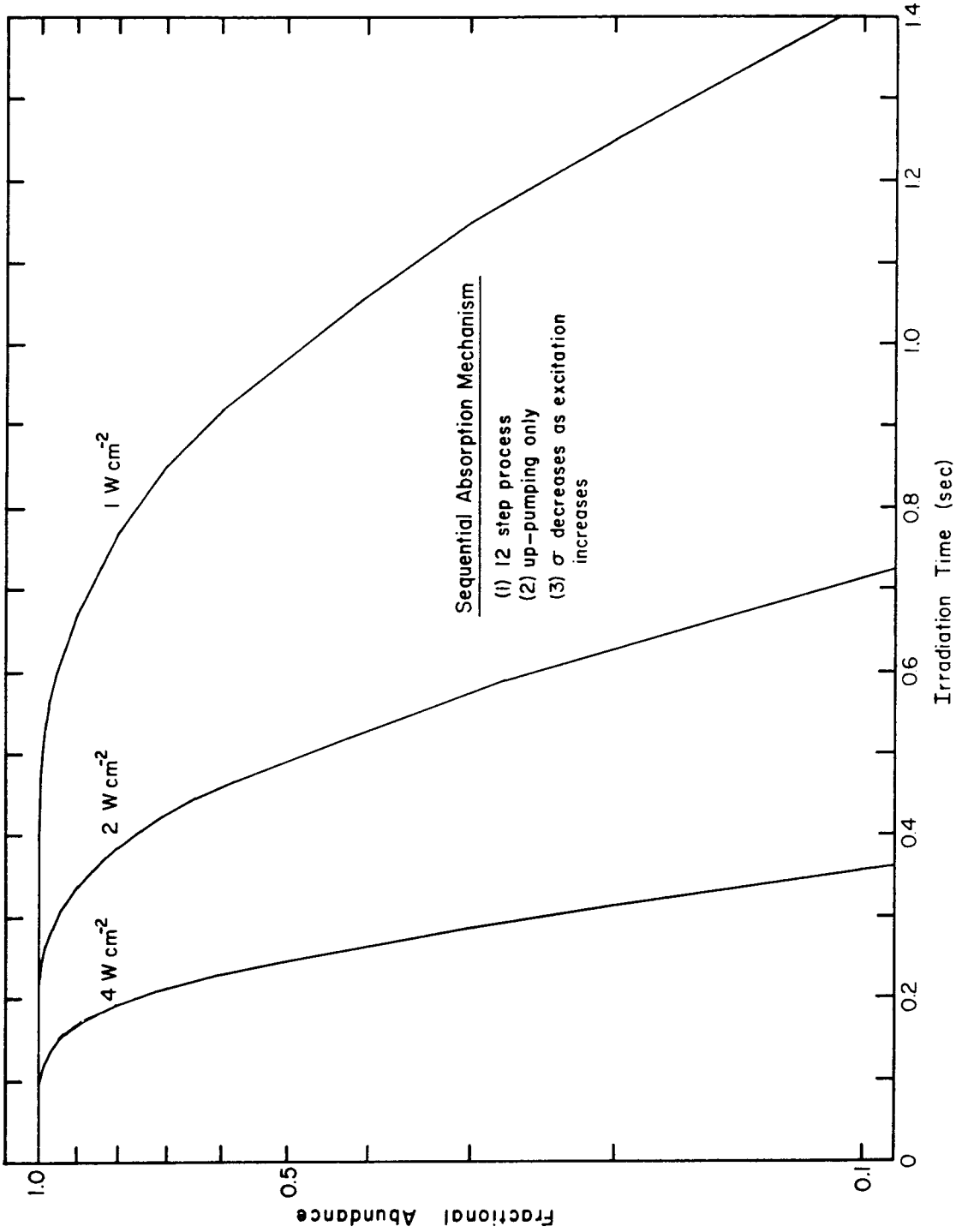
Fractional Abundance
1.0
0.5
0.1
0
0.2
0.4
0.6
0.8
1.0
1.2
1.4
Irradiation Time (sec)
4 W cm⁻²
2 W cm⁻²
1 W cm⁻²
Sequential Absorption Mechanism
(1) 12 step process
(2) up-pumping only
(3) σ decreases as excitation increases

$$\sigma(n) = \exp(-42.9 - 0.029n) \quad (16)$$

it is the number of photons absorbed. The calculation in Figure 14 assumes twelve excitation steps corresponding to the excitation required for $[(C_2H_5)_2O]_2H^+$ and that dissociation is rapid compared to excitation above threshold. Calculation of decomposition rates near threshold indicates rates which are rapid compared to the excitation rates ($< 50\ s^{-1}$) used in the model. It is apparent from Figure 14 that even though the calculation uses data for SF_6 and includes only excitation, both the induction period and decomposition rates agree qualitatively with experimental data, Figure 7. However, the calculated induction periods are considerably longer than those experimentally observed and the calculated lines show more curvature than the experimental graphs. The preliminary calculation serves to illustrate the utility of the model and inclusion of more realistic cross sections in addition to deactivation processes should allow reasonable modeling of the low intensity photolyses.

Conclusions

The large temporal and spatial inhomogeneities of the laser field inherent in pulsed laser studies of multiphoton dissociation are avoided by the use of low intensity unfocused cw radiation. In many respects the present results are similar to pulsed laser experiments. In all cases studied, low intensity multiphoton dissociation proceeds via the lowest energy pathway, as seen in pulsed laser experiments. However, in low intensity photolyses dissociation appears to be very

nearly at threshold, unlike multiphoton dissociation using pulsed lasers in which excitation may be substantially above threshold because of the much faster excitation rates. Unlike high power pulsed laser photodissociation, no appreciable shift to lower energies in the photodissociation spectrum is found with low intensity excitation. This is likely due to the inherently different nature of initial excitation in the two processes. Whereas pulsed laser experiments rely on power broadening to coherently absorb 3-5 photons in a single mode (and hence exhibit a spectral shift to lower energy because of anharmonicity effects) the low intensity excitation precludes power broadening and the photodissociation spectrum is expected to be similar to the ground state spectrum. Isotopic substitution resulting in shifts of bands in absorption spectra is expected to allow isotopic selectivity in slow multiphoton dissociation. In the case of $[(C_2H_5)_2O]_2H^+$ a single resonant absorption may populate the vibrational quasi-continuum. However, the mechanism for excitation to the quasi-continuum in $(C_2H_5)_2OH^+$, $CH_3CHOC_2H_5^+$, and $C_2H_5OH_2^+$ is not obvious. In agreement with pulsed laser experiments, low intensity multiphoton dissociation yields are proportional to energy fluence and an energy fluence threshold is observed. The magnitudes of the energy fluence threshold and photodissociation cross section for $[(C_2H_5)_2O]_2H^+$ measured in the low intensity experiment (0.3 J cm^{-2} and 2×10^{-20} cm^2, respectively) are similar in magnitude to those measured for SF_6 in pulsed laser experiments (1.4 J cm^{-2}[14] and 1.5×10^{-20} cm^2,[8] respectively). For ions derived from diethyl ether

the effect of collisions during low intensity irradiation is only to deactivate excited species, as observed in high intensity pulsed experiments.

There are many possible extensions and applications of the present work. Collisional and radiative relaxation mechanisms can be probed in great detail by observing their effect on multiphoton dissociation. Low intensity multiphoton dissociation provides a convenient method for obtaining hitherto unknown vibrational spectra of gas phase ions. The availability of CO, hydrogen halide, optically pumped far infrared lasers, F-center lasers and optically pumped parametric oscillators will extend the spectral range beyond the 9-11 μm region. Photodissociation spectra should allow differentiation among structural isomers of ions.

Acknowledgment. This work was supported in part by the United States Department of Energy and the President's Fund of the California Institute of Technology.

References and Notes

(1) NSF Pre-Doctoral Fellow, 1976-1979.

(2) Present address: Exxon Research and Engineering Company, Corporate Research Laboratories, Linden, New Jersey 07036.

(3) R. V. Ambartzumian and V. S. Letokhov, in "Chemical and Biochemical Applications of Lasers," C. Bradley Moore, ed., Vol. III, Academic Press, New York, N. Y., 1977, and references contained therein.

(4) H. S. Kwok and E. Yablonovitch, Phys. Rev. Lett., 41, 745 (1978); D. S. Frankel, Jr. and T. J. Manuccia, Chem. Phys. Lett., 54, 451 (1978).

(5) E. R. Grant, P. A. Schulz, Aa. S. Sudbo, Y. R. Shen, and Y. T. Lee, Phys. Rev. Lett., 40, 115 (1978).

(6) P. J. Robinson and K. A. Holbrook, "Unimolecular Reactions," Wiley-Interscience, New York, N. Y., 1972.

(7) J. G. Black, E. Yablonovitch, N. Bloembergen, and S. Mukamel, Phys. Rev. Lett., 38, 1131 (1977); M. J. Shultz and E. Yablonovitch, J. Chem. Phys., 68, 3007 (1978).

(8) M. J. Coggiola, P. A. Schulz, Y. T. Lee, and Y. R. Shen, Phys. Rev. Lett., 38, 17 (1977); E. R. Grant, P. A. Schulz, Aa. S. Sudbo, M. J. Coggiola, Y. R. Shen, and Y. T. Lee, Proceedings International Conference on "Multiphoton Processes," Rochester, N. Y., J. H. Eberly and P. Lambropoulos, eds. John Wiley and Sons, N. Y., 1978.

(9) D. M. Brenner, Chem. Phys. Lett., 57, 357 (1978); R. N. Rosenfeld, J. I. Brauman, J. R. Barker, and D. M. Golden, J. Am. Chem. Soc., 99, 8063 (1977).

(10) A. Hartford, Jr., Chem. Phys. Lett., 53, 503 (1978).

(11) D. S. King and J. C. Stephenson, J. Am. Chem. Soc., 100, 7151 (1978).

(12) J. J. Tiee and C. Wittig, Appl. Phys. Lett., 32, 236 (1978).

(13) P. Kolodner, C. Winterfeld, and E. Yablonovitch, Optics Com., 20, 119 (1977).

(14) N. Bloembergen and E. Yablonovitch, "Laser Spectroscopy," Vol. III, J. L. Hall and J. L. Carlsten, eds., Springer Series in Optical Sciences, Springer, Berlin, Heidelberg, New York, 1977.

(15) E. Grunwald, K. J. Olszyna, D. F. Dever, and B. Knishkowy, J. Am. Chem. Soc., 99, 6515 (1977).

(16) G. P. Quigley, in "Advances in Laser Chemistry," A. H. Zewail, ed., Springer Series in Chemical Physics, Springer, Berlin, Heidelberg, New York, 1978, and references contained therein.

(17) A. J. Colussi, S. W. Benson, R. J. Hwang, and J. J. Tiee, Chem. Phys. Lett., 52, 349 (1977).

(18) R. L. Woodin, D. S. Bomse, and J. L. Beauchamp, J. Am. Chem. Soc., 100, 3248 (1978).

(19) T. A. Lehman and M. M. Bursey, "Ion Cyclotron Resonance Spectrometry," Wiley-Interscience, New York, N. Y., 1976; J. L. Beauchamp, Ann. Rev. Phys. Chem., 22, 527 (1971).

(20) T. B. McMahon and J. L. Beauchamp, Rev. Sci. Inst., 43, 509 (1972).

(21) R. L. Woodin, D. S. Bomse, T. B. McMahon, and J. L. Beauchamp, to be published.

(22) J. L. Beauchamp, Ph. D. Thesis, Harvard University, 1967.

(23) T. B. McMahon, P. G. Miasek, and J. L. Beauchamp, Int. J. Mass Spectrom. Ion Phys., 21, 63 (1976)

(24) Ion-molecule collision frequencies are calculated using average-dipole-orientation theory; L. Bass, T. Su, W. J. Chesnavich, and M. T. Bowers, Chem. Phys. Lett., 34, 119 (1975).

(25) H. Wieser, W. G. Laidlaw, P. J. Krueger, and H. Fuhrer, Spectrochim. Acta, Part A, 24, 1055 (1968); J. P. Perchard, J. C. Monier, and P. Dizabo, ibid., 27, 447 (1971).

(26) The estimated enthalpy change for reaction 1 is based on measured enthalpy changes for analogous reactions of H_3O^+, $CH_3OH_2^+$ and $(CH_3)_2OH^+$; P. Kebarle, Ann. Rev. Phys. Chem., 28, 445 (1977).

(27) $[(C_2H_5)_2O]_2H^+$ collision rate constants, calculated using ADO theory,[24] are 1.2×10^{-9} $cm^3 molecule^{-1} sec^{-1}$ for $(C_2H_5)_2O$, 6.1×10^{-10} $cm^3 molecule^{-1} sec^{-1}$ for SF_6 and 1.0×10^{-9} $cm^3 molecule^{-1} sec^{-1}$ for i-C_4H_{10}.

(28) Similar observations have been made for multiphoton dissociation of bishexafluoroacetylacetonate uranyl-tetrahydrofuran in a molecular beam; A. Kaldor, R. B. Hall, D. M. Cox, J. A. Horsley, P. Rabinowitz, and G. M. Kramer, submitted to J. Am. Chem. Soc.

(29) C. W. Tsang and A. G. Harrison, Org. Mass Spectrom., 3, 647 (1970).

(30) Ion heats of formation obtained from appropriate proton affinity data, neutral heats of formation and tabulated ion thermochemistry. J. F. Wolf, R. H. Staley, I. Koppel, M. Taagepera, R. T. McIver, Jr., J. L. Beauchamp, and R. W. Taft, J. Am. Chem. Soc., 99, 5417 (1977); H. M. Rosenstock, K. Draxl, B. W. Steiner, and J. T. Herron, J. Phys. Chem. Ref. Data, 6, Sup. 1 (1977); J. D. Cox and G. Pilcher, "Thermochemistry of Organic and Organometallic Compounds," Academic Press, London, New York, 1970.

(31) R. Botter, J. M. Pechine, and H. M. Rosenstock, Int. J. Mass. Spectrom. Ion Phys., 25, 7 (1977).

(32) Analogous 1, 2 eliminations of H_2 from gas phase ions have activation energies $>$ 80 kcal/mol. D. H. Williams, Acct. Chem. Rsch., 10, 280 (1977).

(33) D. Holtz and J. L. Beauchamp, unpublished results.

(34) Dudley Williams and George Hvistendahl, J. Am. Chem. Soc., 96, 6753 (1974).

(35) Frequencies in the transition state estimated using bond-order arguments.[6] Frequencies used for proton motion are 3600 cm^{-1}, 1600 cm^{-1}, and 500 cm^{-1}.[41] In the transition state, both $-CH_3$ and $-C_2H_5$ rotations are frozen out. All internal rotations are treated as torsions. Activation energies are assumed the same as for process 11, with zero point energy differences due to deuterium substitution taken into account.

(36) W. T. Huntress, Jr., D. K. Sen Sharma, K. R. Jennings, and M. T. Bowers, Int. J. Mass Spectrom. Ion Phys., 24, 25 (1977).

(37) We have erroneously identified the products of this reaction in another publication. R. L. Woodin, D. S. Bomse, and J. L. Beauchamp, "Multiphoton Dissociation of Gas Phase Ions Using Low Intensity CW Laser Radiation," in Chemical and Biochemical Applications of Lasers, Vol. IV, C. B. Moore, ed., Academic Press, New York, N. Y., 1979.

(38) (a) C. D. Cantrell, S. M. Freund, and J. L. Lyman, in "Laser Handbook," Vol. III, North Holland Publishing, Amsterdam, to be published.

(b) C. D. Cantrell, in "Laser Spectroscopy," Vol. III, J. L. Hall and J. L. Carlsten, eds., Springer Series in Optical Sciences, Springer, Berlin, Heidelberg, New York, 1977.

(c) N. Bloembergen, Opt. Commun., 15, 416 (1975).

(d) M. F. Goodman, J. Stone, and D. A. Dows, J. Chem. Phys., 65, 5052 (1976).

(e) S. Mukamel and J. Jortner, Chem. Phys. Lett., 40, 150 (1976).

(f) S. Mukamel and J. Jortner, J. Chem. Phys., 65, 5204 (1976).

(g) M. Tamir and R. D. Levine, Chem. Phys. Lett., 46, 208 (1977).

(h) D. P. Hodgkinson and J. S. Briggs, Chem. Phys. Lett., 43, 451 (1976).

(i) M. Quack, J. Chem. Phys., 69, 1294 (1978).

(39) G. Herzberg, "Infrared and Raman Spectra of Polyatomic Molecules," Van Nostrand, New York, N. Y., 1945, p. 251.

(40) For typical infrared transition moments of 0.01-0.20 D and laser intensity of 1 W cm^{-2}, the Rabi frequency is $\sim 10^5$ sec^{-1} corresponding to power broadening of $\ll 0.001$ cm^{-1}.

(41) G. H. F. Diercksen, W. P. Kraemer, and B. O. Roos, Theoret. Chim. Acta (Berl.), 36, 249 (1975).

CHAPTER III

Multiphoton Dissociation of Molecules with Low Power CW Infrared Lasers: Collisional Enhancement of Dissociation Probabilities

R. L. Woodin,[†] D. S. Bomse[‡] and J. L. Beauchamp

Contribution No. 5937 from the Arthur Amos Noyes Laboratory of Chemical Physics. California Institute of Technology, Pasadena, California 91125

[†]Present address: Exxon Research and Engineering Company, Corporate Research Laboratories, Linden, New Jersey 07036.

[‡]NSF Pre-Doctoral Fellow, 1976-1979.

ABSTRACT

Low intensity multiphoton dissociation of $C_3F_6^+$ is observed using cw CO_2 laser radiation. Ion cyclotron resonance techniques are used to store ions for irradiation. Multiphoton dissociation is observed at laser intensities below 100 W cm^{-2} and at pressures below 10^{-7} Torr. Only the lowest energy decomposition of $C_3F_6^+$, to give $C_2F_4^+$ and CF_2, is observed. Multiphoton dissociation probabilities show a sharp wavelength dependence in contrast to typical pulsed laser multiphoton dissociation experiments. Photodissociation probabilities for $C_3F_6^+$ are compared with the infrared absorption spectrum of C_3F_6 at both low and high resolution. Collisions between $C_3F_6^+$ and unreactive buffer gases (Ar, N_2, SF_6) are seen to enhance multiphoton dissociation, while collisions with C_2F_6 deactivate the laser excited species. The results are discussed in terms of mechanisms for slow multiphoton dissociation.

1. Introduction

The detailed study of multiphoton dissociation (1,2) using high power pulsed infrared lasers is rendered difficult by the short time interval during which excitation and dissociation occurs. Further difficulties in interpretation result from the spatial and temporal inhomogeneities in photon flux associated with focused laser pulses. As a logical extension of the experiments by Yablonovitch and co-workers which demonstrate that dissociation yields are dependent only on laser energy fluence and not peak power (3), we recently observed and reported dissociation of isolated molecules with unfocused radiation from a cw infrared laser using powers of only a few watts (4). Our approach is unique in that it provides for direct monitoring of reactant and product concentrations during laser photolysis. This is made possible by ion cyclotron resonance techniques which allow for electromagnetic confinement of infrared active species. Irradiation times can approach several seconds and pressures can be varied to allow for up to several thousand collisions. In the present study we report investigations of the dissociation of the molecular ion of perfluoropropylene, $C_3F_6^+$. Details are provided relating to dependence of the photodissociation rate on laser frequency, netural gas pressure, and internal energy content of $C_3F_6^+$.

2. Experimental

Ion cyclotron resonance (ICR) techniques (5, 6) and their application to ion photochemistry (7-13) have been described in detail in the literature. Approximately 10^5 ions formed by electron impact ionization are stored in crossed electric and magnetic fields for times up to 5 seconds and then mass analyzed. Neutral pressures are varied from 10^{-8} to 10^{-5} Torr. The instrument used in this study was built in the Caltech shops and is of standard design, utilizing a 23.4 kG electromagnet and marginal oscillator detector. Pressures are measured using a Schulz-Phelps type ionization guage calibrated against a MKS Baratron Model 90H1-E capacitance manometer. It is estimated than absolute pressure determinations are within ± 20%, with pressure ratios being somewhat more accurate.

Figure 1 illustrates the experimental configuration for laser excitation of ions. The 6 mm diameter unfocused beam from a grating tuned Apollo 550A cw CO_2 laser is directed through a 92% transmittance mesh into the ICR cell where it is reflected. back to a beamstop by the mirror finish on the back source plate. A calibrated beam splitter diverts a fraction of the beam for continuous power measurement. Laser wavelength is measured with an Optical Engineering Model 16A spectrum analyzer. The estimated laser bandwidth is 50 MHz ($\sim 1.6 \times 10^{-3}$ cm^{-1}). Ions are irradiated with intensities up to 100 W cm^{-2}. The laser beam profile is nearly Gaussian (FWHM = 6 mm) as determined by

Figure 1

Schematic view of the experimental apparatus.

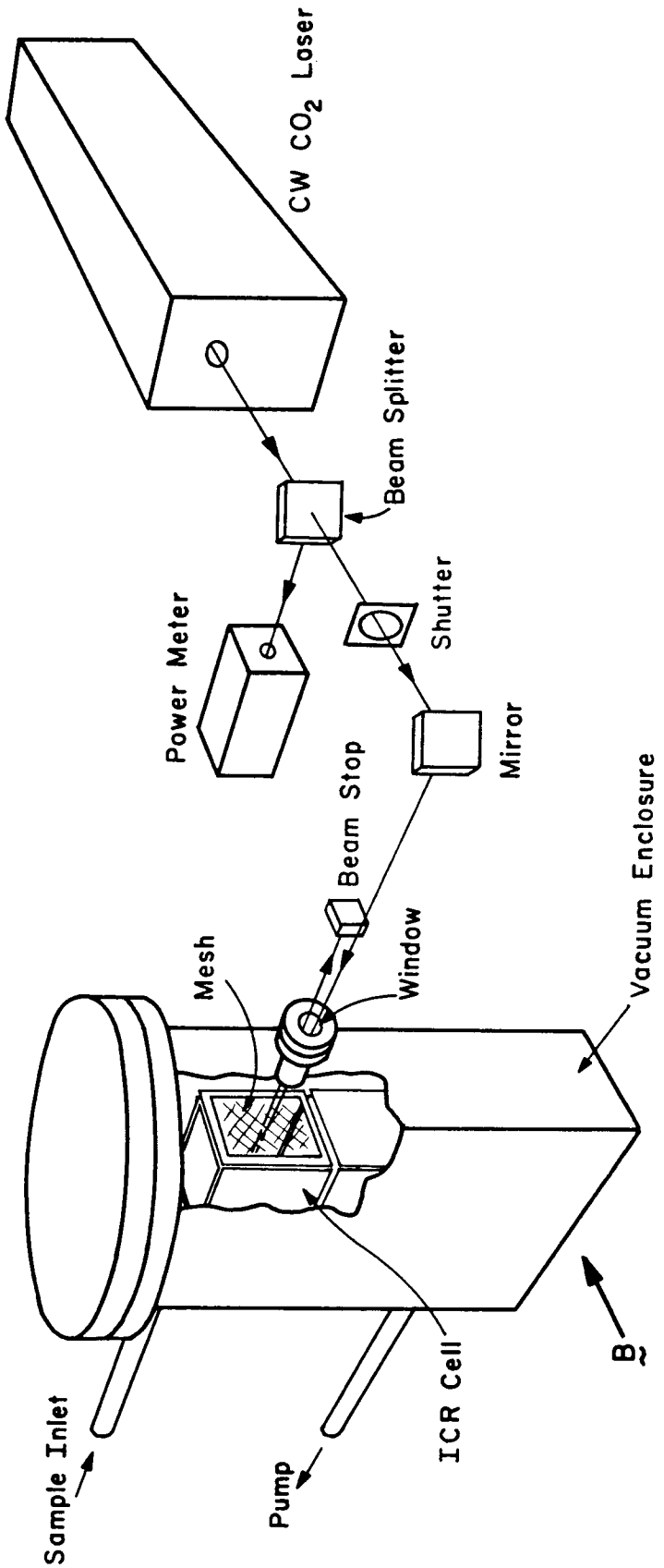
CW CO_2 Laser
Beam Splitter
Power Meter
Shutter
Mirror
Beam Stop
Window
Mesh
Vacuum Enclosure
Sample Inlet
Pump
ICR Cell
B

measuring the power transmitted through a 1 mm diameter pin hole translated across the beam. Infrared beam intensities quoted in this paper are calculated by dividing the total power in the beam by the area of a 6 mm diameter beam. Irradiation of stored ions is uniform as indicated by the fact that small translations of the laser beam do not alter dissociation rates. Additional experimental details are provided in ref. 14.

Low resolution infrared spectra were recorded with a Beckman IR-12 spectrometer. Moderate resolution absorption spectra were obtained with the cw CO_2 laser described above. High resolution absorption measurements utilized a grating tuned cw CO_2 waveguide laser. The waveguide laser is similar to one described in the literature (15) and was built by the Hughes Research Laboratories. For a given transition the laser was tuned over ~ 300 Mhz with 1 Mhz resolution. All absorption experiments were carried out with a 10 cm path length cell equipped with NaCl windows.

3. Results

The ion-molecule chemistry of perfluoropropylene is reported elsewhere (7). Briefly, the major ions formed by electron impact ionization (20-70 eV) of C_3F_6 are $C_3F_6^+$, $C_3F_5^+$, $C_2F_4^+$ and CF_3^+. The only observed reaction which involves these species is the fluoride transfer, reaction (1).

$$CF_3^+ + C_3F_6 \rightarrow C_3F_5^+ + CF_4 \quad (1)$$

$C_3F_6^+$, $C_3F_5^+$ and $C_2F_4^+$ do not react with perfluoropropylene and are suitable candidates for studies of multiphoton dissociation processes. Reactions 2-4 are the plausible ion decomposition pathways based on available thermochemistry (7).

		ΔH (kcal/mole)	
$C_3F_6^+$	$\rightarrow C_2F_4^+ + CF_2$	56	(2)
	$\rightarrow C_3F_5^+ + F$	85	(3)
$C_3F_6^+ \longrightarrow$	$CF_3^+ + C_2F_2$	<52	(4)

Enthalpy changes for $C_3F_6^+$ fragmentation reactions are obtained from a recent photoionization study (16). The uncertainty in the thermochemistry of reaction 4 is due to discrepancies in the reported C_2F_2 heat of formation (7). Laser irradiation of ions derived from C_3F_6 effects a decrease in $C_3F_6^+$ abundance with a concomitant increase in $C_2F_4^+$ abundance. The intensities of CF_3^+ and $C_3F_5^+$ are unaffected by laser irradiation. Double resonance experiments confirm process 2, which is the lowest energy $C_3F_6^+$ decomposition channel. At 14 eV electron energy only the molecular ion is formed. Figure 2 shows the temporal variations of $C_3F_6^+$ and $C_2F_4^+$ with and without continuous laser irradiation. The decrease in $C_3F_6^+$

Figure 2

Ion intensity versus trapping time for photodissociated ion, $C_3F_6^+$, and product ion, $C_2F_4^+$. The intensities of the two ions are not directly comparable (note change of scale of ordinates). Ions formed by a 40 msec electron beam pulse at 14 eV. Other conditions include laser frequency 1047 cm^{-1}; intensity 48 W cm^{-2}; C_3F_6 pressure 7.5×10^{-7} Torr; Ar added to make total pressure 1.6×10^{-6} Torr.

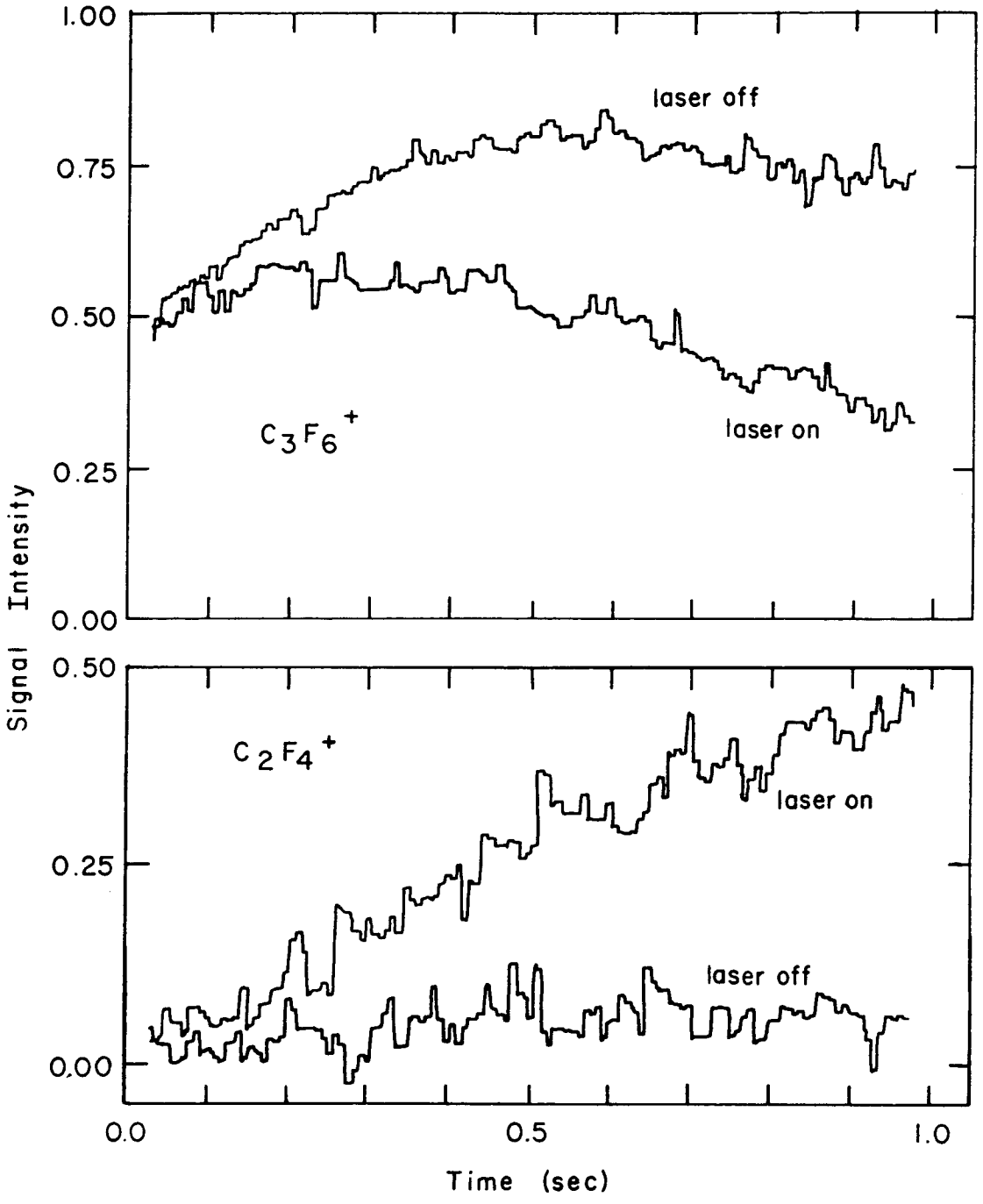
1.00
0.75
0.50
0.25
0.00
laser off
laser on
$C_3F_6^+$
0.50
0.25
0.00
$C_2F_4^+$
laser on
laser off
Signal Intensity
0.0
0.5
1.0
Time (sec)

intensity equals the increase in $C_2F_4^+$ intensity. Semilog plots of $C_3F_6^+$ fractional abundance as a function of irradiation time are linear for all pressures used and laser intensities up to 70 W cm^{-2}. Photodissociation rates are obtained from the slopes of such plots.

The $C_3F_6^+$ dissociation yield (P_D) as a function of laser frequency is shown in fig. 3. Data are included in fig. 3 for the dissociation of ions formed by both 70 eV and 20 eV electron impact. P_D is defined as fraction of $C_3F_6^+$ decomposed during two seconds of irradiation at a laser intensity of 34 W cm^{-2}. Also presented in fig. 3 is the gas phase infrared spectrum of neutral perfluoropropylene in the same spectral region. The dotted line is data taken at ~ 1 cm^{-1} resolution, while the solid data points are absorption measurements using the cw CO_2 laser. Measurements using monochromatic radiation are superimposable on the low resolution data indicating that no rotational fine structure is observable at ~ 50 Mhz resolution. Further investigation of the spectral region near 1037 cm^{-1} using a CO_2 waveguide laser revealed no discernable fine structure at 1 Mhz resolution for a room temperature sample at pressures down to ~ 0.01 Torr.

The effect of collisions on the $C_3F_6^+$ photodissociation rate is shown in figs. 4 and 5. When hexafluoropropylene is used as the buffer gas (fig. 4) the $C_3F_6^+$ photodissociation rate is enhanced as the pressure is increased up to 1.4×10^{-6} Torr. Further addition of C_3F_6 inhibits the decomposition process. Figure 5

Figure 3

Photodissociation spectrum of $C_3F_6^+$ over the CO_2 laser spectral range. Left ordinate is fraction of $C_3F_6^+$ dissociated after two seconds of irradiation at 34 W cm^{-2}. The two solid curves are for ionization energies of 70 eV (□) and 20 eV (○). Perfluoropropylene pressure is 4.8×10^{-7} Torr. Dotted line is infrared absorption spectrum of perfluoropropylene at 0.8 Torr in a 10 cm path length cell. Solid data points are absorption spectrum taken using cw CO_2 laser radiation (0.5 W cm^{-2}). Sample pressure was ~ 1 Torr in a 10 cm path length cell. The solid data points are scaled to match low resolution spectrum.

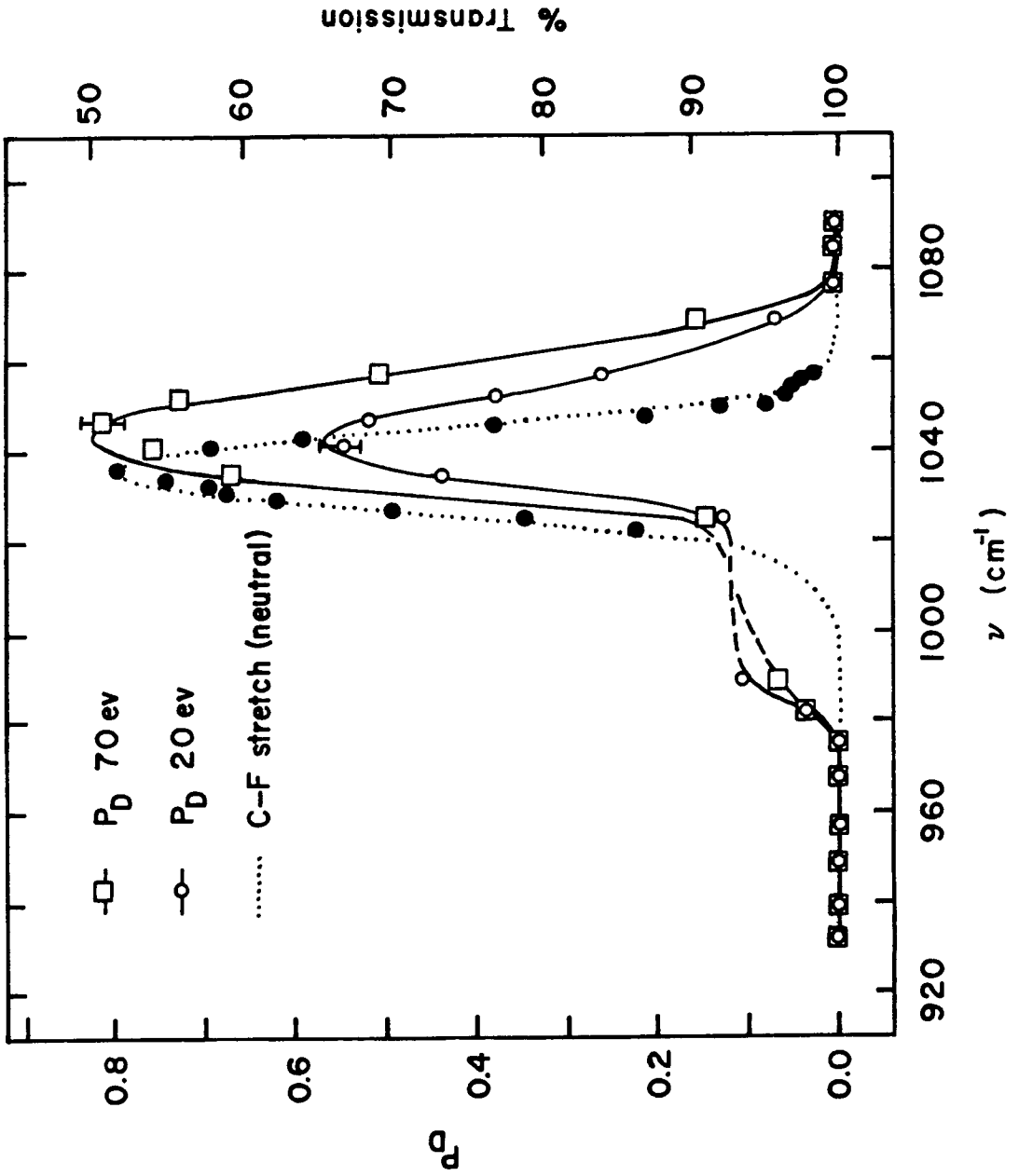
% Transmission
50
60
70
80
90
100
P_D
0.8
0.6
0.4
0.2
0.0
P_D 70 ev
P_D 20 ev
C-F stretch (neutral)
920
960
1000
1040
1080
ν (cm^{-1})

Figure 4

$C_3F_6^+$ multiphoton dissociation rate as a function of perfluoropropylene pressure. Laser frequency is 1047 cm^{-1} and laser intensity is 48 W cm^{-2}. Ionization energy is 14 eV. Trapping time is 0.5 sec.

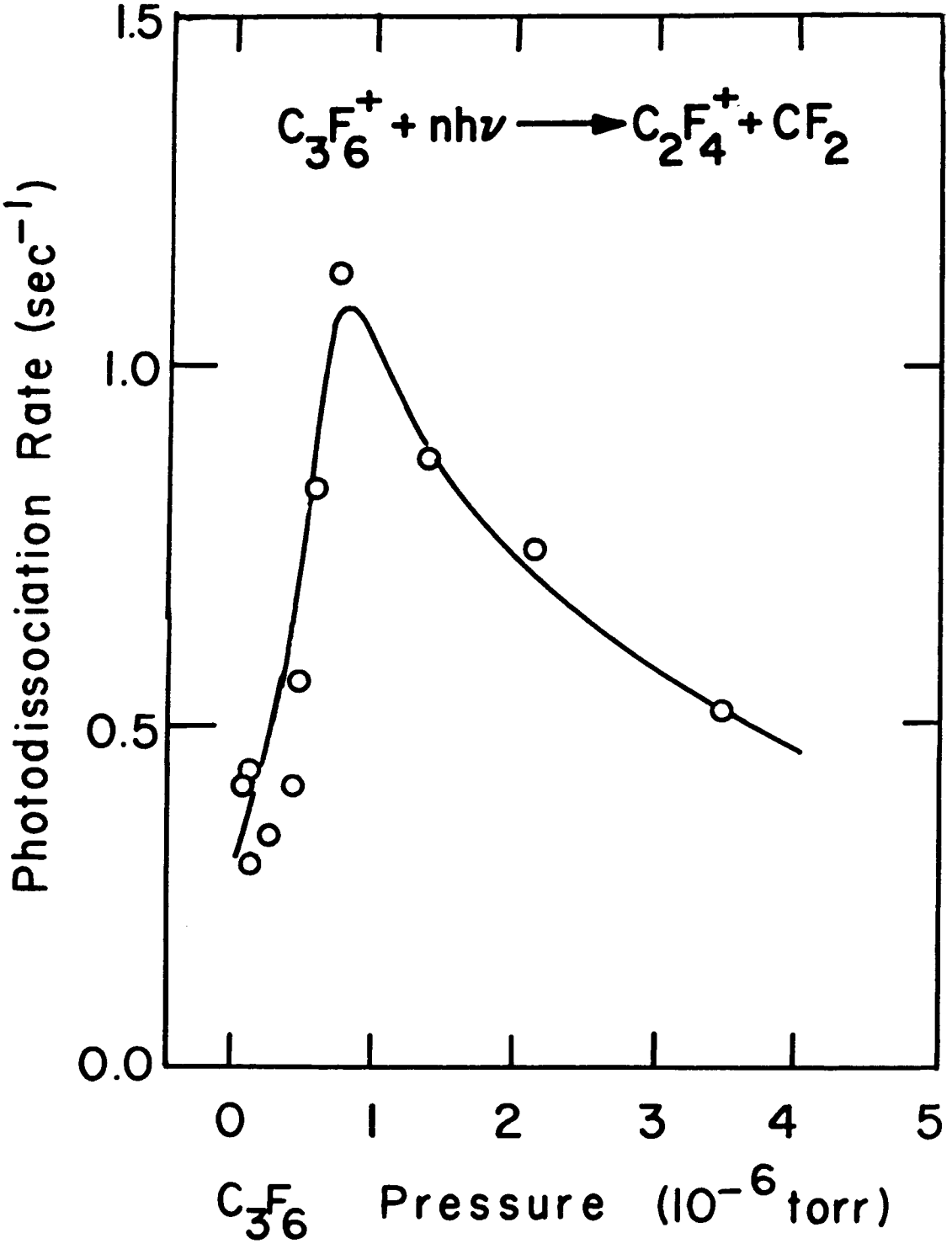
$C_3F_6^+ + nh\nu \longrightarrow C_2F_4^+ + CF_2$
Photodissociation Rate (sec^{-1})
1.5
1.0
0.5
0.0
0
1
2
3
4
5
C_3F_6 Pressure (10^{-6} torr)

Figure 5

$C_3F_6^+$ multiphoton dissociation rate as a function of added buffer gases: Ar (Δ), N_2 (∇) and SF_6 ($\square$). The dashed line indicates $C_3F_6^+$ multiphoton dissociation rate with C_3F_6 as the added buffer gas. Ar, N_2 or SF_6 are added to 1.2×10^{-7} Torr C_3F_6. The abscissa indicates total pressure.

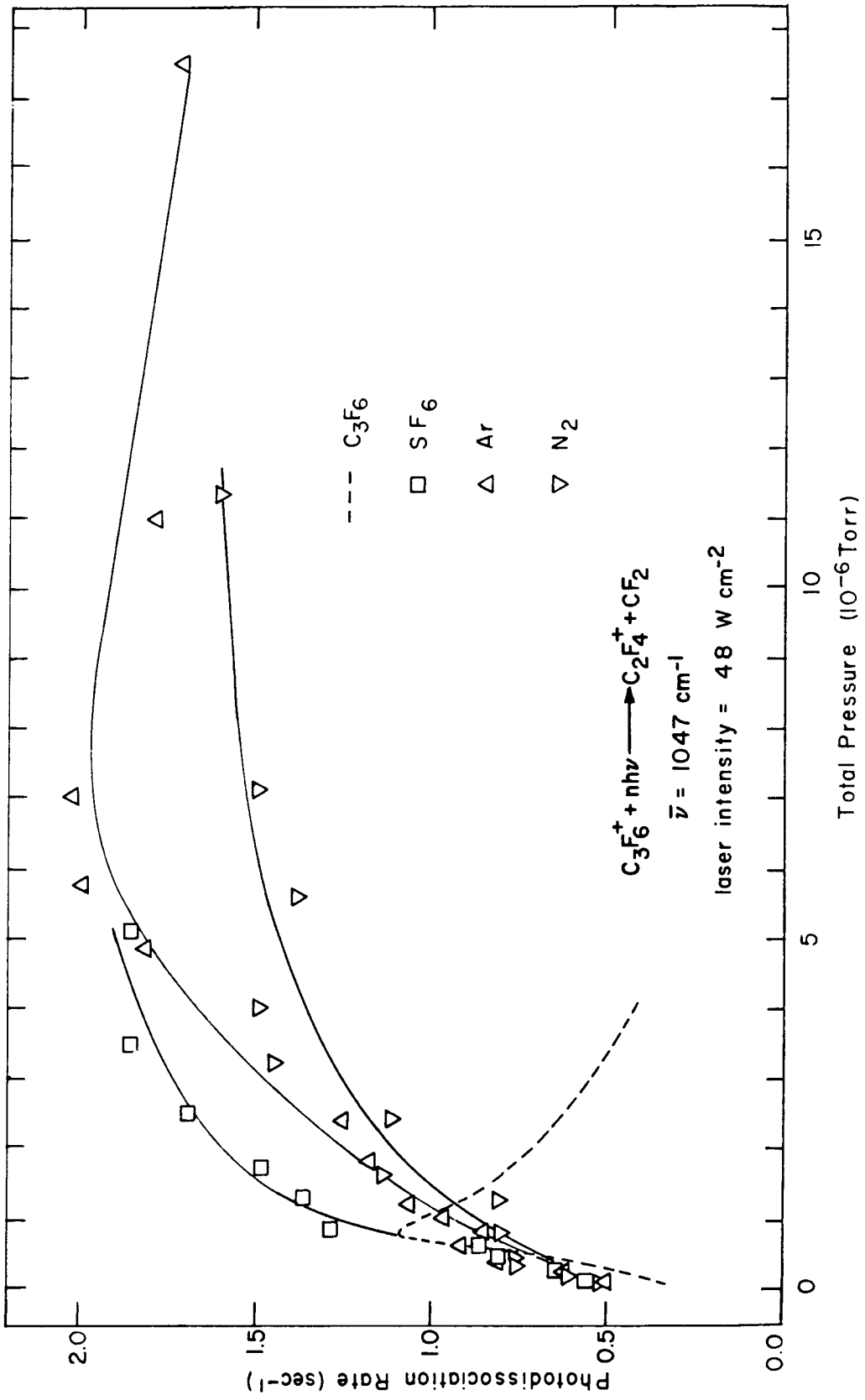
Photodissociation Rate (sec⁻¹)
2.0
1.5
1.0
0.5
0.0
0
5
10
15
Total Pressure (10⁻⁶ Torr)
C3F6
SF6
Ar
N2
C3F6+ + nhν ⟶ C2F4+ + CF2
ν̄ = 1047 cm⁻¹
laser intensity = 48 W cm⁻²

shows the effect on the $C_3F_6^+$ dissociation rate when unreactive buffer gases, N_2, Ar, or SF_6 are added to 1.2×10^{-7} Torr of perfluoropropylene. In these experiments the ionization energy was maintained at 14 eV to prevent ionization of the buffer gas. The rate of dissociation increases substantially with increasing buffer gas pressure for all three diluents. From fig. 5 there is little evidence for significant deactivation by Ar, N_2, or SF_6 within the accessible range of higher pressures, even though ions undergo up to $\sim 10^3$ collisions during irradiation.

The role of collisions prior to laser excitation was examined by allowing for a delay period between $C_3F_6^+$ formation (14 eV ionization energy) and irradiation. At a pressure of 2×10^{-7} Torr delay times up to 0.5 sec allow up to 10 collisions prior to irradiation. For all delay times used the observed photodissociation rates were identical within experimental error.

The effect of laser excitation of neutrals was explored in the mixture of C_3F_6 with SF_6. Irradiating a 2:1 mixture of SF_6 and C_3F_6 at 1047 cm^{-1} with 48 W cm^{-2} produces dissociation of $C_3F_6^+$ at a rate of ~ 2 sec^{-1}. No dissociation is effected by irradiating the same mixture at an SF_6 absorption maxima (947 cm^{-1}) (1). This experiment was repeated at several SF_6 pressures up to 5×10^{-6} Torr (SF_6:C_3F_6 = 40:1) with the same result.

4. Discussion

From the experimental results detailed in Section 3, it is apparent that low intensity multiphoton dissociation of $C_3F_6^+$ is observed. The strong frequency dependence for $C_3F_6^+$ photodissociation and the invariance of $C_3F_5^+$ and CF_3^+ intensities to laser irradiation eliminate the possibility that non-specific heating of the icr cell leads to the observed change in ion intensities. A mechanism in which laser excitation of neutrals followed by collisional V-V transfer to stored ions leads to $C_3F_6^+$ dissociation is not consistent with the observation that $C_3F_6^+$ in the presence of SF_6 is stable when irradiated at an SF_6 absorption maxima.

The IR absorption band in neutral C_3F_6 (λ_{max}: 1037 cm^{-1}) shown in fig. 3 has been identified as a C-F stretch of A' symmetry (17). Comparison with other fluorinated species suggests that this vibrational mode involves only the CF_3 group. Since the lowest energy ionization process in C_3F_6 entails removing an electron from the C-C double bond, this particular vibrational frequency is unperturbed in going from the neutral to the cation. Therefore, the photodissociation spectrum and the netural absorption band are nearly superimposed.

Experiments at high sensitivity show a weak band in the absorption spectrum of C_3F_6 at 978 cm^{-1} (not apparent in fig. 3) which is assigned as a combination band (17). The intensity of the absorption at 978 cm^{-1} relative to the major peak at 1037 cm^{-1} is

considerably smaller than the magnitude of the 985 cm^{-1} features relative to the major peak at 1047 cm^{-1} in the $C_3F_6^+$ photodissociation spectrum (fig. 3). The small peak in the photodissociation spectrum occurs at an energy which is too low to attribute to a v = 1 to v = 2 resonance (typical anharmonicities for C-F stretch modes are 18 cm^{-1} (18)) and is tentatively assigned as a combination band. If this interpretation is correct, then the marked difference in multiphoton dissociation probabilities for the two infrared bands implies that resonant absorption is not rate limiting in the photolysis. For typical infrared transition moments of 0.01-0.10 D and a laser intensity of 1 W cm^{-2}, the Rabi frequency (19) is $\sim 10^5$ sec^{-1}, far in excess of observed photodissociation rates.

Energy deposition into internal degrees of freedom of ions formed by electron impact ionization tends to increase with increasing electron energy. Hence, the population of vibrationally excited $C_3F_6^+$ will be greater when formed with 70 eV electrons than with 20 eV electrons. The increase in photodissociation yield at 70 eV compared to 20 eV (fig. 3) is attributed to an increased facility for multiphoton dissociation of vibrationally excited species.

The data in figs. 4 and 5 provide clear evidence that collisions can enhance multiphoton dissociation. The contrasting behavior between C_3F_6 and the buffer gases can be attributed to either symmetric electron transfer (20) or near-resonant V-V transfer between $C_3F_6^+$ and C_3F_6 making the parent molecule uniquely

efficient in deactivating vibrationally excited $C_3F_6^+$. This accounts for the decrease in photodissociation probability at higher pressures of C_3F_6. Symmetric charge transfer has been shown to be effective at removing up to several eV of energy from $C_6H_6^+$ and $C_6H_5CN^+$ (8, 12).

Assuming that collisional processes are rate limiting in the multiphoton dissociation of $C_3F_6^+$, then at low pressures the slopes of the curves in fig. 5 should give rate constants for collisional enhancement of photodissociation. For the data in fig. 5 approximately one out of every two collisions serves to enhance the multiphoton process. In C_3F_6 alone, it is seen in fig. 5 that collision rates approximately 80 times larger than photodissociation rates are required to reduce the latter by a factor of two.

The sharp frequency dependence observed in fig. 3 for $C_3F_6^+$ photodissociation is in contrast with reported experiments on SF_6 using high power pulsed lasers, in which photodissociation maxima are shifted to lower wavelengths by $\sim 8\ cm^{-1}$ and broadened by at least a factor of two (1). Whereas in pulsed laser experiments excitation is thought to be to $v = 3\text{-}5$ in a single mode (1), it appears that in low intensity multiphoton dissociation excitation is only to $v = 1$ of the pumped mode, giving rise to a sharp photodissociation spectrum. Following intramolecular energy transfer, the resonant mode is returned to $v = 0$ and may absorb another photon. This mechanism is similar to that proposed by

Tamir and Levine (21). Such resonant transitions followed by intramolecular V-V transfer are required until the molecule is energized to a level such that the density of vibrational states is large compared with the laser bandwidth ($\sim 0.001\ cm^{-1}$), and the molecule may then absorb in the "quasi-continuum" (1,22). Density of states calculations (23) using frequencies for C_3F_6 indicate that a density of states of approximately 2000 states/cm^{-1} is obtained with four quanta of 1000 cm^{-1} radiation. In the case of SF_6, estimated lifetimes for relaxation from v = 3 of the pumped mode are from 30 psec to 1μsec (22,24). At lower levels of excitation intramolecular energy transfer rates are expected to be slower. Collisions may then act to enhance intramolecular V-V transfer, in accordance with fig. 5. Alternatively, the narrow laser linewidth may excite only a small portion of the $C_3F_6^+$ absorption band, and collisions may serve to redistribute rotational states and hence increase photodissociation.

The lack of fine structure in the C_3F_6 absorption band implies that either there exists a dense manifold of initial and final states associated with the vibrational transition or there is a large homogeneous linewidth for each rotational component. The calculated Doppler linewidth is $\sim$ 30 Mhz for C_3F_6 at room temperature. Both inferences agree with the observed ability of narrow band low intensity radiation to dissociate the entire population of $C_3F_6^+$. Even at the lowest pressures saturation

with respect to laser intensity is not observed. This is consistent with a homogeneously broadened line where collisions are not required to tune molecules to the laser.

5. Conclusions

From the present work it is apparent that multiphoton dissociation of stored ions is possible with low intensity infrared radiation. Even with the current lack of ion spectral data, suitable candidates for infrared laser photolysis may be found by paying careful attention to neutral precursor vibrational frequencies and the nature of the ionization process. The sharp features in the photodissociation spectrum suggest that low intensity multiphoton dissociation is very selective with respect to both isotopic substitution and molecular structure.

The observed enhancement of photodissociation rates by both collisions and prior excitation offers intriguing possibilities. In particular, it should be possible to observe both pulsed and cw low power multiphoton dissociation of neutral molecules since the constraint of a collision free environment can be relaxed.

Acknowledgments

The waveguide laser data were obtained by Drs. John Peterson, Gerard Megie and Robert Menzies of the Jet Propulsion Laboratory.

Their assistance is gratefully acknowledged. This work was supported in part by the United States Department of Energy and the President's Fund of the California Institute of Technology.

References

(1) R. V. Ambartzumian and V. S. Letokhov, in "Chemical and Biochemical Applications of Lasers," C. Bradley Moore, ed., Vol. III, Academic Press, New York, N. Y., 1977, and references contained therein.

(2) E. Grunwald, D. F. Dever, and P. M. Keehn, "Megawatt Infrared Laser Chemistry," John Wiley and Sons, New York, N. Y., 1978.

(3) P. Kolodner, C. Winterfeld, and E. Yablonovitch, Optics Com., 20, 119 (1977).

(4) R. L. Woodin, D. S. Bomse, and J. L. Beauchamp, J. Am. Chem. Soc., 100, 3248 (1978).

(5) T. A. Lehman and M. M. Bursey, "Ion Cyclotron Resonance Spectrometry," Wiley-Interscience, New York, N. Y., 1976; J. L. Beauchamp, Ann. Rev. Phys. Chem., 22, 527 (1971).

(6) T. B. McMahon and J. L. Beauchamp, Rev. Sci. Inst., 43, 509 (1972).

(7) B. S. Freiser and J. L. Beauchamp, J. Am. Chem. Soc., 96, 6260 (1974).

(8) B. S. Freiser and J. L. Beauchamp, Chem. Phys. Lett., 35, 35 (1975).

(9) B. S. Freiser and J. L. Beauchamp, J. Am. Chem. Soc., 98, 3136 (1976).

(10) B. S. Freiser and J. L. Beauchamp, J. Am. Chem. Soc., 98, 265 (1976).

(11) B. S. Freiser, R. H. Staley, and J. L. Beauchamp, Chem. Phys. Lett., 39, 49 (1976).

(12) T. E. Orlowski, B. S. Freiser and J. L. Beauchamp, Chem. Phys., 16, 439 (1976).

(13) B. S. Freiser and J L. Beauchamp, J. Am. Chem. Soc., 99, 3214 (1977).

(14) D. S. Bomse, R. L. Woodin, and J. L. Beauchamp, J. Am. Chem. Soc., submitted for publication.

(15) R. L. Abrams, Appl. Phys. Lett., 25, 304 (1974).

(16) D. W. Berman, D. S. Bomse, and J L. Beauchamp, unpublished results.

(17) J. R. Nielsen, H. H. Classen, and D. C. Smith, J. Chem. Phys. 20, 1916 (1952).

(18) R. S. Sheorey, R. C. Slater, and G. W. Flynn, J. Chem. Phys., 68, 1058 (1978).

(19) L. Allen and J. H. Eberly, "Optical Resonance and Two-Level Atoms," Wiley-Interscience, New York, N.Y., 1975.

(20) T. B. McMahon, P. G. Miasek, and J. L. Beauchamp, Int. J. Mass Spectrom. Ion Phys., 21, 63 (1976).

(21) M. Tamir and R. D. Levine, Chem. Phys. Lett., 46, 208 (1977).

(22) D. S. Frankel Jr. and T. J. Manuccia, Chem. Phys. Lett., 54, 451 (1978).

(23) P. J. Robinson and K. A. Holbrook, "Unimolecular Reactions," Wiley-Interscience, New York, N.Y., 1972.

(24) H. S. Kwok and E. Yablonovitch, Phys. Rev. Lett., 41, 745 (1978).

CHAPTER IV

Bimolecular Infrared Radiative Association Reactions. Attachment of Li^+ to Carbonyl Compounds in the Gas Phase

R. L. Woodin[†] and J. L. Beauchamp

Contribution No. 5938 from the Arthur Amos Noyes Laboratory of Chemical Physics, California Institute of Technology, Pasadena, California 91125

[†] Present address: Exxon Research and Engineering Co., Corporate Research Laboratories, Linden, New Jersey 07036.

ABSTRACT

Direct clustering of Li^+ with $(C_2H_5)_2CO$, $CH_3COC_2H_5$, $(CD_3)_2CO$, $(CH_3)_2CO$, CH_3CHO and H_2CO is examined in the gas phase by ion cyclotron resonance spectroscopy. Initial interaction of Li^+ with the carbonyl compound leads to formation of a vibrationally excited adduct which can be stabilized by energy loss in collisional or infrared radiative processes. At pressures where the time between collisions exceeds 100 msec the dominant stabilization mechanism is assumed to be infrared emission; calculations of radiative rates are presented. Calculated rates for Li^+ attachment at low pressures are found to be in good agreement with experiment. Implications of bimolecular infrared radiative association reactions for molecular synthesis in interstellar space are discussed.

1. Introduction

An excited intermediate can readily be generated by the interaction of an ion with a neutral molecule due to the usually small or negligible activation barrier to association [1] and the appreciable binding energies which often exist between the collision partners. The ability to select from a wide range of reactant species facilitates studies of the stabilization and fragmentation processes of activated species. In the absence of exothermic reaction channels, the fate of an excited intermediate formed in an ion-molecule collision, process (1), is generally thought to be governed by collisions stabilization,

$$A^+ + B \underset{k_a(E)}{\overset{k_f}{\rightleftharpoons}} [AB^+]^\ddagger \qquad (1)$$

$$[AB^+]^\ddagger + M \xrightarrow{k_s} AB^+ + M \qquad (2)$$

process (2), (where M may be the molecule B) or unimolecular decomposition to reactants which is the reverse of process (1). The unimolecular decomposition rate $k_a(E)$ is a sensitive function of the internal energy content of $[AB^+]^\ddagger$. Recent studies have shown that association reactions may exhibit bimolecular reaction kinetics even at very low pressures. These include investigations of electron attachment to SF_6 [2], reactions in fluoromethyl silanes [3] and adduct formation in the interactions of SiH_3^+ with ethylene and benzene (at somewhat higher pressures) [4]. Under conditions where collisions

are infrequent, an alternative mechanism for deactivation of $[AB^+]^\ddagger$ may be radiative stabilization, process (3). The radiative rate $k_r(E)$

$$[AB^+]^\ddagger \xrightarrow{k_r(E)} AB^+ + h\nu \tag{3}$$

is also a function of the internal energy content of $[AB^+]^\ddagger$. Assuming steady-state conditions for $[AB^+]^\ddagger$ the overall rate constant for disappearance of A^+ and formation of stabilized AB^+ is given by eq. (4),

$$k_2(E) = \frac{k_f(k_r(E) + k_s[M])}{k_r(E) + k_a(E) + k_s[M]} \tag{4}$$

where E is the internal energy content of $[AB^+]^\ddagger$. An obvious requirement for process (3) to be efficient is that $k_r \gg k_s[M]$ which for a given k_r will be satisfied at sufficiently low pressures.

The possible importance of radiative association processes is especially apparent for molecular synthesis in interstellar space where particle densities range from 10 to 10^7 particles cm^{-3} [5]. Assuming $k_f = 10^{-9}$ cm^3 $molecule^{-1}$ sec^{-1}, times between ion-molecule collisions range from one hour to 100 years [5] and a process such as eq. (3) can be significant for molecular aggregation and synthesis. Formation of even one molecule every 100 years leads to significant amounts of products on the time scale of interstellar processes! For dipole allowed electronic transitions, radiative lifetimes are on the order of 10^{-8} sec [6] giving $k_2 \cong 10^{-15} - 10^{-9}$ cm^3 $molecule^{-1}$ sec^{-1} if k_a ranges from 10^{-12} to 10^{-6} sec^{-1}. Interstellar formation of CH^+ and CH_2^+ has

been ascribed to such electronic radiative processes [7]. In the absence of electronic excitations, infrared emission is the radiative stabilization mechanism. For infrared emission, $k_r \cong 10^2$ sec^{-1} [8] implying from eq. (4) that $k_2 \cong 10^{-18} - 10^{-9}$ cm^3 molecule^{-1} sec^{-1} for the range $k_a = 10^{12} - 10^2$ sec^{-1}. Loss of a single infrared photon (1-9 kcal/mole) stabilizes the species with respect to dissociation but leaves it vibrationally excited. Infrared radiative association is becoming increasingly popular as a possible mechanism for interstellar chemistry. Infrared emission has been postulated in the formation of H_3CO^+ in interstellar space, process (5) [9-11].

$$HCO^+ + H_2 \rightarrow H_3CO^+ + h\nu \qquad (5)$$

Experimental studies in which collisional stabilization leads to formation of an adduct of H_2 and HCO^+ are consistent with an adduct lifetime which suggests that process (5) is entirely reasonable. However, the structure is most likely a loose association product $HCO^+ \cdots H_2$ rather than protonated formaldehyde or the methoxy cation [12]. Association reactions of CH_3^+, processes (6) - (8) [13,14], H_2CN^+, process (9) [9], and H_4CN^+, process (10) [9], involving

$$CH_2^+ + H_2 \rightarrow CH_5^+ + h\nu \qquad (6)$$

$$CH_3^+ + NH_3 \rightarrow CH_3 \cdot NH_3^+ + h\nu \qquad (7)$$

$$CH_3^+ + H_2O \rightarrow CH_3 \cdot OH_2^+ + h\nu \qquad (8)$$

$$H_2CN^+ + H_2 \rightarrow H_4CN^+ + h\nu \qquad (9)$$

$$H_4CN^+ + H_2 \rightarrow H_6CN^+ + h\nu \qquad (10)$$

infrared emission have been recently proposed. Experimental studies of reactions (6) - (8) under conditions of collisional stabilization allow estimates of decomposition lifetimes to be made [13,14]. As in the case of H_3CO^+ the decomposition lifetimes are compatible with radiative stabilization at low pressures, and such data have been used to calculate interstellar molecular abundances [13-15].

In order to experimentally examine processes such as (1) - (3) under nearly collision-free conditions, an ion-trap method appears to be uniquely suited. Ion cyclotron resonance spectroscopy (ICR) can be used to study ion-molecule reactions over the pressure range 10^{-8} - 10^{-3} Torr, allowing ion-molecule collision frequencies from 1 sec^{-1} to 10^4 sec^{-1} [16]. In this work the attachment of Li^+ to a series of Lewis bases, B, including H_2CO, CH_3CHO, $(CH_3)_2CO$, $(CD_3)_2CO$, $CH_3COC_2H_5$ and $(C_2H_5)CO$ is studied by ICR and the results interpreted in terms of an infrared radiative stabilization mechanism. Association reactions of Li^+ with small molecules are particularly appropriate to study because the binding energetics for a range of neutral species have recently been quantified [17], the structures of several Li^+ complexes (BLi^+) have been elucidated [18,19], and the only fragmentation process which needs to be considered is dissociation to reactants, process (1). The model used to interpret the data is similar to models discussed in the literature [9,10]. Section 2 contains experimental details, section 3 deals with theoretical calculations of $k_r(E)$ and $k_a(E)$, and section 4 presents results and their interpetation. Conclusions which may be drawn from this work are discussed in section 5.

2. Experimental

Techniques of ICR spectroscopy have been described in detail in the literature [16]. Ions are formed and stored in an electrostatic trap located in a strong magnetic field. While the ions are stored they may react with neutral molecules present at pressures from 10^{-8} to 10^{-3} Torr. In trapping or pulsed mode ions are formed in the initial 10 msec of a cycle and stored for up to several seconds. The ions are then mass analyzed to determine concentrations. In drift mode operation the ions are continuously formed and mass analyzed several milliseconds later. The primary advantage of drift mode is the ability to operate at higher pressures.

The instrument used in this study was built in the Caltech shops and utilizes a 15-inch electromagnet capable of a 23.4 kG field. The detection system consists of a marginal oscillator detector accompanied by a phase sensitive amplifier in drift mode and a boxcar integrator in trapping mode. Most experiments are carried out in trapping mode with ion storage times of up to one second.

Vacuum in the instrument is maintained by either a two-inch diffusion pump or a 20 ℓ sec^{-1} ion pump. Pressure is measured with a Schulz-Phelps type ionization gauge calibrated against an MKS Instruments Baratron Model 90H1-E capacitance manometer. It is expected that absolute pressure determinations are within ± 20%.

Chemicals used in this study were obtained from commercial sources with the exception of formaldehyde. Formaldehyde was prepared fresh before each experiment from thermal decomposition of

commercially obtained paraformaldehyde. All samples were degassed by several freeze-pump-thaw cycles prior to use. Mass spectra of the compounds showed no discernible impurities.

Lithium cations are generated by a glass bead filament made according to the procedure described by Hodges and Beauchamp [20]. This produces a glass bead of $Li_2O : Al_2O_3 : SiO_2 = 1 : 1 : 2$ composition on 7 mil rhenium wire. The filament (approximately 1 mm diameter) requires 1-2 amps of current to produce adequate Li^+ emission. The filament extends into the ion source region and is biased on with an appropriate voltage during the beginning of a trapping sequence. Temperature measurements indicate that the temperature rise in the source region after several hours of operation is less than 5° C. All experiments are carried out at ambient temperature, 298°K.

3. Theory

3.1. Calculations of infrared radiative rates

Rates of spontaneous emission are calculated according to the method described by Dunbar [21]. The total radiative rate k_r from all active modes of a species with internal energy E is given by eq. (11)

$$k_r(E) = \sum_i \left(\sum_n P_n^i (E) A_{n,n-1}^i \right) \tag{11}$$

where $A_{n,n-1}^i$ is the Einstein coefficient for spontaneous emission from the n^{th} level of the i^{th} active mode. (Only transitions of $\Delta n = 1$ are considered.) P_n^i is the probability that the n^{th} level of the i^{th} mode is populated. The summations in eq. (11) are over all active modes and all populated vibrational levels of each mode, respectively. Within the harmonic oscillator approximation $A_{n,n-1}^i$ can be replaced by $nA_{1,0}^i$ and eq. (12) results. As described in reference [21], $A_{1,0}^i$ is calculated

$$k_r(E) = \sum_i \left(\sum_n nP_n^i (E) A_{1,0}^i \right) \tag{12}$$

from the integrated absorption intensity, $\mathcal{A}^i$, by eq. (13) where $\bar{\nu}_i$ is

$$A_{1,0}^i = 8\pi \bar{\nu}_i^2 \mathcal{A}^i \tag{13}$$

the frequency of the i^{th} mode in wavenumbers and $\mathcal{A}^i$ is the integrated absorption intensity of the i^{th} mode in IUPAC absolute units [22].

In order to calculate $k_r(E)$ the vibrational spectra and integrated absorption intensities for the adducts BLi^+ need to be known. While experimental spectroscopic data are not available, reasonable estimates

of vibrational frequencies are made based on ab initio calculations [18,19] which indicate that Li^+ has little effect on the structure of the neutral partner. Vibrational frequencies of BLi^+ are thus taken to be the same as for isolated molecules B [23,24], with the addition of three new frequencies associated with the B-Li^+ bond. Estimates of the three additional frequencies have been made for H_2OLi^+ (520 cm^{-1}, 450 cm^{-1}, and 390 cm^{-1}) [19] and are assumed to be nearly the same for molecules considered here. These frequencies are not included in calculating k_r because their oscillator strengths are not known. This approximation should not be serious since low frequency modes tend to have smaller Einstein coefficients than high frequency modes [eq. (13)]. Integrated absorption intensities for molecules B are taken from published work [25,26] or estimated from published spectra [24,27,28].

To calculate P_n^i a Boltzmann distribution is assumed, eq. (14).

$$P_n^i = \frac{e^{-E_n^i/kT_{int}}}{\sum_n e^{-E_n^i/kT_{int}}} \tag{14}$$

E_n^i is the energy of the n^{th} level of the i^{th} mode and T_{int} is an effective vibrational temperature for the species. T_{int} is calculated from tabulated data for the heat content function $(H-H_0)/T$ of molecule B [29-32], the internal energy E of the species and eq. (15) [21]. It is

$$H-H_0 = E + 4RT_{int} \tag{15}$$

assumed that tabulated heat content functions for isolated molecules B

apply to corresponding ions since the molecules are perturbed only slightly by addition of Li^+.

Combining eqs. (12)-(15) allows $k_r(E)$ to be calculated. Results of such calculations for the ions considered here are shown in Fig. 1. Since the species $[BLi^+]^\ddagger$ formed at room temperature are assumed to be very near to threshold for decomposition, it is expected that loss of a single photon stabilizes the species with respect to dissociation and k_r is then the radiative stabilization rate. Radiated photon energies are from 1-9 kcal/mole with the most probable energy approximately 5 kcal/mole. As can be seen in Fig. 1, a monotonic increase in $k_r(E)$ with internal energy is calculated, which is nearly linear at higher energies. It is interesting to note from Fig. 1 that differences in molecular structure have a relatively small effect on radiative rates, with $k_r(E)$ for H_2COLi^+ not greatly different from $k_r(E)$ for $(C_2H_5)_2COLi^+$.

3.2. Calculations of unimolecular dissociation rates

The decomposition of $[BLi^+]^\ddagger$ to B and Li^+ is treated by standard techniques of RRKM theory [33]. Due to potential inaccuracies in other sections of this study, e.g., calculations of $k_r(E)$, more extensive phase-space type calculations [34] of the unimolecular decompositions are not considered here. The RRKM formalism has given reasonable results for association reactions at higher pressures [4,35].

The microscopic unimolecular rate of dissociation, $k_a(E)$, of $[BLi^+]^\ddagger$ is given by eq. (16), where E is the internal energy of the

FIGURE 1

Radiative stabilization rates $k_r(E)$ as a function of internal energy of the chemically activated species $[BLi^+]^{\ddagger}$. Details of calculation of $k_r(E)$ are in section 3. 1.

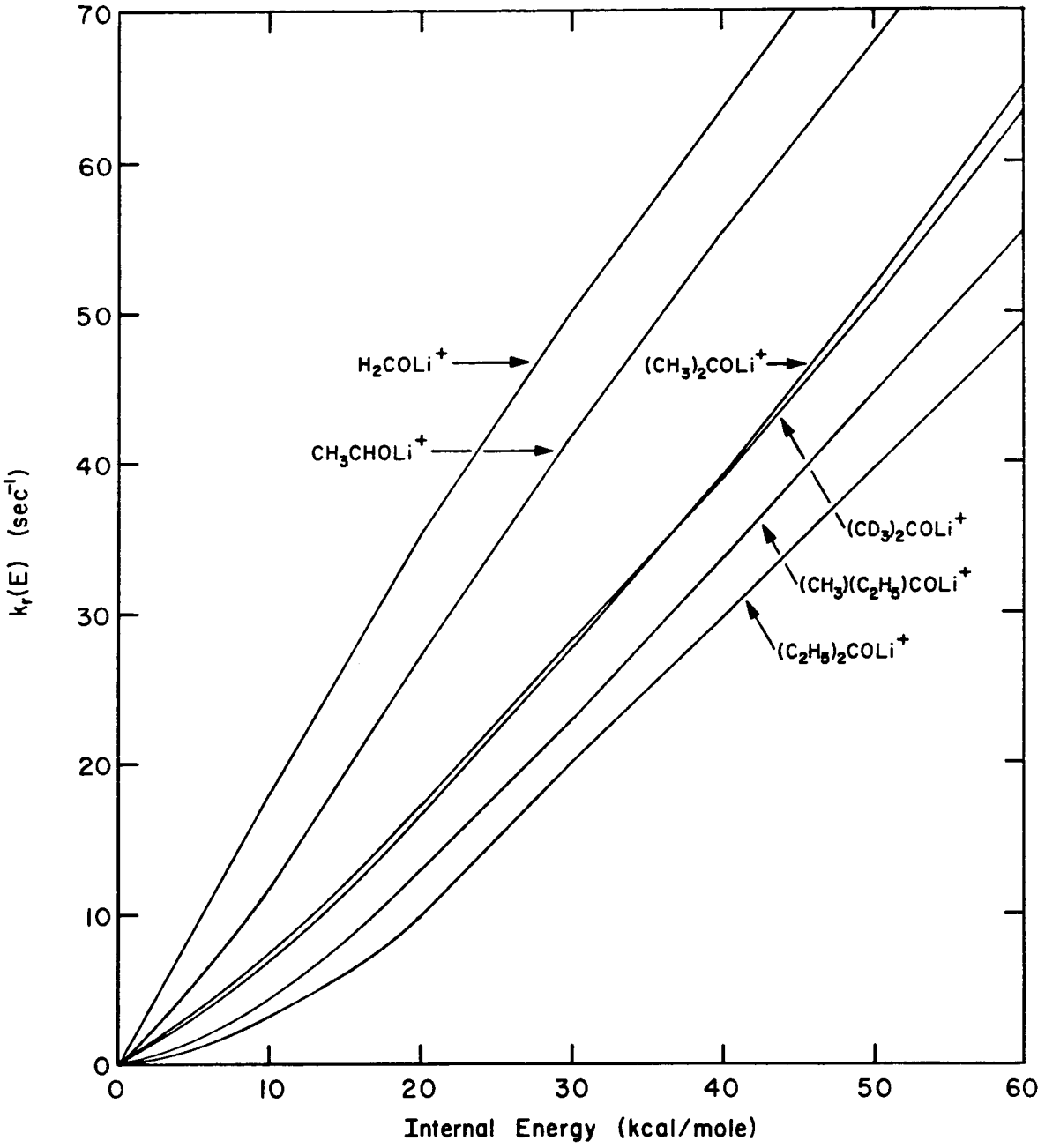
70
60
50
40
30
20
10
0
0
10
20
30
40
50
60
$k_r(E)$ (sec^{-1})
Internal Energy (kcal/mole)
H_2COLi^+
CH_3CHOLi^+
$(CH_3)_2COLi^+$
$(CD_3)_2COLi^+$
$(CH_3)(C_2H_5)COLi^+$
$(C_2H_5)_2COLi^+$

$$k_a(E) = \frac{\sum_{E^\ddagger=0}^{E^\ddagger} P(E^\ddagger)}{hN^*(E)} \qquad (16)$$

energized molecule, $E^\ddagger$ is the internal energy of the activated complex, h is Planck's constant, $\sum_{E^\ddagger=0}^{E^\ddagger} P(E^\ddagger)$ is the sum of states of the activated complex at all energies up to and including $E^\ddagger$, and $N^*(E)$ is the density of states of the energized molecule at energy E. The quantity $E^\ddagger$ is given by eq. (17), where E_0 is the activation energy for decomposition

$$E^\ddagger = E - E_0 \qquad (17)$$

of $[BLi^+]^\ddagger$. The species $[BLi^+]^\ddagger$ is formed by chemical activation and thus retains the reaction exothermicity, $D_0(B\text{-}Li^+)$, plus the thermal energy content of the molecule B as internal excitation. In these calculations for 298°K, translational energy converted to internal energy during collision is assumed negligible. Accurate determinations of $D_0(B\text{-}Li^+)$ have been made for a variety of Lewis bases and estimates of Li^+ binding energies for compounds not studied experimentally may be made by considering trends for similar molecules [17]. Table 1 gives values for $D_0(B\text{-}Li^+)$ used in this study. Since the exact nature of the long range potential surface and transition state for decomposition (in particular the extended O-Li^+ bond lengths) are not known for these systems, rotational effects are not considered in calculating $k_a(E)$. The calculations were carried out in several ways, assuming various transition states, with similar results in all cases. Hence for

Table 1

D_0 (B-Li^+) for Li^+ complexes studied [17]

Complex	D_0 (B-Li^+)[(a)]
H_2COLi^+	36.0
CH_3CHOLi^+	41.7
$(CH_3)_2COLi^+$	44.6
$(CD_3)_2COLi^+$	44.6
$(CH_3)(C_2H_5)COLi^+$	46.0
$(C_2H_5)_2COLi^+$	47.0

(a) Units are kcal/mole.

simplicity calculations ignoring rotational effects are presented. Activation energies for decomposition of $[BLi^+]^\ddagger$ are then taken to be equal to $D_0(B\text{-}Li^+)$ from Table 1. Results of calculations for $k_a(E)$, using eq. (16), are shown in Fig. 2 as a function of internal energy above decomposition threshold for $(C_2H_5)_2COLi^+$, $(CH_3)(C_2H_5)COLi^+$, $(CD_3)_2COLi^+$, $(CH_3)_2COLi^+$, CH_3CHOLi^+, and H_2COLi^+. Sums and densities of states in eq. (16) are evaluated using the Whitten-Rabinovitch approximation [33]. Comparison of $\sum_{E^\ddagger=0}^{E^\ddagger} P(E^\ddagger)$ calculated this way to a direct count calculation gives agreement to within 10%. Internal rotations are treated as torsions. Vibrational frequencies for BLi^+ are taken to be the same as for molecules B [23,24] with the addition of three new frequencies associated with the $B\text{-}Li^+$ bond (see section 3.1). These three additional frequencies are assumed to be the same for all BLi^+ complexes considered here. The 520 cm^{-1} vibration ($B\text{-}Li^+$ stretch) is chosen as the reaction coordinate. In the transition state only the two remaining frequencies associated with the $B\text{-}Li^+$ bond are expected to change and they are taken to be 100 cm^{-1}. Variation of these frequencies from 50 cm^{-1} to 200 cm^{-1} has no substantial effect on the results. Of particular interest in Fig. 2 are the lifetimes of species formed near threshold. Decomposition rates less than 100 sec^{-1} indicate that radiative processes (Fig. 1) can compete effectively with dissociation to deactivate the vibrationally excited adduct.

FIGURE 2

RRKM unimolecular dissociation rates $k_a(E)$ as a function of internal energy in excess of decomposition threshold. The decomposition process is $[BLi^+]^{\ddagger} \rightarrow B + Li^+$.

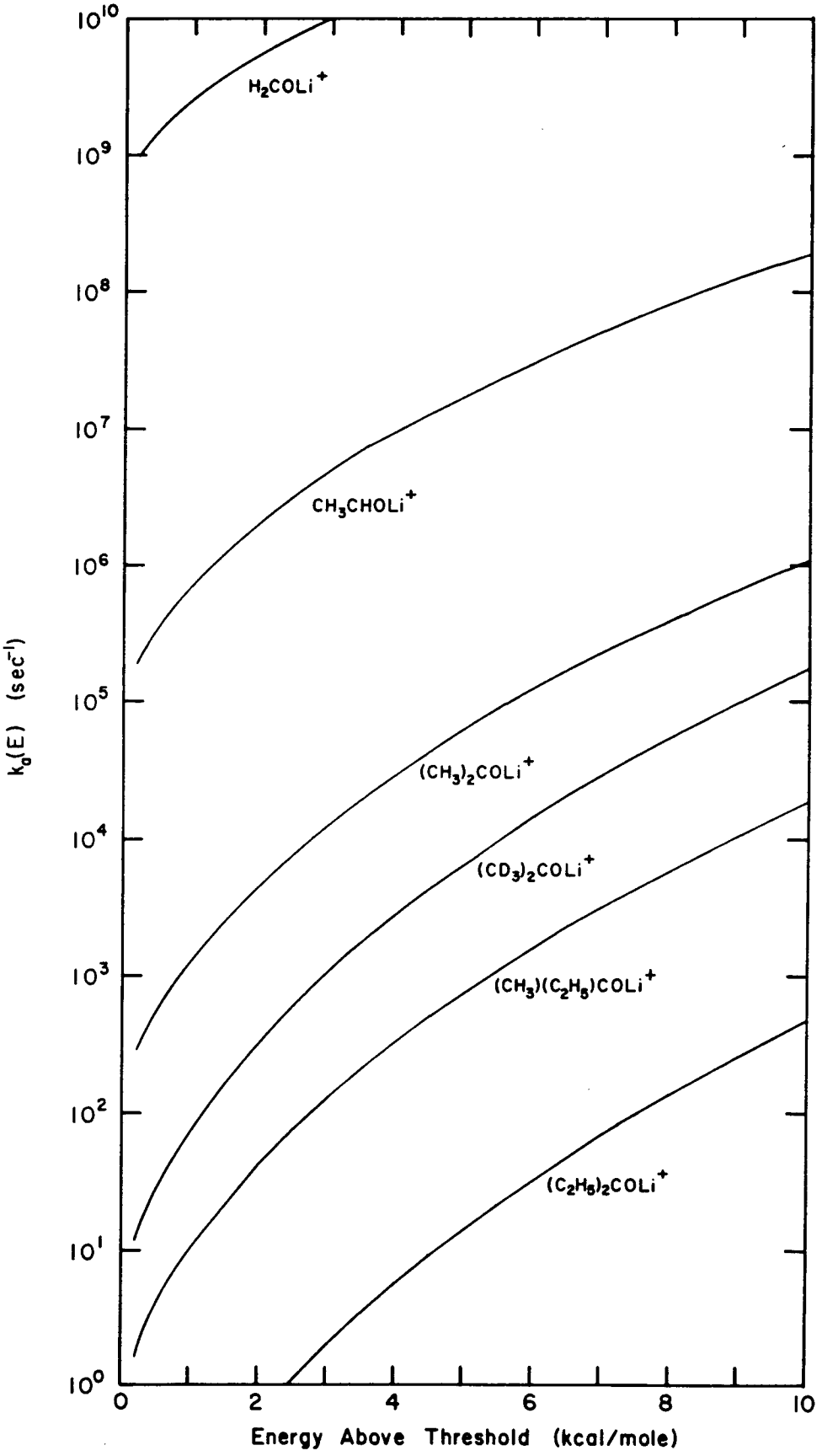
10^{10}
10^{9}
10^{8}
10^{7}
10^{6}
10^{5}
10^{4}
10^{3}
10^{2}
10^{1}
10^{0}
$k_d(E)$ (sec^{-1})
H_2COLi^+
CH_3CHOLi^+
$(CH_3)_2COLi^+$
$(CD_3)_2COLi^+$
$(CH_3)(C_2H_5)COLi^+$
$(C_2H_5)_2COLi^+$
0
2
4
6
8
10
Energy Above Threshold (kcal/mole)

4. Results and Discussion

4.1. Experimental determination of k_2

Figure 3 displays a typical trapped-ion spectrum of Li^+ attachment to $(C_2H_5)_2CO$ at a pressure of 3×10^{-7} Torr. Observed processes are those given by reactions (18)-(20). BLi^+ and B_2Li^+ are directly

$$B + Li^+ \rightarrow BLi^+ \tag{18}$$

$$B + BLi^+ \rightarrow B_2Li^+ \tag{19}$$

$$B + B_2Li^+ \rightarrow B_3Li^+ \tag{20}$$

observed. To measure the Li^+ signal a delayed ejection double resonance [16] technique is used. The B_2Li^+ ion is monitored at a trapping time such that BLi^+ has reacted away and B_3Li^+ has not formed to an appreciable extent; typically 900-1000 msec. The concentration of B_2Li^+ under these conditions should equal the initial Li^+ concentration $[Li^+]_0$. Ejecting all Li^+ ions in the trap at a given time causes the B_2Li^+ signal to decrease by an amount equal to the concentration of Li^+ in the trap at that time. A plot of $[Li^+]$ versus time is obtained by scanning the Li^+ ejection time and utilizing eq. (21).

$$[Li^+] = [Li^+]_0 - [B_2Li^+]_{ej} \tag{21}$$

$[B_2Li^+]_{ej}$ is the concentration of B_2Li^+ remaining after Li^+ is ejected. Since neutral pressures are approximately a factor of 10^5 larger than ion concentrations, pseudo-first order kinetics apply. Semi-logarithmic plots of $[Li^+]$ versus time (found to be linear over two orders of magnitude) yield k_2 from their slopes. Agreement between

FIGURE 3

Typical trapped ion data from $(C_2H_5)_2CO$ experiment. $(C_2H_5)_2CO$ pressure is 3×10^{-7} Torr. The plot of $[Li^+]$ is obtained by a delayed ejection experiment as discussed in section 4.1. Li^+ ions are formed in the first 10 msec.

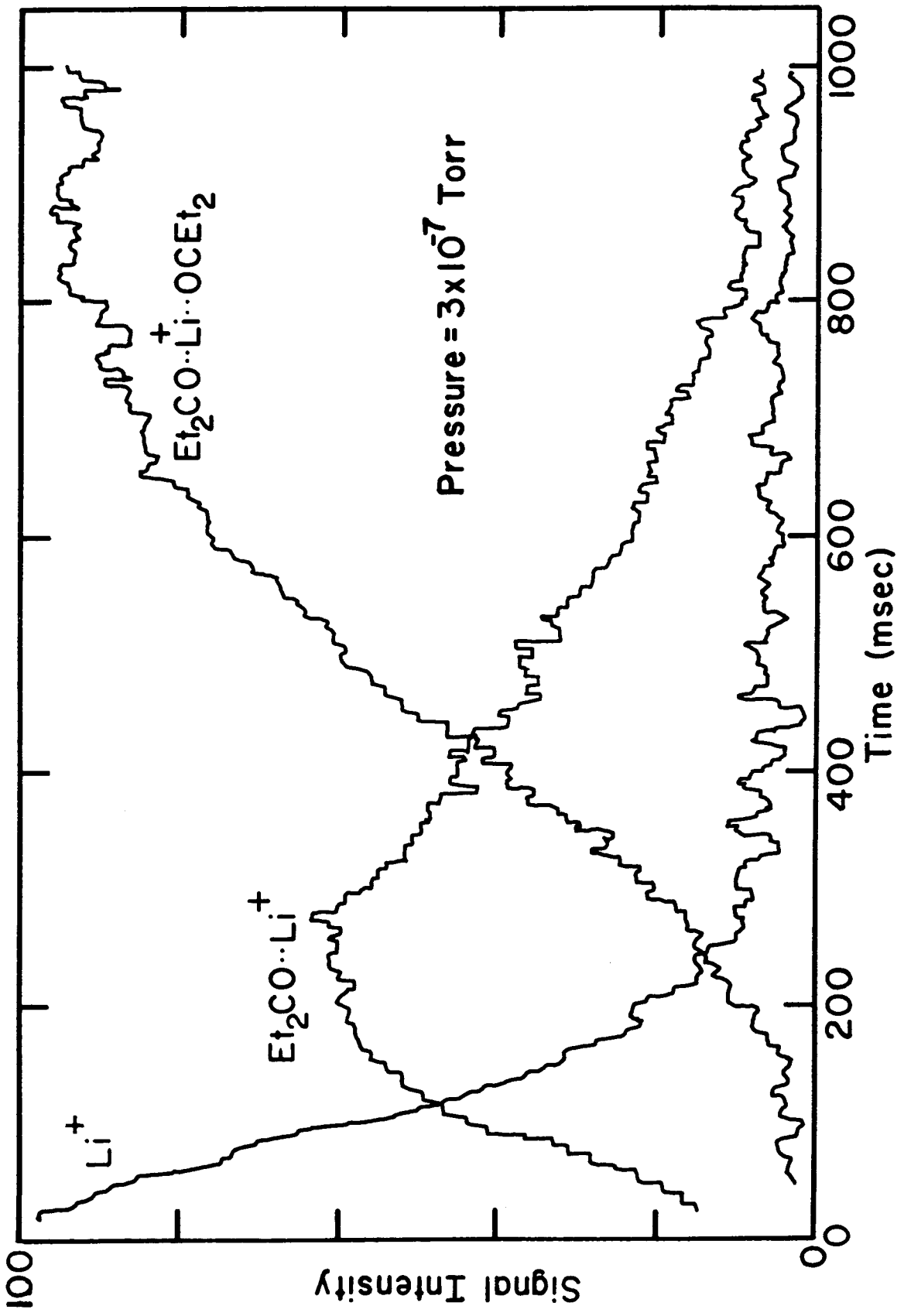
100
0
Signal Intensity
0
200
400
600
800
1000
Time (msec)
Pressure = 3x10^-7 Torr
Li+
Et2CO··Li+
Et2CO··Li··OCEt2+

k_2 determined from Li^+ decay and from total product formation (a less precise method) is within 10%. Rate constants determined for Li^+ attachment to $(C_2H_5)_2CO$, $(CH_3)(C_2H_5)CO$, $(CH_3)_2CO$ and $(CD_3)_2CO$ from trapped ion experiments are presented in Table 2. The rate constants in Table 2 are found to be independent of pressure in the range from 10^{-7} to 10^{-6} Torr (~ 6 collisions sec^{-1} to ~ 60 collisions sec^{-1}). Higher pressures could not be investigated in trapped ion experiments because of excessive ion loss and competitive formation of B_3Li^+.

Reactions of H_2CO and CH_3CHO with Li^+ are too slow to be studied by trapped ion techniques and are studied in drift mode. Over the pressure range of 10^{-5} to 10^{-3} Torr, Li^+ attachment rates are observed to increase with pressure. Because of Li^+ filament instability at higher pressures these studies were not extensively pursued. Table 3 presents measured rate constants for formation of H_2COLi^+ and CH_3CHOLi^+ at pressures of 2×10^{-3} Torr and 3×10^{-5} Torr, respectively.

4.2. Calculation of k_2

In order to utilize the quantities $k_r(E)$ and $k_a(E)$ calculated in sections 3.1 and 3.2 to calculate $k_2(E)$ [eq. (4)], rate constants for formation, k_f, and collisional stabilization, k_s, are needed. For ion-molecule reactions involving polar neutrals, collision rates are generally calculated according to average-dipole-orientation (ADO) theory [36]. However, due to the orientation of the carbonyl group and bulky alkyl groups, it is probable that not every collision results

Table 2

Calculated and experimental rate constants k_2[(a)] for $Li^+ + B \rightarrow BLi^+$; $(CH_3)_2CO$, $(CD_3)_2CO$, $CH_3COC_2H_5$, $(C_2H_5)_2CO$

	k_2 ($k_r \neq 0$)		k_2 ($k_r = 0$)		
	@ 1×10^{-7} Torr	@ 1×10^{-6} Torr	@ 1×10^{-7} Torr	@ 1×10^{-6} Torr	k_2(Exp.)[(b)]
$(C_2H_5)_2CO$	1.37	1.45	1.37	1.85	1.37 ± 0.56
$CH_3COC_2H_5$	0.79	0.97	0.46	1.12	0.84 ± 0.16
$(CH_3)_2CO$	0.10	0.16	0.02	0.15	0.30 ± 0.15
$(CD_3)_2CO$	0.43	0.59	0.18	0.63	0.22 ± 0.12

(a) Units are 10^{-9} cm^3 $molecule^{-1}$ sec^{-1}.

(b) Quoted errors are for one standard deviation. Average of measurements up to 10^{-6} Torr, performed in trapped ion mode.

Table 3

Calculated and experimental rate constants[a] for $Li^+ + B \rightarrow BLi^+$; H_2CO and CH_3CHO

B	k_2 ($k_r \neq 0$)	k_2 ($k_r = 0$)	k_2 (Exp.)[b]
CH_3CHO	1.7×10^{-2}	$1.7 \quad 10^{-2}$	$(8.1 \pm 1.0) \times 10^{-3}$
H_2CO	1.7×10^{-4}	1.7×10^{-4}	$(7.4 \pm 2.0) \times 10^{-4}$

(a) Units are 10^{-9} cm^3 $molecule^{-1}$ sec^{-1}. CH_3CHO calculations and experimental data for $[CH_3CHO] = 3 \times 10^{-5}$ Torr, H_2CO calculations and experimental data for $[H_2CO] = 2 \times 10^{-3}$ Torr.

(b) Quoted errors are for one standard deviation. These measurements carried out in drift mode.

in formation of an adduct. From Fig. 2 it is apparent that k_a for $[(C_2H_5)_2COLi^+]^{\ddagger}$ is very small at all energies of interest. Hence for $(C_2H_5)_2CO$ k_2 equals k_f. For the rest of the systems studied, ADO collision rates are scaled by a factor of 0.278 which is equal to k_2/k_{ADO} for $(C_2H_5)_2CO$. Since the vibrationally excited adduct is close to the decomposition threshold, a single collision is assumed adequate for stabilization with respect to dissociation, hence collision rate constants calculated from ADO theory are used for k_s. Table 4 presents the calculated ADO rate constant $k_f(ADO)$ and scaled values k_f. Also included are calculated ADO stabilization rate constants k_s.

Comparison of calculated $k_2(E)$ with measured rate constants requires averaging $k_2(E)$ over the internal energy distribution of $[BLi^+]^{\ddagger}$ adduct. Assuming the internal energy distribution of $[BLi^+]^{\ddagger}$ is the same as the neutral species B displaced in energy by the reaction exothermicity, $D_0(B\text{-}Li^+)$ [37], the averaged k_2 is calculated from eq. (22) where K(E) is the Boltzmann factor [33] for molecule B

$$k_2 = \int_{E_0}^{\infty} k_2(E)\,K(E-E_0)dE \qquad (22)$$

calculated from eq. (23). N(E) is the density of vibrational states at

$$K(E) = \frac{N(E)e^{-E/kT}}{\int_0^{\infty} N(E)e^{-E/kT}dE} \qquad (23)$$

energy E for the neutral species B. The Whitten-Rabinovitch approximation is used to calculated N(E) for $(C_2H_5)_2CO$, $(CH_3)(C_2H_5)CO$, $(CH_3)_2CO$ and $(CD_3)_2CO$. A direct count of vibrational states is used

Table 4

Forward rate constants k_f and collisional stabilization rate constants k_s [a]

Molecule	k_f(ADO) [b]	k_f [c]	k_s [b]
$(C_2H_5)_2CO$	4.92	1.37	1.87
$CH_3COC_2H_5$	4.81	1.35	1.98
$(CH_3)_2CO$	4.74	1.33	2.18
$(CD_3)_2CO$	4.71	1.32	2.08
CH_3CHO	4.41	1.24	2.23
H_2CO	3.57	1.00	2.09

(a) Units are 10^{-9} cm^3 $molecule^{-1}$ sec^{-1}.

(b) Calculated according to ADO theory [36]. Dipole moments are from ref. [39]. Polarizabilities for H_2CO, CH_3CHO and $(CH_3)_2CO$ are from ref. [40]. Polarizabilities for $CH_3COC_2H_5$ and $(C_2H_5)_2CO$ are from ref. [41]. The dipole moment and polarizability of $(CD_3)_2CO$ are assumed the same as for $(CH_3)_2CO$.

for H_2CO and CH_3CHO. Calculated values of k_2 for the trapped ion experiments using data from Figs. 1 and 2, Table 4 and averaged according to eq. (22) are presented in Table 2. Included for comparison are values of k_2 calculated assuming spontaneous emission does not occur ($k_r = 0$). Comparable results for higher pressure experiments with H_2CO and CH_3CHO, calculated at 2×10^{-3} and 3×10^{-5} Torr, respectively, are shown in Table 3. It is clear from Table 2 that data calculated excluding radiative stabilization exhibit termolecular behavior and are too small in magnitude compared to experiment. Data calculated including radiative stabilization are seen to exhibit bimolecular behavior, as observed experimentally. The pressure dependence of k_2 when k_r is included is comparable to the experimental uncertainty in the measured rate constants, while excluding k_r results in a pressure dependence which is too large when compared with experiment. It is not possible to totally exclude collisional stabilization since collisions do occur at a rate of about $5\ sec^{-1}$ at 10^{-7} Torr. In either case it is clear that the lifetimes of intermediates can easily be long enough for infrared radiative stabilization to be important. The present work does not prove that infrared emission is responsible for adduct stabilization; observation of infrared emission would be required. However, the calculations indicate that radiative stabilization is a reasonable deactivation mechanism at low pressure, and the observed pressure dependence supports this conclusion.

The calculations for k_2 at higher pressure for H_2CO and CH_3CHO

(Table 3) are in reasonable agreement with measured rate constants. Differences are most likely due to errors in pressure determination, difficulties associated with rate constant measurement in drift mode experiments [16, 39] and errors in estimating k_f. In Table 3 there is no difference between k_2 calculated with and without k_r. For H_2CO and CH_3CHO the decomposition rates are large enough (section 3.2, Fig. 2) that radiative processes (section 3.1) cannot compete. Thus under conditions where H_2COLi^+ and CH_3CHOLi^+ are observed $k_r \ll k_s$ [M] and k_r does not contribute to the stabilization process.

The discrepancy between calculated rate constants for $(CH_3)_2CO$ and $(CD_3)_2CO$ association with Li^+ illustrates the sensitivity of the calculations to the decomposition lifetime when k_r competes closely with k_a. $(C_2H_5)_2COLi^+$ and $(CH_3)(C_2H_5)COLi^+$ represent a "large molecule" limit for which $k_r > k_a$ and hence nearly every complex formed is stabilized. Similarly, CH_3CHO and H_2CO represent a "small molecule" limit in which k_a is very large compared to k_r and hence few complexes are stabilized. However, for $(CH_3)_2COLi^+$ and $(CD_3)_2COLi^+$, k_a and k_r compete closely and hence the overall rate constant becomes very sensitive to the RRKM calculation.

5. Conclusions

Results of this work support postulated infrared radiative stabilization mechanisms proposed for molecular synthesis in interstellar space. While observation of infrared emission would be necessary to prove the infrared emission mechanism, the pressure dependence of k_2 at very low pressure (Table 2) indicates that collisional stabilization is not occuring and radiative stabilization may be important. It is of interest to note that while $k_r(E)$ varies between 50 and 100 sec^{-1} for all compounds studied (at typical energies), Fig. 1, $k_a(E)$ varies over nine orders of magnitude depending on molecular complexity, Fig. 2. Since $k_r(E)$ depends mainly on energy released into the adduct from reaction exothermicity, energy present in molecule B prior to adduct formation is relative unimportant and $k_r(E)$ is not strongly temperature dependent. $k_a(E)$ depends directly upon energy in the adduct in excess of the decomposition threshold, Fig. 2, and hence on the internal energy of the neutral prior to reaction. The internal energy of species B is determined by its temperature and hence $k_a(E)$ is strongly temperature dependent. At sufficiently low temperatures the large and small molecule distinctions (section 4) begin to lose meaning as decomposition occurs closer and closer to threshold and dissociation lifetimes become very large. Under conditions found in interstellar space where temperatures are typically less than 100°K radiative stabilization may become effective enough that k_2 approaches the gas kinetic limit, even for small molecules [14].

Acknowledgments

R. L. W. would like to thank F. H. Houle and Dr. R. R. Corderman for many helpful discussions during the course of this study. This work was supported in part by the United States Department of Energy Grant EX-76-G-03-1305, Exxon Corp. and the Ford Motor Co. Fund for Energy Research administered by the California Institute of Technology.

References

[1] T. Su and M. T. Bowers, Int. J. Mass Spectrom. Ion Phys. 12 (1973) 347.

[2] M. S. Foster and J. L. Beauchamp, Chem. Phys. Lett. 31 (1975) 482.

[3] M. K. Murphy and J. L. Beauchamp, J. Am. Chem. Soc. 98 (1976) 5781.

[4] W. N. Allen and F. W. Lampe, J. Am. Chem. Soc. 99 (1977) 6816; W. N. Allen and F. W. Lampe, ibid. 99 (1977) 2943.

[5] E. Herbst and W. Klemperer, Phys. Tod. June (1976) 32.

[6] J. I. Steinfeld, Molecules and radiation, an introduction to modern molecular spectroscopy (MIT Press, Cambridge, Massachusetts, 1974) p. 28.

[7] A. Dalgarno and J. H. Black, Rep. Prog. Phys. 39 (1976) 573.

[8] G. Herzberg, Molecular spectra and molecular structure (Van Nostrand Reinhold Company, New York, 1945) Vol. 2.

[9] E. Herbst, Astrophys. J. 205 (1976) 94.

[10] E. Herbst and W. Klemperer, Astrophys. J. 185 (1973) 505.

[11] D. A. Williams, Astrophys. Lett. 10 (1971) 17.

[12] F. C. Fehsenfeld, D. B. Dunkin and E. E. Ferguson, Astrophys. J. 188 (1974) 43.

[13] D. Smith and N. G. Adams, Astrophys. J. 217 (1977) 741.

[14] D. Smith and N. G. Adams, Astrophys. J. 220 (1978) L87.

[15] G. F. Mitchell, Astrom. Astr. 55 (1977) 303.

[16] J. L. Beauchamp, Ann. Rev. Phys. Chem. 22 (1971) 527; T. A. Lehman and M. M. Bursey, Ion cyclotron resonance spectroscopy (John Wiley and Sons, Inc., New York, 1976); T. B. McMahon and J. L. Beauchamp, Rev. Sci. Instr., 43 (1972) 509.

[17] R. H. Staley and J. L. Beauchamp, J. Am. Chem. Soc. 97 (1975) 5920; R. L. Woodin and J. L. Beauchamp, J. Am. Chem. Soc. 100 (1978) 501.

[18] R. L. Woodin, F. A. Houle and W. A. Goddard III, Chem. Phys. 14 (1976) 461.

[19] G. H. F. Diercksen, W. P. Kraemer and B. O. Roos, Theoret. Chim. Acta 36 (1975) 249.

[20] R. V. Hodges and J. L. Beauchamp, Anal. Chem. 48 (1976) 825.

[21] R. C. Dunbar, Spectrochim. Acta 31A (1975) 797.

[22] K. E. Seshadri and R. N. Jones, Spectrochim. Acta 19 (1963) 1013.

[23] T. Shimanouchi, Tables of molecular vibrational frequencies consolidated (National Bureau of Standards, NSRDS-NBS 39, 1972), Vol. 1.

[24] Z. Buric and P. J. Krueger, Spectrochim. Acta 30A (1974) 2069.

[25] V. I. Vakhlyueva, A. G. Finkel, L. M. Sverdlov and A. I. Andreeva, Opt. Spectrosc. 25 (1968) 234.

[26] V. I. Vakhlyueva, A. G. Finkel, L. M. Sverdlov and L. A. Zaitseva, Opt. Spectrosc. 25 (1968) 160.

[27] E. S. Ebers and Harold Nielson, J. Chem. Phys. 5 (1937) 822.

[28] H. W. Thompson and P. Torkington, J. Chem. Soc. (1945) 640.

[29] L. O. Dworjanyn, Aust. J. Chem. 13 (1960) 175.

[30] K. S. Pitzer and W. Weltner, Jr., J. Am. Chem. Soc. 71 (1949) 2842.

[31] R. E. Pennington and K. A. Kobe, J. Am. Chem. Soc. 79 (1957) 300.

[32] J. K. Nickerson, K. A. Kobe and J. J. McKetta, J. Phys. Chem. 65 (1961) 1037.

[33] P. J. Robinson and K. A. Holbrook, Unimolecular reactions (John Wiley and Sons, Ltd., London, 1972).

[34] W. J. Chesnavich and M. T. Bowers, J. Am. Chem. Soc. 98 (1976) 8301; W. J. Chesnavich and M. T. Bowers, ibid., 99 (1977) 1705.

[35] W. N. Olmstead, M. Lev-On, D. M. Golden and J. I. Brauman, J. Am. Chem. Soc. 99 (1977) 992.

[36] L. Bass, T. Su, W. J. Chesnavich and M. T. Bowers, Chem. Phys. Lett. 34 (1975) 119.

[37] R. J. McCluskey and R. W. Carr, Jr., Int. J. Chem. Kinet. 10 (1978) 171.

[38] S. E. Buttrill, Jr., J. Chem. Phys. 50 (1969) 4125.

[39] A. L. McClellan, Tables of experimental dipole moments (W. H. Freeman and Company, San Francisco, 1963).

[40] J. Applequist, J. R. Carl and K. K. Fung, J. Am. Chem. Soc. 94 (1972) 2952.

[41] J. A. Beran and L. Kevan, J. Phys. Chem. 73 (1969) 3860.

CHAPTER V

Formation of Interstellar Molecules by Bimolecular Association Reactions: Experimental Evidence for Infrared Radiative Stabilization in Laboratory Studies

R. L. Woodin* and J. L. Beauchamp

Contribution No. 5934 from the Arthur Amos Noyes Laboratory of Chemical Physics, California Institute of Technology, Pasadena, California 91125

*Present address: Exxon Research and Engineering Co., Corporate Research Laboratories, Linden, New Jersey 07036.

ABSTRACT

Ion cyclotron resonance techniques are used to observe direct clustering of Li^+ with $(C_2H_5)_2CO$, $CH_3COC_2H_5$, $(CH_3)_2CO$, $(CD_3)_2CO$, CH_3CHO, and H_2CO. Initial interaction of Li^+ with the carbonyl compound leads to formation of a vibrationally excited adduct. For several of the molecules, adduct formation is observed to be bimolecular at pressures low enough ($< 10^{-6}$ Torr) such that the collisional stabilization of the vibrationally excited species is unlikely. Experimental results are interpreted in terms of an infrared radiative stabilization mechanism, and calculated attachment rate constants are in good agreement with experiment. The present results are discussed in terms of the significance of infrared radiative association reactions for molecular synthesis in interstellar space.

As increasingly complex molecules are discovered in interstellar space, the question of their origin becomes more and more intriguing. Molecules containing up to nine carbon atoms have been discovered to date (Gammon, 1978). A number of mechanisms have been suggested to explain synthesis of large molecules in interstellar space, including bimolecular processes (Herbst and Klemperer, 1973) and reactions on grain surfaces (Dalgarno and Black, 1976). Since high-energy stellar radiation ionizes an appreciable fraction of the atoms and molecules, and ion-molecule reactions often do not have appreciable activation energies (Su and Bowers, 1973), ion-molecule association reactions may occur as in process (1). The species $[AB^+]^\ddagger$ is usually a

$$A^+ + B \xrightarrow{k_f} [AB^+]^\ddagger \qquad (1)$$

vibrationally excited adduct (Herbst, 1976); in some cases the excitation is electronic (Black and Dalgarno, 1973). Collisional stabilization of the energy-rich species $[AB^+]^\ddagger$, eq. (2), is unlikely because of the

$$[AB^+]^\ddagger + M \xrightarrow{k_f} AB^+ + M \qquad (2)$$

extremely low pressures (10 to 10^7 particles cm^{-3}) characteristic of interstellar space (Herbst and Klemperer, 1976). In the absence of collisional stabilization one of three processes may occur: unimolecular decomposition to reactants, eq. (3), unimolecular decomposition to products different from reactants, eq. (4), and radiative stabilization, eq. (5). Process (3) results in no net reaction. Reactions such as (4)

$$[AB^+]^{\ddagger} \longrightarrow A^+ + B \quad (3)$$

$$[AB^+]^{\ddagger} \longrightarrow C^+ + D \quad (4)$$

$$[AB^+]^{\ddagger} \longrightarrow AB^+ + h\nu \quad (5)$$

have been assumed for a variety of species, for example, eq. (6)

$$CN + H_3^+ \rightarrow HCN^+ + H_2 \quad (6)$$

(Herbst and Klemperer, 1973). In cases where the lifetime with respect to dissociation of $[AB^+]^{\ddagger}$ is relatively long, emission of radiation [eq. (5)] may be an important stabilization mechanism (Williams, 1971). Electronic radiative stabilization is proposed for formation of CH^+ and CH_2^+ in interstellar space (Black and Dalgarno, 1973), while vibrational radiative stabilization is proposed for a number of reactions, eqs. (7)-(11), (Smith and Adams, 1977; Smith and Adams, 1978; Herbst, 1976). Laboratory investigations of such

$$CH_3^+ + H_2 \rightarrow CH_5^+ + h\nu \quad (7)$$

$$CH_3 + NH_3 \rightarrow CH_3 \cdot NH_3^+ + h\nu \quad (8)$$

$$CH_3^+ + H_2O \rightarrow CH_3 \cdot OH_2^+ + h\nu \quad (9)$$

$$H_2CN^+ + H_2 \rightarrow H_4CN^+ + h\nu \quad (10)$$

$$H_4CN^+ + H_2 \rightarrow H_6CN^+ + h\nu \quad (11)$$

reactions are difficult due to the usually short lifetime of $[AB^+]^{\ddagger}$ intermediates. Most studies of radiative association processes use high pressure data to calculate dissociation lifetimes which are then used in conjunction with estimates of radiative rates to calculate overall bimolecular radative association rate constants (Smith and

Adams, 1977; Smith and Adams, 1978).

The techniques of ion cyclotron resonance spectroscopy (ICR) appear to be uniquely suited for studying processes such as (5) under nearly collision-free conditions (Beauchamp, 1971; Lehman and Bursey, 1976). We report here observation of association reactions of Li^+ to $(C_2H_5)_2CO$, $CH_3COC_2H_5$, $(CH_3)_2CO$, $(CD_3)_2CO$, CH_3CHO and H_2CO in ICR experiments. Experimentally determined rate constants are modeled using an infrared radiative stabilization mechanism. Details of the calculations will be published elsewhere (Woodin and Beauchamp, 1979).

Reactions of Li^+ with Lewis bases such as alkyl ketones follow processes (12)-(14), where B is a Lewis base. No decomposition

$$Li^+ + B \rightarrow BLi^+ \quad (12)$$

$$BLi^+ + B \rightarrow B_2Li^+ \quad (13)$$

$$B_2Li^+ + B \rightarrow B_3Li^+ \quad (14)$$

processes [such as (4)] are observed. Figure 1 shows a trapped ion plot for Li^+ with $(C_2H_5)_2CO$. Li^+ ions are generated by thermionic emission from a glass bead filament (Hodges and Beauchamp, 1976). All experiments are carried out at ambient temperature. Decay of the Li^+ signal plotted on a semi-logarithmic scale as a function of time is linear, and the slope in conjunction with the neutral pressure provides the apparent bimolecular rate constant for reaction (12). Results for Li^+ association with $(C_2H_5)_2CO$, $CH_3COC_2H_5$, $(CH_3)_2CO$ and $(CD_3)_2CO$ are given in Table I. Of particular importance is that these rate

FIGURE 1

Typical trapped ion data from $(C_2H_5)_2CO$ experiment. Li^+ ions generated in the first 10 msec react to form $(C_2H_5)_2COLi^+$, which in turn reacts to form $[(C_2H_5)_2CO]_2Li^+$.

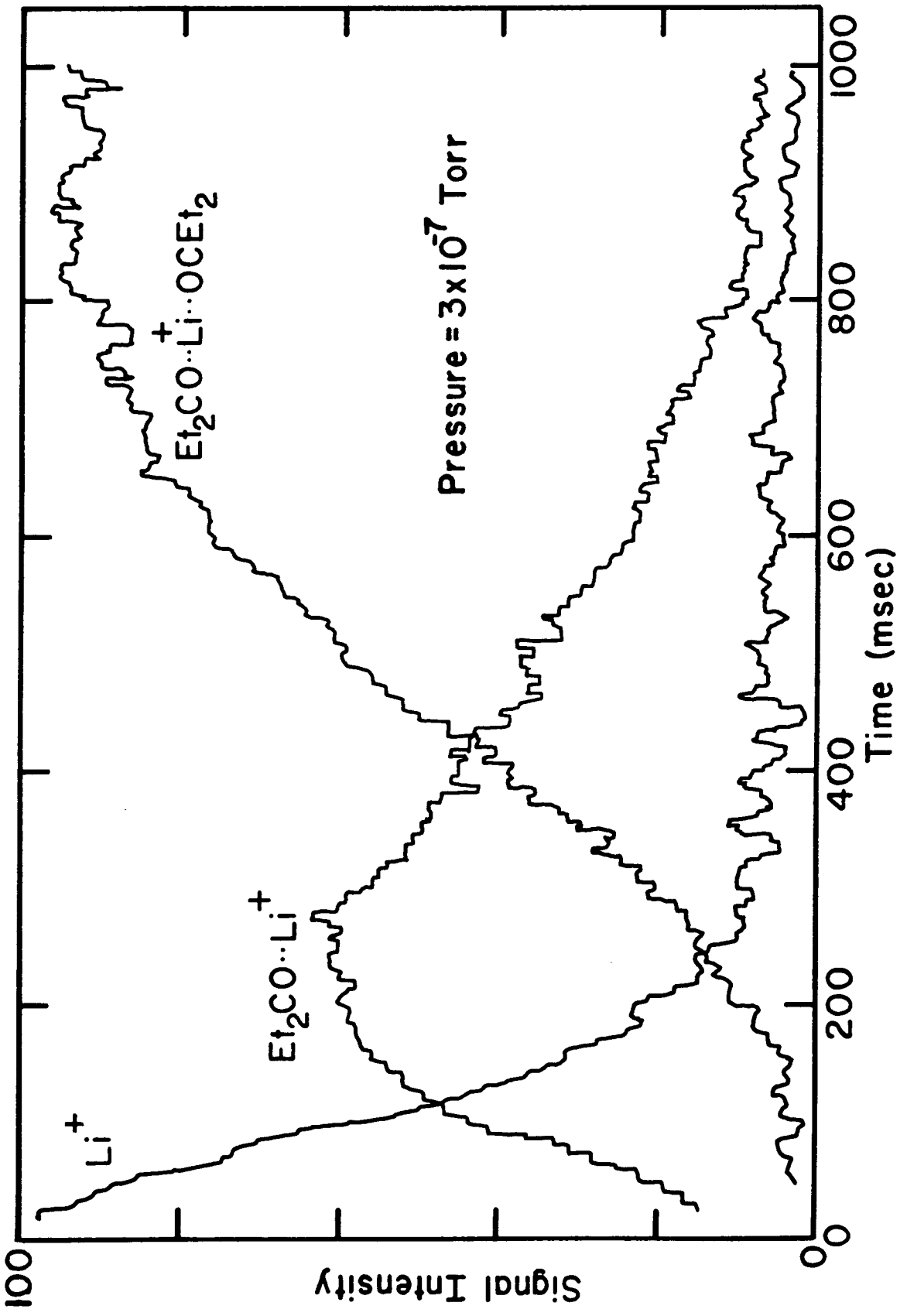
100
0
Signal Intensity
0
200
400
600
800
1000
Time (msec)
Pressure = 3x10⁻⁷ Torr
Li+
Et2CO··Li+
Et2CO··Li··OCEt2+

TABLE I

Calculated and experimental association rate constants k_2[(a)] for $Li^+ + B \rightarrow BLi^+$; $(C_2H_5)_2CO$, $CH_3COC_2H_5$, $(CH_3)_2CO$ and $(CD_3)_2CO$

B	k_f[(b)]	$k_2(k_r \neq 0)$[(c)]		$k_2(k_r = 0)$[(d)]		k_2(exp.)[(e)]
		@ 1×10^{-7} Torr	@ 1×10^{-6} Torr	@ 1×10^{-7} Torr	@ 1×10^{-6} Torr	
$(C_2H_5)_2CO$	4.92	1.37	1.45	1.37	1.85	1.37 ±0.56
$CH_3COC_2H_5$	4.81	0.79	0.97	0.46	1.12	0.84 ±0.16
$(CH_3)_2CO$	4.74	0.10	0.16	0.02	0.15	0.30 ±0.15
$(CD_3)_2CO$	4.71	0.43	0.59	0.18	0.63	0.22 ±0.12

(a) Units are 10^{-9} cm^3 $molecule^{-1}$ sec^{-1}

(b) Calculated according to ADO theory (Bass, et al., 1975).

(c) Calculated including radiative stabilization.

(d) Calculated excluding radiative stabilization.

(e) Average value of measurements at pressures up to 10^{-6} Torr. Quoted errors are for one standard deviation.

constants are independent of pressure from 10^{-7} to 10^{-6} Torr. Association reactions of Li^+ with CH_3CHO and H_2CO increase with increasing pressure at all pressures such that the adduct is observed. Data for CH_3CHO and H_2CO are given in Table II at 3×10^{-5} Torr and 2×10^{-3} Torr, respectively.

In order to calculate the overall bimolecular reaction rate constant, the mechanism of eq. (15) is used. The radiative rate $k_r(E)$

$$Li^+ + B \underset{k_a(E)}{\overset{k_f}{\rightleftharpoons}} [BLi^+]^{\ddagger} \xrightarrow{k_r(E)+k_s[B]} BLi^+ \qquad (15)$$

(Dunbar, 1975) and unimolecular dissociation rate $k_a(E)$ (Robinson and Holbrook, 1972) are both functions of the internal energy content, E, of $[BLi^+]^{\ddagger}$. k_f is the rate constant for formation of $[BLi^+]^{\ddagger}$ and k_s is the collisional stabilization rate constant. Assuming a steady-state concentration for $[BLi^+]^{\ddagger}$, the apparent bimolecular association rate, $k_2(E)$, for formation of BLi^+ is given by (16). Clearly, for radiative

$$k_2(E) = \frac{k_f(k_r(E) + k_s[B])}{k_r(E) + k_a(E) + k_s[B]} \qquad (16)$$

stabilization to be important, the condition $k_r \gg k_s[B]$ must hold. Given the internal energy content of the chemically activated $[BLi^+]^{\ddagger}$ species, $k_r(E)$ may be calculated according to the method outlined by Dunbar (1975) and $k_a(E)$ is calculated by standard RRKM theory (Robinson and Holbrook, 1972). k_s and k_f are assumed to be the collisional rate constants calculated by ADO theory (Bass et al., 1975).

TABLE II

Calculated and experimental association rate constants k_2[(a)] for $Li^+ + B \rightarrow BLi^+$; CH_3CHO and H_2CO

B	k_f[(b)]	$k_2(k_r \neq 0)$[(c)]	$k_2(k_r = 0)$[(d)]	k_2(exp.)[(e)]
CH_3CHO	4.41	1.7×10^{-2}	1.7×10^{-2}	$(8.1 \pm 1.0) \times 10^{-3}$
H_2CO	3.57	1.7×10^{-4}	1.7×10^{-4}	$(7.4 \pm 2.0) \times 10^{-4}$

(a) Units are 10^{-9} cm^3 $molecule^{-1}$ sec^{-1}. CH_3CHO calculations and experimental data for $[CH_3CHO] = 3 \times 10^{-5}$ Torr; H_2CO calculations and experimental data for $[H_2CO] = 2 \times 10^{-3}$ Torr.

(b) Calculated according to ADO theory (Bass et al., 1975).

(c) Calculated including radiative stabilization.

(d) Calculated excluding radiative stabilization.

(e) Quoted errors are for one standard deviation.

The internal energy content of $[BLi^+]^{\ddagger}$ is given by the thermal energy content of B and $D_0(B\text{-}Li^+)$ which have been determined for a variety of Lewis bases (Staley and Beauchamp, 1975; Woodin and Beauchamp, 1978), and may be estimated for compounds not studied by considering trends of similar molecules. For the bases studied here, $D_0(B\text{-}Li^+)$ is given in Table III. For the decomposition of $[BLi^+]^{\ddagger}$ to reactants the activation energy is assumed to be $D_0(B\text{-}Li^+)$, and centrifugal effects are not considered. A variety of calculations assuming different transition states give essentially the same results.

Assuming that the presence of Li^+ does not appreciably perturb the Lewis base (Woodin et al., 1976; Diercksen et al., 1975), then integrated absorption intensities and thermodynamic functions of B may be used to approximate those of BLi^+. Calculated values of $k_r(E)$ vary almost linearly with energy. Table III shows $k_r(E)$ for the ions when the internal energy equals $D_0(B\text{-}Li^+)$ and assuming that emission of a single photon stabilizes the adduct with respect to dissociation.

Vibrational frequencies of species such as BLi^+ are not known. However, since li^+ is found not to perturb the base (Woodin et al., 1976, Diercksen et al., 1975), vibrational frequencies of B may be used with the addition of suitable frequencies associated with the $B\text{-}Li^+$ bond. Values of $O\text{-}Li^+$ frequencies estimated for H_2OLi^+ (Diercksen et al., 1975) of 520 cm^{-1}, 450 cm^{-1} and 390 cm^{-1} are used here in all cases. The 520 cm^{-1} $B\text{-}Li^+$ stretch is assumed to be the reaction coordinate. Calculated results for $k_a(E)$ are plotted as a function of excess energy above threshold in Fig. 2 for $(C_2H_5)_2COLi^+$,

TABLE III

$D_0(B\text{-}Li^+)$ and k_r calculated at $D_0(B\text{-}Li^+)$ for the Li^+ complexes considered in this work

Complex	$D_0(B\text{-}Li^+)$[a]	k_r[b]
H_2COLi^+	36.0	58
CH_3CHOLi^+	41.7	57
$(CH_3)_2COLi^+$	44.6	45
$(CD_3)_2COLi^+$	44.6	44
$(CH_3)(C_2H_5)COLi^+$	46.0	40
$(C_2H_5)_2COLi^+$	47.0	37

(a) Units are kcal/mole.

(b) Units are sec^{-1}. Calculated at an energy equal to $D_0(B\text{-}Li^+)$.

FIGURE 2

RRKM unimolecular dissociation rates $k_a(E)$ as a function of internal energy in excess of decomposition threshold. The dissociation process is $[BLi^+]^{\ddagger} \rightarrow B + Li^+$.

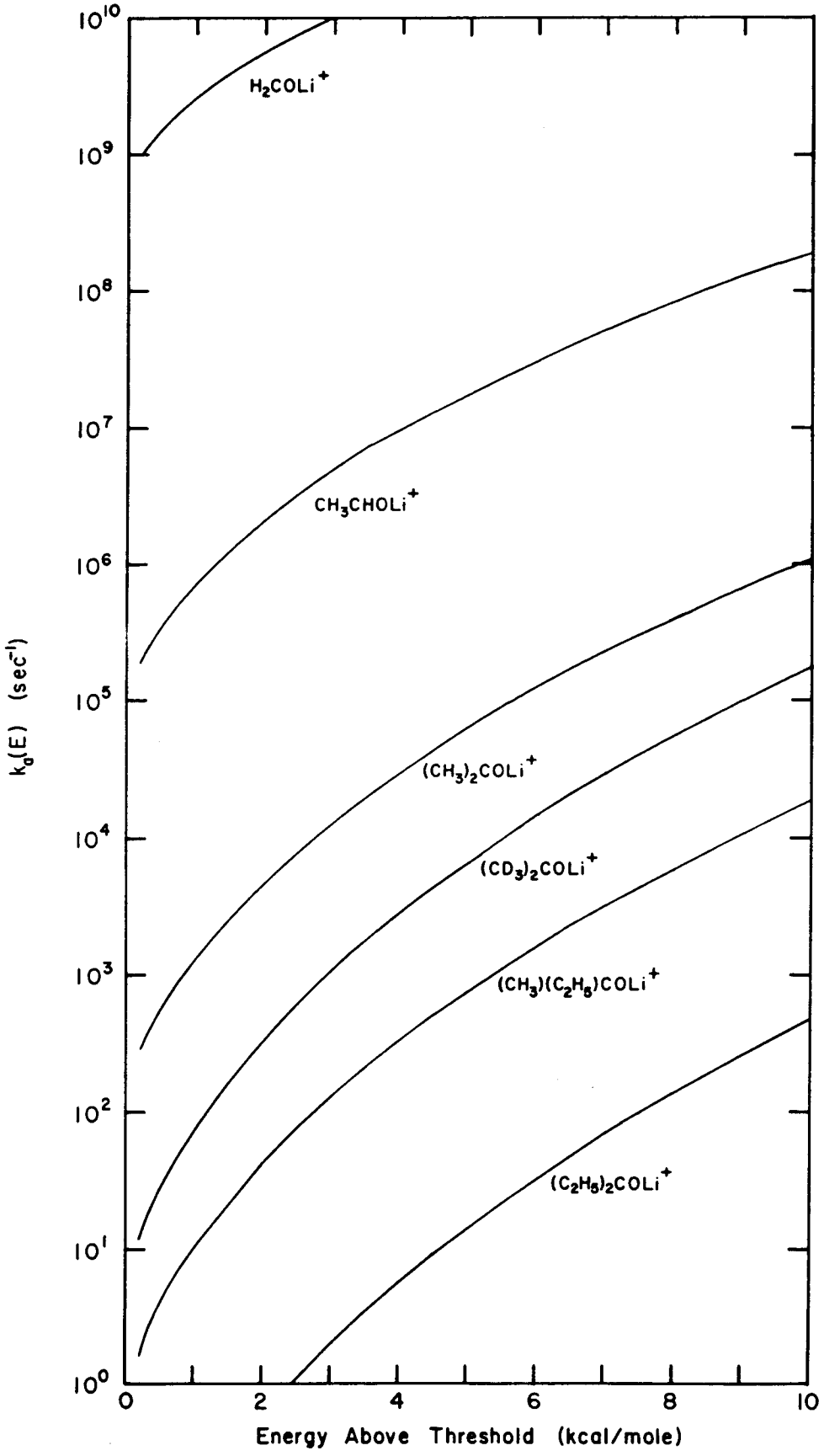
10^{10}
10^{9}
10^{8}
10^{7}
10^{6}
10^{5}
10^{4}
10^{3}
10^{2}
10^{1}
10^{0}
$k_d(E)$ (sec^{-1})
H_2COLi^+
CH_3CHOLi^+
$(CH_3)_2COLi^+$
$(CD_3)_2COLi^+$
$(CH_3)(C_2H_5)COLi^+$
$(C_2H_5)_2COLi^+$
0
2
4
6
8
10
Energy Above Threshold (kcal/mole)

$(CH_3)(C_2H_5)COLi^+$, $(CH_3)_2COLi^+$, $(CD_3)_2COLi^+$, CH_3CHOLi^+, and H_2COLi^+. It is apparent from Figure 2 and Table III that radiative processes compete favorably with dissociation at energies near threshold.

Combining calculated values for $k_r(E)$, $k_a(E)$ and $k_s[B]$ and k_f at a given pressure allows calculation of $k_2(E)$, eq. (16). Tables I and II include ADO rate constants for k_f. That the ADO rate constant for $(C_2H_5)_2CO$ is approximately a factor of three larger than the experimental value of k_2 indicates that not every collision forms an adduct, since from Figure 2, $k_a(E)$ is small for $(C_2H_5)_2COLi^+$ and from eq. (16) k_2 should equal k_f. To take this effect into account values of k_f used to calculate $k_2(E)$ are from ADO rate constants scaled appropriately to give the correct value for $(C_2H_5)_2COLi^+$. Averaging $k_2(E)$ over the Boltzmann distribution of B prior to reaction (Robinson and Holbrook, 1972) gives a value for k_2 to compare with experiment. Table I shows calculated apparent rate constants, k_2, for pressures of 10^{-7} and 10^{-6} Torr ($\sim$6 collisions sec^{-1} and $\sim$60 collisions sec^{-1}) with and without radiative stabilization. Table II includes results for k_2 calculated with and without infrared emission at appropriate pressures.

The calculated rate constants agree well for $(C_2H_5)_2COLi^+$, $(CH_3)(C_2H_5)COLi^+$, $(CH_3)_2COLi^+$ and $(CD_3)_2COLi^+$ when radiative stabilization is included. The pressure dependence with infrared emission included also agrees with the experimental observation that these rate constants are bimolecular from 10^{-7} to 10^{-6} Torr. Excluding radiative processes results in termolecular behavior, in disagreement with experiment (Table I). These results support

radiative stabilization as a viable relaxation mechanism. The data in Table II show no effect of radiative processes upon the association rate constants for CH_3CHO and H_2CO. This is because for smaller molecules dissociation is fast compared to infrared emission (Figure 2 and Table III) and collisional stabilization is necessary to observe the adduct on the time scale of the experiment.

The present results do not prove the radiative association mechanism; observation of infrared emission would be required. However, the observed pressure dependence under nearly collisionless conditions strongly supports a radiative stabilization mechanism. The calculations indicate that molecular synthesis via radiative association may be facile under the low temperature conditions of interstellar space. While radiative rates depend on the total energy of the activated molecule, dissociation rates depend strongly on the excess energy above the decomposition threshold (Figure 2) which is derived mainly from the thermal energy content of molecule B. At typical interstellar temperatures of ~50K (Gammon, 1978) association complexes thus may have very long lifetimes before decomposition, allowing radiative stabilization to be effective. It is even possible that under suitable conditions association reactions may occur at the gas-kinetic rate (Smith and Adams, 1978), making radiative association reactions an efficient mechanism of molecular synthesis in interstellar space.

ACKNOWLEDGMENTS

This research supported in part by the United States Department of Energy Grant No. EX-76-G-03-1305, Exxon Corporation,and the Ford Motor Co. Fund for Energy Research administered by the California Institute of Technology.

REFERENCES

Bass, L., Su, T., Chesnavich, W. J., and Bowers, M. T., 1975, Chem. Phys. Lett., 34, 119.

Beauchamp, J. L., 1971, Ann. Rev. Phys. Chem., 22, 527.

Black, J. H., and Dalgarno, A., 1973, Astrophys. Lett., 15, 79.

Dalgarno, A., and Black, J. H., 1976, Rep. Prog. Phys., 39, 573.

Diercksen, W. P., Kraemer, W. P., and Roos, B. O., 1975, Theoret. Chim. Acta, 36, 249.

Dunbar, R. C., 1975, Spectrochim. Acta, 31A, 797.

Gammon, R. H., 1978, Chemical and Engineering News, Oct.2, 21.

Herbst, E., 1976, Astrophys. J., 205, 94.

Herbst, E., and Klemperer, W., 1973, Astrophys. J., 185, 505.

Herbst, E., and Klemperer, W., 1976, Phys. Tod., June, 32.

Hodges, R. V., and Beauchamp, J. L., 1976, Anal. Chem., 48, 825.

Lehman, T. A., and Bursey, M. M., 1976, Ion Cyclotron Resonance Spectroscopy, (New York; John Wiley and Sons).

Robinson, P. J., and Holbrook, K. A., 1972, Unimolecular Reactions, (London: John Wiley and Sons).

Smith, D., and Adams, N. G., 1977, Astrophys. J., 217, 741.

Smith, D., and Adams, N. G., 1978, Astrophys. J., 220, 187.

Staley, R. H., and Beauchamp, J. L., 1975, J. Am. Chem. Soc., 97, 5920.

Su, T., and Bowers, M. T., 1973, Int. J. Mass Spectrom. Ion Phys., 12, 347.

Williams, D. A., 1971, Astrophys. Lett., 10, 17.

Woodin, R. L., and Beauchamp, J. L., 1978, J. Am. Chem. Soc., 100, 501.

Woodin, R. L., and Beauchamp, J. L., 1979, Chem. Phys., to be submitted.

Woodin, R. L., Houle, F. A., and Goddard, W. A., III, 1976, Chem. Phys., 14, 461.

CHAPTER VI

Ion Cyclotron Resonance Studies of Radiative and Dissociative Electron Attachment Processes at Low Pressures

R. L. Woodin,[†] M. S. Foster,[‡] and J. L. Beauchamp

Contribution No. 5939 from the Arthur Amos
Noyes Laboratory of Chemical Physics
California Institute of Technology, Pasadena, California 91125

[†] Present address: Exxon Research and Engineering Company, Corporate Research Laboratories, Linden, New Jersey 07036.

[‡] Present address: Chevron Research Company, Richmond, California 94802.

ABSTRACT

Ion cyclotron resonance spectroscopy is used to measure non-dissociative electron attachment rate constants for C_6F_6 (perfluorobenzene), C_7F_8 (perfluorotoluene), c-C_4F_8 (perfluorocyclobutane) and C_7F_{14} (perfluoromethylcyclohexane) at low pressure ($< 10^{-6}$ Torr). Infrared emission is assumed to stabilize excited species leading to long-lived molecular negative ions. Combining the present data with negative ion lifetimes measured at low pressures by time-of-flight methods and electron attachment rates measured at high pressures in swarm experiments allows estimates of radiative lifetimes to be made. These all fall in the range from 0.4-3.0 msec, which are typical of infrared radiative lifetimes. Data are also presented for dissociative electron attachment to CCl_4. In this case the ion cyclotron resonance results extrapolate smoothly to yield the attachment rate measured in high pressure swarm experiments.

I. INTRODUCTION

Studies of electron attachment processes using ion cyclotron resonance (ICR) techniques at first glance might appear to have generated more confusion than understanding relating to this important phenomenon.[1,2] ICR experiments yield negative ion lifetimes[1] which are orders of magnitude longer than those measured using time-of-flight techniques.[2,3] In addition, rate constants for electron attachment measured at the low pressures typical of ICR experiments (10^{-8} - 10^{-5} Torr) are orders of magnitude less than those measured in high pressure (0.1 - 10 Torr) swarm experiments.[2,3,4] It is well known that lifetimes and attachment rates are sensitive functions of the electron energy distribution.[3,5,6] However, this alone does not adequately account for the apparent discrepancies among the reported studies of negative ion lifetimes and attachment rates.

The scheme depicted in Eq. (1), can be employed to describe

$$A + e^-(E_{kin}) \underset{1/\tau_a}{\overset{k_f}{\rightleftharpoons}} [A^-]^* \xrightarrow[k_s[M]]{k_d} B^- + C \qquad (1)$$

$$[A^-]^* \xrightarrow{1/\tau_r} [A^-]^{\ddagger} + h\nu$$

$$[A^-]^* \xrightarrow{k_s[M]} [A^-]^{\ddagger}$$

electron attachment.[1] Reaction of molecule A with an electron of kinetic energy E_{kin} results in formation of the excited negative ion $[A^-]^*$ which contains internal excitation at least equal to the electron affinity of A. The species $[A^-]^*$ may then autodetach an electron

(with autodetachment lifetime τ_a), decompose (k_d), radiate (with radiative lifetime τ_r) or be collisionally stabilized ($k_s[M]$). The species $[A^-]^{\ddagger}$ may still possess internal excitation, but it is insufficient for autodetachment to be energetically possible. Further radiative or collisional events lead to thermal equilibrium. Processes involving $[A^-]^*$ are expected to be sensitive to the internal energy content of $[A^-]^*$ and hence to the initial electron energy. In general, cross sections for electron attachment show sharp maxima for low energy ($\sim$ 0 eV) electrons.[3,4,6,7]

Earlier we presented an ICR study of SF_6 in which the radiative mechanism for formation of stable SF_6^- at low pressure was inferred.[1] In the present study we present results for non-dissociative electron attachment to a wide variety of molecules, including C_6F_6 (perfluorobenzene), C_7F_8 (perfluorotoluene), c-C_4F_8 (perfluorocyclobutane), and C_7F_{14} (perfluoromethylcyclohexane). In addition, results for dissociative attachment to CCl_4 are presented. Data are now available from a variety of other experiments such that comparison of high and low pressure data is possible. The present results are interpreted in terms of the mechanism of Eq. (1).

II. EXPERIMENTAL

Trapped ion ICR techniques have been described in detail in the literature.[8] An initial electron beam pulse fills the source region of the ICR cell with electrons which may react with neutral species to form negative ions. After a suitable trapping time mass spectrometic

analysis provides relative ion abundances. The instrument used in these studies was built in the Caltech shops and utilizes a 23.4 kG electromagnet, flat ICR cell, and standard marginal oscillator detector. All experiments are carried out at ambient temperature (298° K).

Pressure measurement is made with a Schulz-Phelps type ionization gauge calibrated against a MKS Baratron Model 90H1-E capacitance manometer. Error in pressure measurement is estimated to be ± 20%, and is the major source of inaccuracy in rate constant measurements.

All chemicals used in this study were obtained from commercial sources and used without further purification. Condensible gases were removed by several freeze-pump-thaw cycles; impurities were negligible as determined by mass spectrometry.

III. RESULTS AND DISCUSSION

Electron attachment rate constants are measured in the same manner as for SF_6.[1] It has been shown in previous studies that C_6F_6, C_7F_8, c-C_4F_8 and C_7F_{14} attach low-energy electrons.[6,7,9] In ICR experiments only electrons scattered from the beam and trapped in the source region of the ICR cell attach to SF_6,[10] and the same is assumed for the processes studied here. Consistent with this, negative ion signal intensity increases with increasing electron energy as more inelastically scattered electrons are produced. For C_6F_6, C_7F_8, c-C_4F_8 and C_7F_{14}, non-dissociative attachment is observed.

In addition, a dissociative attachment process, reaction (2), is observed for C_7F_{14}. The ratio of $C_7F_{14}^-$ to $C_6F_{11}^-$ is approximately 25:1.

$$C_7F_{14} + e^- \rightarrow C_6F_{11}^- + CF_3 \qquad (2)$$

Since attachment cross sections peak at very low electron energies ($\sim$ 0 eV), observation of reaction (2) implies that $\sim$4% of the C_7F_{14} molecules possses sufficient internal energy prior to electron attachment such that dissociation of $C_7F_{14}^-$ is then rapid compared to radiative stabilization.

Figure 1 shows typical trapped-ion data for formation of $C_6F_6^-$. Similar results obtain for $C_7F_8^-$, c-$C_4F_8^-$ and $C_7F_{14}^-$. After the initial 10-20 msec, the curve in Fig. 1 is accurately described by a simple exponential function, Eq. (3), where $[M^-]_\infty$ is the anion abundance

$$[M^-] = [M^-]_\infty (1 - e^{-k_{app}[M]t}) \qquad (3)$$

at long time and k_{app} is the apparent bimolecular rate constant. Figure 2 shows the measured electron attachment rate constant, k_{app}, for C_6F_6, C_7F_8, c-C_4F_8 and C_7F_{14} plotted as a function of pressure of the pure gas. Within experimental error the electron attachment rate constants for these molecules are pressure independent at pressures less than 3×10^{-6} Torr. Measurements of the attachment rate constant for C_7F_{14} was not possible at pressures above 2×10^{-7} Torr because the total rate of formation of $C_7F_{14}^-$ becomes comparable to the sampling time of the experiment. Average values of the electron attachment rate constants from Fig. 2 are listed in Table 1 along

FIGURE 1

Typical trapped ion data for electron attachment to C_6F_6. The trap is filled with electrons by a 10 msec electron beam pulse. C_6F_6 pressure is 2×10^{-7} Torr.

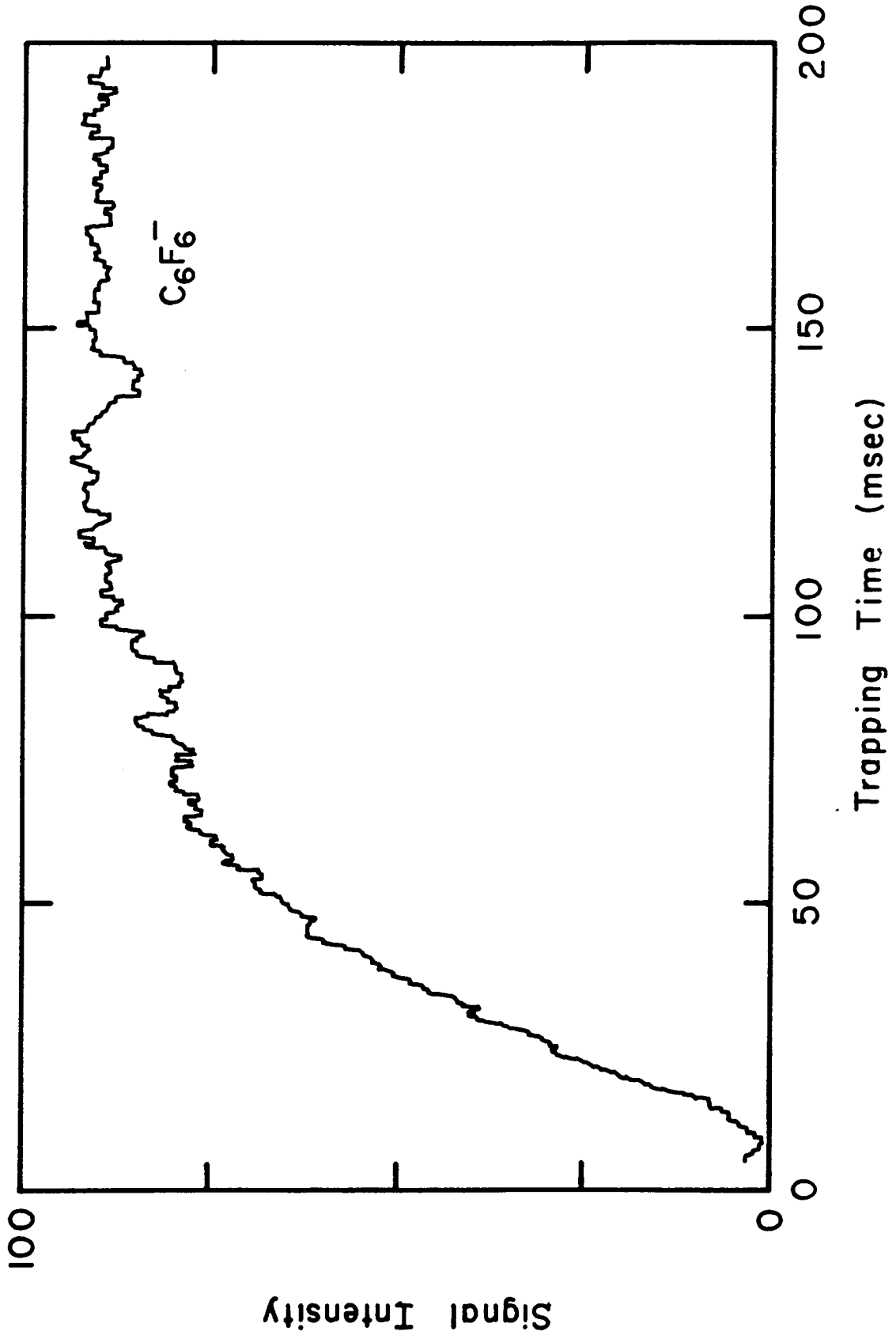
Signal Intensity
100
0
0
50
100
150
200
Trapping Time (msec)
$C_6F_6^-$

FIGURE 2

Electron attachment rate constants as a function of pressure for C_6F_6 (perfluorobenzene), C_7F_8 (perfluorotoluene), c-C_4F_8 (perfluorocyclobutane) and C_7F_{14} (perfluoromethylcyclohexane).

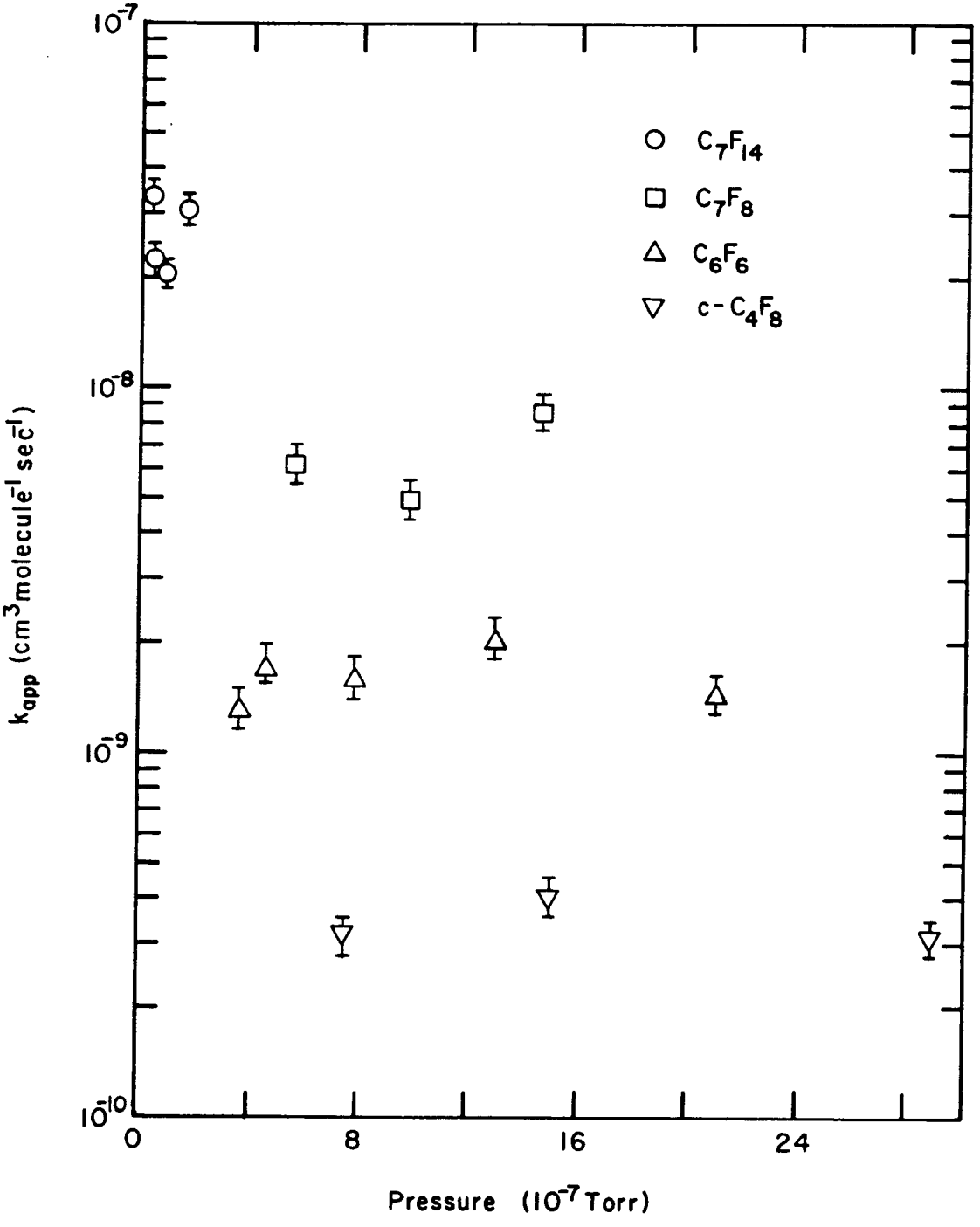
10^{-7}
10^{-8}
10^{-9}
10^{-10}
k_{app} ($cm^3 molecule^{-1} sec^{-1}$)
C_7F_{14}
C_7F_8
C_6F_6
c-C_4F_8
0
8
16
24
Pressure (10^{-7} Torr)

TABLE 1. Attachment rate constants, autodetachment lifetimes and radiative lifetimes for electron attachment to SF_6, C_6F_6, C_7F_8, c-C_4F_8 and C_7F_{14}. Also included are known electron affinities.

Molecule	k_{app}[a]	k_f[b]	τ_a[c]	τ_r[d]	EA[e]
SF_6	1.6 ± 0.2[f]	2.72	25	0.4	>0.6[g]
C_6F_6	0.16 ± 0.03[h]	1.02	12	0.8	≥ 1.8[g]
C_7F_8	0.66 ± 0.15[h]	2.44	12.2	0.5	≥ 1.7[g]
c-C_4F_8	0.04 ± 0.01[h]	0.11	14.8	0.5	0.4[i]
C_7F_{14}	2.7 ± 0.5[h]	0.99	793	2.9	NA[j]

[a]Units are 10^{-8} cm^3 $molecule^{-1}$ sec^{-1}. Errors quoted are for one standard deviation.

[b]High pressure thermal attachment rate constants, equated with k_f in accordance with Eq. (1). Units are 10^{-7} cm^3 $molecule^{-1}$ sec^{-1}. Data from Ref. 2.

[c]Units are μsec. Data from Ref. 2.

[d]Units are msec. Calculated according to Eq. (4).

[e]Units are eV.

[f]Ref. 1.

[g]Ref. 2.

[h]Measured in this work.

[i]Ref. 16.

[j]Data not available.

with literature values of thermal attachment rate constants determined in swarm experiments. Also included are data for SF_6 at low pressures. Data from swarm experiments are obtained at high buffer gas pressures such that every ion formed is collisionally stabilized.[3] In accord with the scheme shown in Eq. (1), we equate the high pressure attachment rate constants with k_f.

As described in our previous ICR study of SF_6,[1] scattered electrons in the source region of an ICR cell can have kinetic energy from approximately thermal to 0.9 V_T, where V_T is the trapping voltage. Values of V_T in these experiments range from -1.5 to -2.5 volt, and hence an appreciable fraction of the trapped electrons initially are epithermal. Since k_f, τ_a and k_d are sensitive functions of the electron kinetic energy, variations of V_T may have a large effect on k_{app}. Measurements of k_{app} as a function of V_T are shown in Fig. 3 for $C_6F_6^-$. For trapping voltages from 1-5 volts, an initial period of slower $C_6F_6^-$ formation is followed by rapid electron attachment with limiting slope independent of trapping voltage. This is analogous to results obtained with SF_6. Since k_{app} is calculated from the limiting slope, Fig. 3, k_{app} is independent of the initial electron distribution. The increased time required for electron thermalization with increasing V_T is a consequence of the electron energy distribution peaking at higher energy with higher trapping voltage. It is evident from Fig. 3 that electron thermalization is rapid compared to attachment and subsequent autoionization is expected to be very efficient at relaxing the electron energy distribution. Results obtained for C_7F_8,

with literature values of thermal attachment rate constants determined in swarm experiments. Also included are data for SF_6 at low pressures. Data from swarm experiments are obtained at high buffer gas pressures such that every ion formed is collisionally stabilized.[3] In accord with the scheme shown in Eq. (1), we equate the high pressure attachment rate constants with k_f.

As described in our previous ICR study of SF_6,[1] scattered electrons in the source region of an ICR cell can have kinetic energy from approximately thermal to 0.9 V_T, where V_T is the trapping voltage. Values of V_T in these experiments range from -1.5 to -2.5 volt, and hence an appreciable fraction of the trapped electrons initially are epithermal. Since k_f, τ_a and k_d are sensitive functions of the electron kinetic energy, variations of V_T may have a large effect on k_{app}. Measurements of k_{app} as a function of V_T is shown in Fig. 3 for $C_6F_6^-$. For trapping voltages from 1-5 volts, an initial period of slower $C_6F_6^-$ formation is followed by rapid electron attachment with limiting slope independent of trapping voltage. This is analogous to results obtained with SF_6. Since k_{app} is calculated from the limiting slope, Fig. 3, k_{app} is independent of the initial electron distribution. The increased time required for electron thermalization with increasing V_T is a consequence of the electron energy distribution peaking at higher energy with higher trapping voltage. It is evident from Fig. 3 that electron thermalization is rapid compared to attachment and subsequent autoionization is expected to be very efficient at relaxing the electron energy distribution. Results obtained for C_7F_8,

FIGURE 3

Variation of $(1-C_6F_6^-(t)/C_6F_6^-(\infty))$ with time at 5×10^{-7} Torr and at various trapping voltages V_T (in volts). Trapping voltages are negative for negative ions. $C_6F_6^-(\infty)$ is the $C_6F_6^-$ ion abundance when all the electrons have been attached, and is equal to the number of free electrons produced during the electron beam pulse.

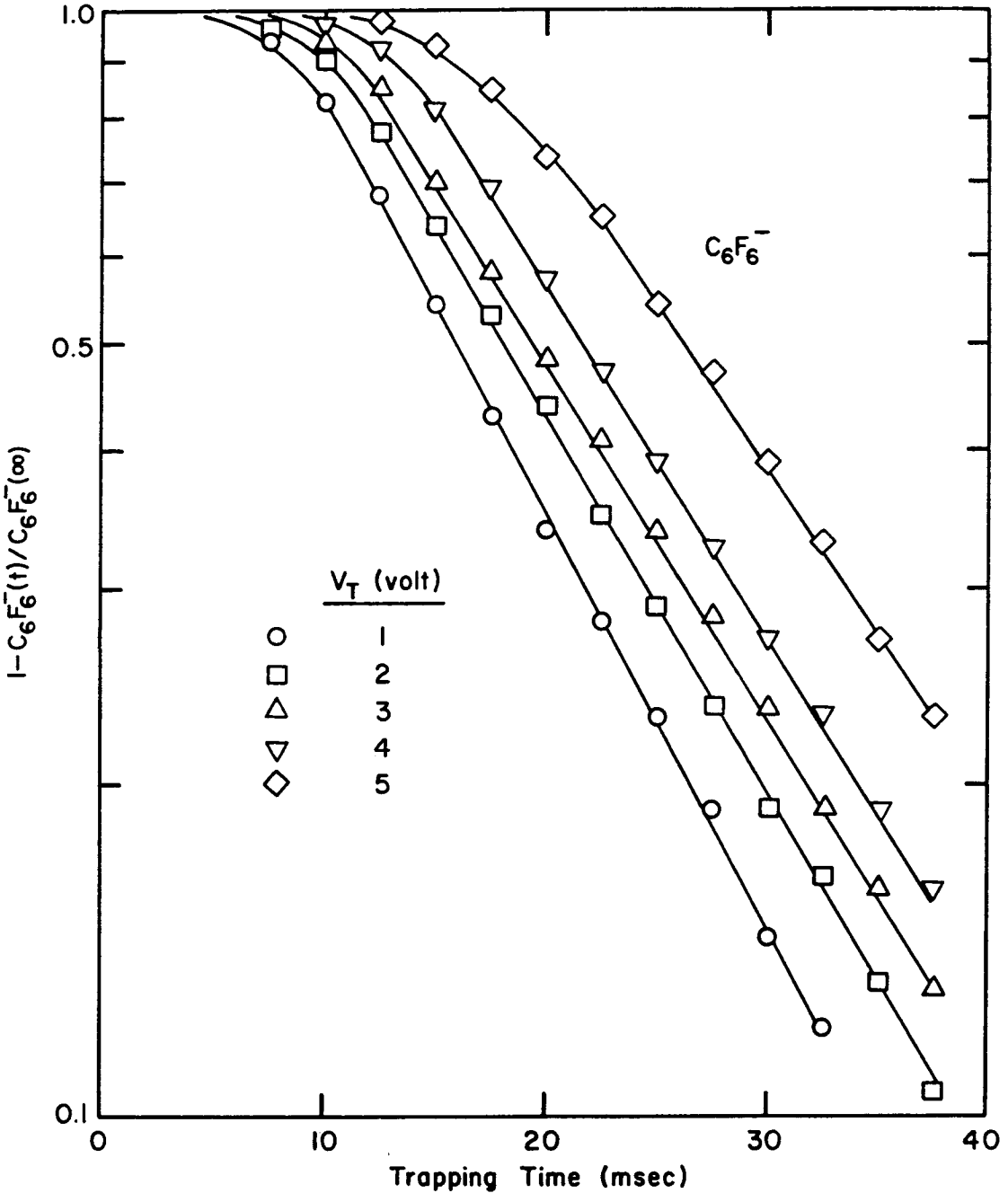
1.0
0.5
0.1
0
10
20
30
40
Trapping Time (msec)
1-C6F6-(t)/C6F6-(∞)
C6F6-
VT (volt)
1
2
3
4
5

$c\text{-}C_4F_8$ and C_7F_{14} indicate behavior similar to that shown in Fig. 3.

Table 1 includes autodetachment lifetimes, τ_a, as determined from time-of-flight experiments. Comparison of autodetachment lifetimes in Table 1 (10 μsec - 1 msec) with the time between collisions for data shown in Fig. 2 (10-1000 msec) indicates that collisional stabilization of the excited molecular ions is much slower than autodetachment at the pressures used in ICR experiments. As dissociative processes are minor for ions in Table 1, radiative stabilization is the most likely mechanism leading to formation of long-lived stable molecular negative ions at low pressure [Eq. (1)]. This conclusion is supported by the bimolecular behavior of the rate constants shown in Fig. 2. Assuming steady-state conditions for $[A^-]^*$ in Eq. (1), Eq. (4) results for k_{app} providing $\frac{1}{\tau_a} \gg \frac{1}{\tau_r} \gg k_s[m]$.

$$k_{app} = \frac{k_f \tau_a}{\tau_r} \tag{4}$$

The data in Table 1 in conjunction with Eq. (4) can be used to estimate radiative lifetimes. Calculated values of τ_r are shown in Table 1. The calculated radiative lifetimes, 0.4 - 3.0 msec, are not unreasonable for infrared emission.[11] Infrared radiative lifetimes (calculated from integrated absorption intensities) for C-F modes in CH_3F, CH_2F_2, CHF_3 and CF_4 are 3, 1.1, 0.4 and 0.2 msec, respectively.[12]

It is of interest to examine the data in Table 1 for $c\text{-}C_4F_8$ and C_7F_{14}. Even though C_7F_{14} rapidly attaches electrons at low pressures,

the radiative lifetime is an order of magnitude larger than for other species. In contrast with C_7F_{14}, c-C_4F_8 is the slowest to attach electrons yet has an autodetachment lifetime and radiative rate comparable to the other ions. In the case of C_7F_{14} the long (793 μsec) autodetachment lifetime is responsible for the rapid attachment process. For a large molecule, internal energy is shared by a large number of modes resulting in a slow unimolecular decomposition (autodetachment) rate. For comparable internal energy content, a larger molecule will also have a lower internal temperature since the energy is distributed over more internal modes. The lower internal temperature results in a longer radiative lifetime, and may explain the long radiative lifetime calculated for C_7F_{14}. On the other hand, c-C_4F_8 has a short radiative lifetime (Table 1). The small attachment rate constant measured at low pressure thus reflects the smaller thermal attachment rate (k_f) measured at high pressure (Table 1). While the electron affinity (included in Table 1) of C_7F_{14} is not known, it is expected to be comparable to or at most slightly higher than the electron affinity of c-C_4F_8.

For electron attachment to the molecules in Table 1 the rate limiting step at low pressure appears to be stabilization of the excited molecular ion. For molecules which undergo dissociative attachment no stabilization is needed and attachment rates at low pressures should not differ from high pressure results. Carbon tetrachloride undergoes dissociative electron attachment of low energy electrons to give Cl^- and CCl_3, Eq. (5).[13] In pure CCl_4, relaxation of the electron energy distribution

$$CCl_4 + e^- (E_{kin}) \rightarrow Cl^- + CCl_3 \qquad (5)$$

is relatively slow and is the rate limiting step at low pressure.[1] Addition of a gas efficient at relaxing the electron energy distribution (such as CO_2) should allow low pressure dissociative attachment rates in CCl_4 to approach high pressure attachment rates. Figure 4 shows CCl_4 low pressure dissociative attachment rates plotted as a function of CO_2 pressure added to 5.7×10^{-8} Torr of CCl_4. The dashed line indicates the attachment rate as calculated from the high pressure attachment rate constant of 2.7×10^{-7} cm^3 molecule^{-1} sec^{-1}.[14] At the CO_2 pressures used attachment rates are proportional to CO_2 concentration as expected. From the slope of the linear portion of the curve in Fig. 4 a rate constant for thermalization of electrons by CO_2 of 2.2×10^{-9} cm^3 molecule^{-1} sec^{-1} is calculated. Higher CO_2 pressures cannot be used because the total rate of Cl^- formation becomes comparable to the experimental sampling time. CH_4 and N_2 were found to be inefficient at relaxing the electron energy distribution, while C_6D_6 was found to relax electrons at a rate slower than CO_2. This is attributed to low-lying temporary electron attachment resonances to CO_2 and C_6D_6,[3,15] not available to CH_4 of N_2, which permit energetic electrons to attach and subsequently autodetach with lower energy. It is apparent from Fig. 4 that the dissociative attachment rates are approaching the high pressure data, and that the rate limiting step is relaxation of the electron energy distribution.

FIGURE 4

Low pressure dissociative attachment rates (open circles) for CCl_4 as a function of added CO_2 pressure. CCl_4 pressure is 5.7×10^{-8} Torr. Dashed line indicates attachment rate at 5.7×10^{-8} Torr calculated from high pressure rate constant of 2.7×10^{-7} cm^3 $molecule^{-1}$ sec^{-1}.

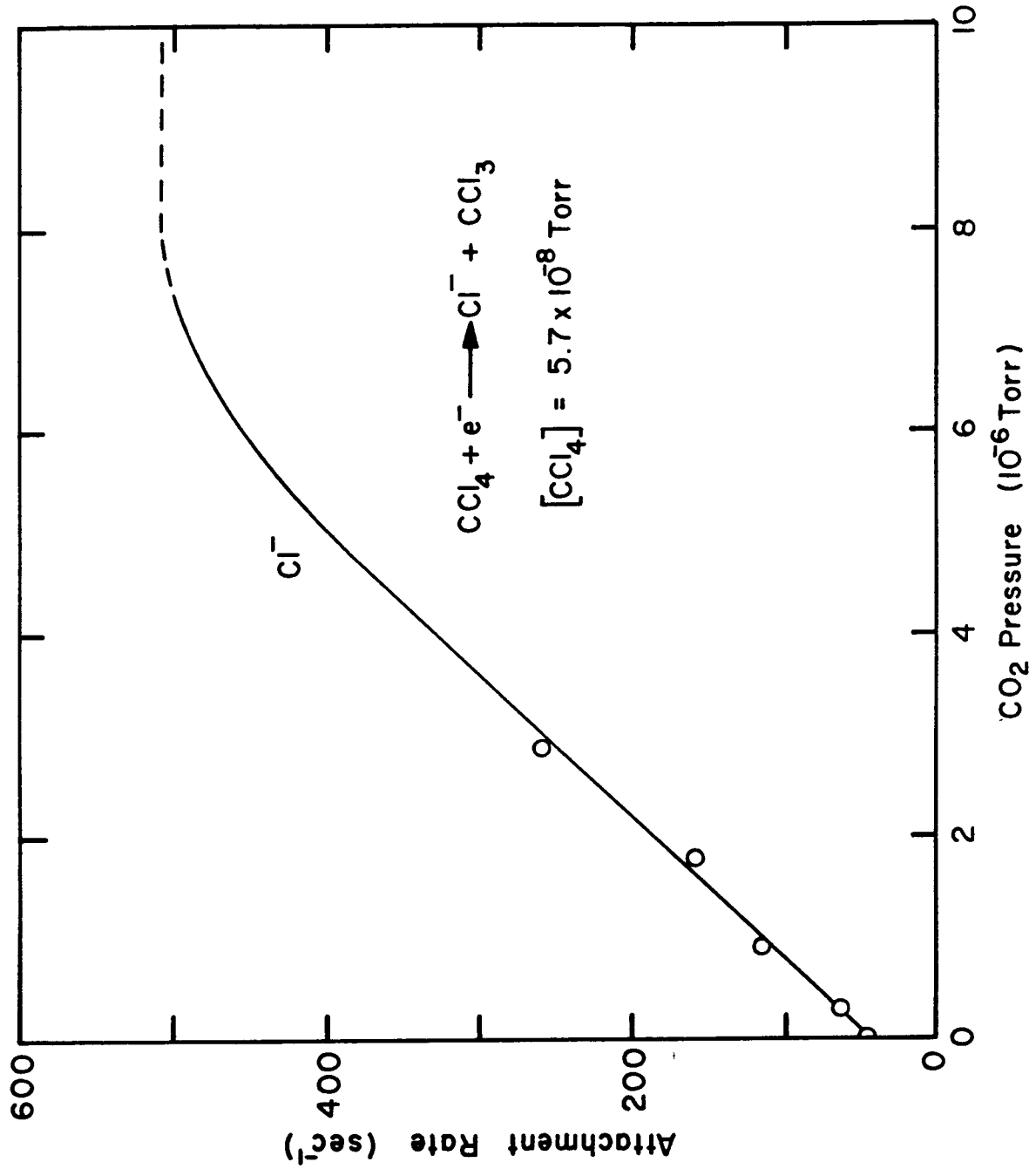
600
400
200
0
Attachment Rate (sec⁻¹)
0
2
4
6
8
10
CO2 Pressure (10⁻⁶ Torr)
Cl⁻
CCl4 + e⁻ ⟶ Cl⁻ + CCl3
[CCl4] = 5.7 x 10⁻⁸ Torr

IV. CONCLUSIONS

With data on electron attachment now becoming available from a variety of experiments under various conditions of pressure, temperature and initial electron energy distribution, the various processes involved [Eq. (1)] are becoming increasingly well characterized. Whereas high pressure experiments yield information on initial attachment rates and autodetachment lifetimes, low pressure ICR techniques are especially well suited for studying processes such as radiative and collisional stabilization. It is seen in this work that formation of stable molecular negative ions at very low pressure is not unique to SF_6, but is observed for a large variety of molecules where autodetachment and dissociation lifetimes are long enough to allow radiative stabilization. Combination of ICR data with high pressure data allows estimates of radiative lifetimes to be made, with results that are consistent with an infrared emission process. Dissociative electron attachment, such as observed in CCl_4, occurs at low pressure with nearly the same facility as at high pressure because no stabilization process is required. In low pressure ICR experiments, the rate limiting step in dissociative electron attachment appears to be relaxation of the electron energy distribution.

Acknowledgments

This work was supported in part by the United States Department of Energy and the President's Fund of the California Institute of Technology.

References

†Present address: Exxon Research and Engineering Company, Corporate Research Laboratories, Linden, New Jersey 07036.

‡Present address: Chevron Research Company, Richmond, California 94802.

[1]M. S. Foster and J. L. Beauchamp, Chem. Phys. Lett. 31, 482 (1975).

[2]L. G. Christophorou, Adv. Electron. and Electron Phys. 46, 55 (1978).

[3]L. G. Christophorou, Atomic and Molecular Radiation Physics, (Wiley-Interscience, New York, 1971).

[4]R. N. Compton, L. G. Christophorou, G. S. Hurst, and P. W. Reinhardt, J. Chem. Phys. 45, 4634 (1966).

[5]R. W. Odom, D. L. Smith, and J. H. Futrell, J. Phys. B. 8, 1349 (1975) and references contained therein.

[6]K. S. Gant and L. G. Christophorou, J. Chem. Phys. 65, 2977 (1976).

[7]L. G. Christophorou, D. L. McCorkle and D. Pittman, J. Chem. Phys. 60, 1183 (1974).

[8]J. L. Beauchamp, Ann. Rev. Phys. Chem. 22, 527 (1971); T. A. Lehman and M. M. Bursey, Ion Cyclotron Resonance Spectroscopy (John Wiley and Sons, Inc., New York, 1976); T. B. McMahon and J. L. Beauchamp, Rev. Sci. Instr. 43, 509 (1972).

[9]W. T. Naff, C. D. Cooper and R. N. Compton, J. Chem. Phys. 49, 2784 (1968).

[10]R. W. Odom, D. L. Smith and J. H. Futrell, Chem. Phys. Lett. 24, 227 (1974) and references contained therein.

[11]G. Herzberg, Infrared and Raman Spectra of Polyatomic Molecules, (Van Nostrand, New York, 1945), p. 251.

[12]J. H. Newton and W. B. Person, J. Chem. Phys. 64, 3036 (1976); J. H. Newton, R. A. Levine, and W. B. Person, J. Chem. Phys. 67, 3282 (1977).

[13]L. G. Christophorou and J. A. D. Stockdale, J. Chem. Phys. 48, 1956 (1968); A. A. Christodoulides and L. G. Christophorou, J. Chem. Phys. 54, 4691 (1971).

[14]L. G. Christophorou, D. L. McCorkle and J. G. Carter, J. Chem. Phys. 54, 253 (1971).

[15]R. N. Compton, L. G. Christophorou and R. H. Huebner, Phys. Lett. 23, 656 (1966).

[16]C. Lifshitz, T. O. Tiernan, and B. M. Hughes, J. Chem. Phys. 59, 3182 (1973).